

# Dynamic Soil Structure Interaction of Seismic Isolated Bridges

by

Spyridoula Maria Papathanasiou

A thesis submitted to the Faculty of Postgraduate Studies and Research of National  
Technical University of Athens, in partial fulfilment of the requirements for the degree of  
Master of Science

in

**“Analysis and Design of Earthquake Resistant Structures”**

Supervisor: Vlasios Koumoussis, Professor at National Technical University of Athens

School of Civil Engineering  
Department of Structural Engineering - Laboratory of Earthquake Engineering  
National Technical University of Athens  
Athens, 2013



## **The Aim of this Thesis**

Since this text is written as the final thesis of the Master's degree in *Analysis and Design of Earthquake Resistant Structures* of the School of Civil Engineering at NTUA, it is primarily aimed to educate the engineers, designers and analysts, interested in the behavior of large structures, more specifically bridges, under seismic loading when soil-foundation-structure interaction effects are present. For purposes of completeness a parametric investigation considering different structures, earthquake excitations, and foundation system properties is conducted in an attempt to identify the important parameters that influence the behavior of a structure with the SSI effects. The study doesn't intend to conclude whether the soil-structure interaction is beneficial or detrimental since this question has been addressed adequately in the literature.

## **Acknowledgements**

I would like to thank Professor Vlasis Koumouisis, for agreeing to serve as my supervisor and for his constant support provided to me throughout the course of this study. His guidance helped me in all the time of research and writing of this thesis. I would also like to express my sincere gratitude to Professor Panos Tsopelas for the continuous support of my research, for his patience, motivation, enthusiasm, and his immense knowledge on the subject.

I would also like to thank Dr. Amir Kaynia, of the Norwegian Geotechnical Institute for his generosity of providing an executable version of the computer software PILES used in this present study to obtain the dynamic impedances of the pile foundations considered.



# ABSTRACT

This thesis focuses on the impact of the Soil-Structure Interaction (SSI) on seismic isolated bridges. The general conception is that the beneficial effects of the structural isolation are amplified due to the dynamic interaction between the soil, the foundation and the structure. Such a misconception is related with the additional flexibility that the design spectrum contributes to the system when the SSI acts. In reality, the spectrum is only a smoothed average of the response spectra. Hence, the lengthening of the period may possibly not correspond to small seismic forces, as it is unlikely for the response at a real seismic event to follow closely the smooth line of the spectrum (Figure A).

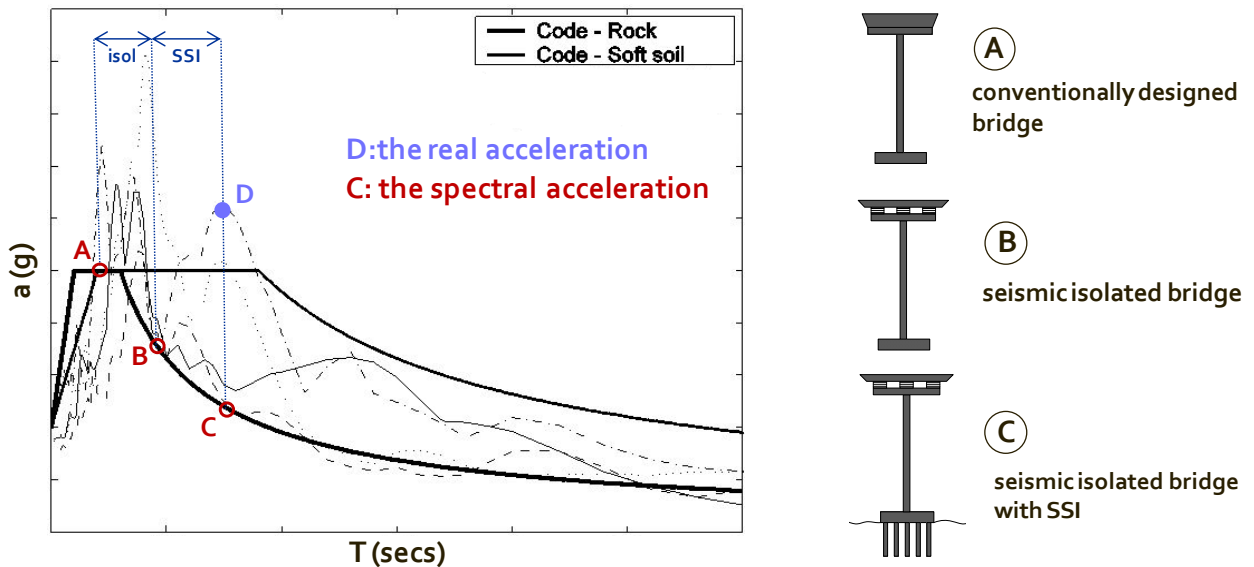
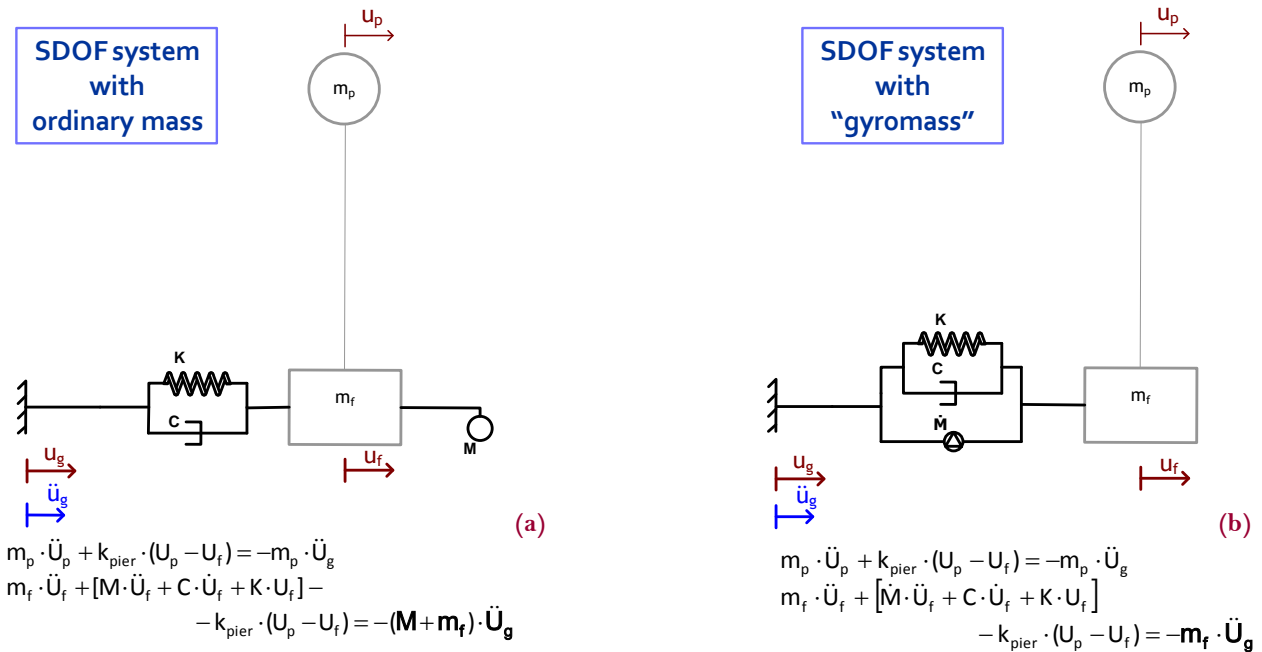


Figure A. The design spectrum and the SSI effects.

The validity of this statement is examined with the help of stick models of 2 seismic isolated bridges and equivalent models of the frequency-dependent impedance functions of the soil and foundation (consists of a pile group). The latter models consist of frequency-independent springs and dashpots as well as "gyromasses", which are elements proposed recently in the literature. Each "gyromass" plays the role of an ordinary mass, with the advantage of not adding inertial forces into the system (Figure B). Appropriate combinations of springs, dashpots, and "gyromasses" can match in the

frequency domain even the most frequency-sensitive impedance functions providing an advantage over simple Voigt models (spring-dashpot in parallel) used frequently in SSI analyses. The models are suitable for use in time domain and are utilized in this study for the nonlinear time history analyses of the bridges, subjected to 2 sets of 20 motions; the near fault and the far field sets.



**Figure B. Modeling of SSI effects at single degree of freedom systems a) including an ordinary mass and b) a gyromass.**

The paper examines factors which influence the SSI effects on a structure: number and geometry of piles, spacing of piles, soil characteristics, flexibility of superstructure etc. The results are presented in terms of displacements and forces of the system and some general conclusions are drawn over the possible vulnerability of a soil–foundation–isolated superstructure system to the SSI effects. To this direction, the dynamic characteristics of the models experiencing the soil–structure interaction in combination with the power spectra of “dangerous” excitations reveal interesting aspects of the total system’s response. Further analysis would possibly predict the cases that the SSI demands detailed modeling due to its detrimental role.

# Contents

Introduction .....	9
1. Soil Structure Interaction Effect.....	11
2. Soil-Foundation-Bridge System Modeling .....	17
2.1. Soil - Foundation System .....	17
2.1.1. Dynamic impedances of pile groups.....	19
2.2. Seismic Isolation System .....	37
2.3. Bridge Systems.....	40
3. Computational modeling .....	43
3.1. Computational Modeling of the Soil-Structure Interaction Problem .....	43
3.1.1. Spring-Mass-Damper Models to account for SSI.....	43
3.1.2. The concept of GYROMASS.....	45
3.2. Calibrating GYROMASS Models.....	50
3.2.1. Levenberg Marquadt Method .....	50
3.2.2. Parameter calibration of Type II model.....	53
3.3. Models.....	60
3.3.1. Voigt Model .....	60
3.3.2. Type II Model .....	62
3.3.3. Simple Type II Model.....	63
3.4. Dynamic properties of the Soil-Foundation-Structure System (Eigenvalue Analysis) .....	65
3.5. Seismic Excitations .....	68
4. Analyses Results and Discussion.....	71
4.1. Non Linear Time History Analyses and Results.....	71
4.2. Bridge I Analyses .....	72
4.3. Bridge II Analyses.....	75
4.4. Qualitative Prediction of SSI Response .....	80
4.4.1. Transfer Function.....	80
4.4.2. White Noise or actual Seismic Motion as Input to the TF .....	82
4.4.3. Structural System Properties.....	82
4.5. Effect of $E_p/E_s$ .....	95

5. Conclusions ..... 105  
Bibliography ..... 107

# Introduction

After years of investigating constructions that have been severely damaged by earthquakes, structural engineers have developed the most intelligent, innovative and technologically safe design theories so as their projects to deal successfully with their environment and transfer safely all their loadings to the soil. In common projects, such as housing buildings, engineers rarely examine in detail the soil's characteristics and the subsequent effects of a possible interaction with the structures during an earthquake event. Some soils are hard, like rock, while others are weak, like loose sand. The different soil properties can affect seismic waves as they pass through a soil layer. This will also influence what needs to be done to structures, especially the heavy ones, to help them perform better in an earthquake. The need of simplifying things during the design of a new project, often leads to generalized considerations, such as the structure being linearly interacting with the soil or even being fixed base. The real image of the problem though, is not exactly this. In fact, the foundation interacts nonlinearly with the surrounding soil and modifies unpredictably the final performance of the total system. The phenomenon is the so-called *soil-structure interaction (SSI)*.

Soil-Structure interaction is often neglected by engineers during the design of their structures. The problem of such a policy is that the designer not only has to be totally aware of the phenomenon's nature but also confident that the ignorance of the soil-structure interaction effects is not going to cause ultimate collapse or even serviceability problems to the structure. The objective of this thesis is to investigate in which cases the interaction effects between the soil and large structures can be stimulated with simple models or further analysis is needed. For this purpose, 2 different bridge models were considered, one representative of short stiff highway overpass systems and another tall flexible multispan highway bridges. The analysis consisted of many stages. Firstly, the dynamic impedance of the soil-foundation interaction was modeled with frequency-dependent springs and dashpots. Then, nonlinear time history analyses were performed for the piers of the two types of bridges, for two sets of seismic motions; far-field and near-fault accelerograms. Finally, the results of these analyses were summarized and reach to a general conclusion: depending on the system's conditions and the earthquake motion's characteristics the negligence of soil-structure interaction may be harmful.



# 1

## Soil Structure Interaction Effect

Soil-structure interaction is the phenomenon where a structure together with its foundation and soil behave as a system, with the soil and the structure motions influencing each other in a way which can't be absolutely decomposable. Many design codes state that the SSI effects may be safely ignored during the design process of heavy structures, however that is not always true. For example in ATC-3 provisions (1978) and also in NEHRP specifications (1997) and its latest revisions it was effectively stated that the response of a structure under earthquake loading could be conservatively evaluated without taking the SSI effects into consideration. The myth of the SSI effects being safely neglected stems from the perception that the phenomenon makes the structural system more flexible when subjected to an earthquake and hence it reduces the overall seismic loading. This belief is reasonable enough for light structures in relatively stiff soil. When it comes to heavy structures resting on soft soil (such as heavy bridges, nuclear power plants etc), the design considerations have to be different, not only because of the significance of such structures, but also because the environment's and system's behavior uncertainties under a certain seismic excitation are high.

The code compliant acceleration design spectrum (see *Figure 1*) decrease monotonically with increasing structural period; a fact that leads to misconceptions over the seismic demand. Considering that the design spectrum is a smoothed average of the response spectra for many different earthquake motions, it is unlikely that the acceleration response from a real seismic excitation will follow it closely. The factors which determine the final performance of the system are the characteristics of the earthquake excitation, the superstructure, the foundation and the soil's profile.

In order to highlight the important features of SSI phenomenon, the appropriate models and excitations have to be considered and their analysis results should be compared. For this purpose, a variety of methods have been proposed and advanced through the years. They can be categorized in two large groups: a) *the direct solving*

methods and b) *the substructure solving methods*. Undoubtedly, the simplest approach for solving accurately problems involving interaction between soil and foundation is to model a big area around the foundation and then subject the boundaries to a bedrock motion (the non linearities of the soil have to be included). In such an analysis though, the dynamic degrees of freedom would be too many and this would increase both the cost and the duration of the analysis procedure.

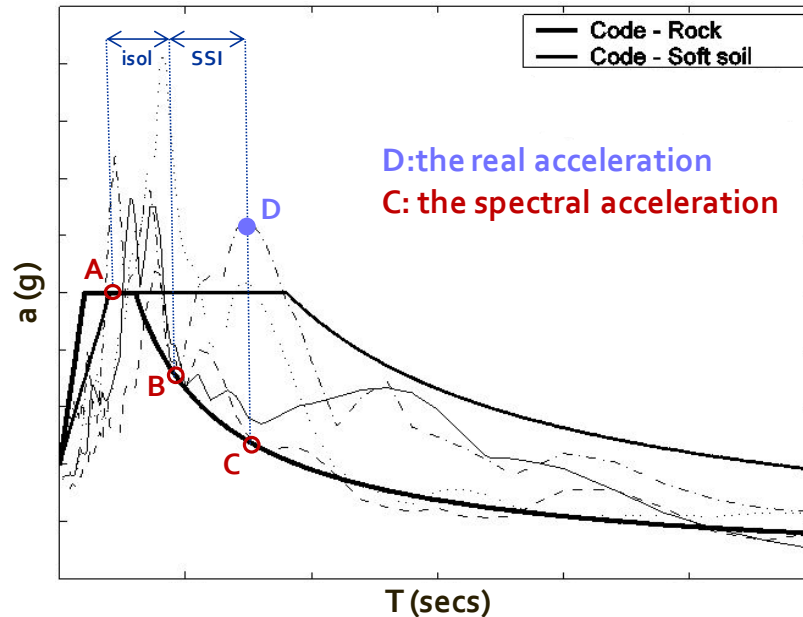


Figure 1. The design spectrum and the SSI effects.

In the substructure method the system is analyzed after considered being composed of separate parts/substructures. The link between the separate parts is established if compatibility conditions are imposed. Such an approach allows for easier identification of the interaction's important parameters and helps quantifying how the interaction influences each part separately. In addition this approach offers independence, as the change of the properties of one subsystem may leave the others unaffected. This is exactly the way that this study deals with the phenomenon of SSI: the structure is not one but three interrelated subsystems; soil, foundation, superstructure.

For a more detailed examination of the substructure method, it is necessary to introduce some components of the soil behavior and the SSI which accompany the substructure method: *free field*, *inertial* and *kinematic* response.

*Free field response* is the response of the soil's surface, without the presence of the structure, as the seismic waves travel from the rock stratum through the soil profile (see

Figure 2, b). It is clear that the excitation that is generated from the source of the earthquake will be different from the motion at the top of the ground, due to the wave reflections and refractions that may occur. The estimation of the “distorted” earthquake motion that accounts for the free field response (requires soil amplification analysis) includes the exact modeling of the soil profile of the region and the dynamic characteristics of each layer, which introduces more uncertainties to the SSI problem. For simplicity purposes, in this study the earthquake excitation is considered to be the same as the free field response, as recorded at the control point (no soil amplification analysis is performed).

The free field response is not the motion that the structure will be exposed to, due to the presence of the structure’s foundation, which experiences both horizontal displacements and rocking. As a result, a scattered wave field may be generated, with the foundation being the source of it. This interaction between the free field motion and the foundation’s motion, in the absence of the superstructure, is the *kinematic response* (Figure 2, c).

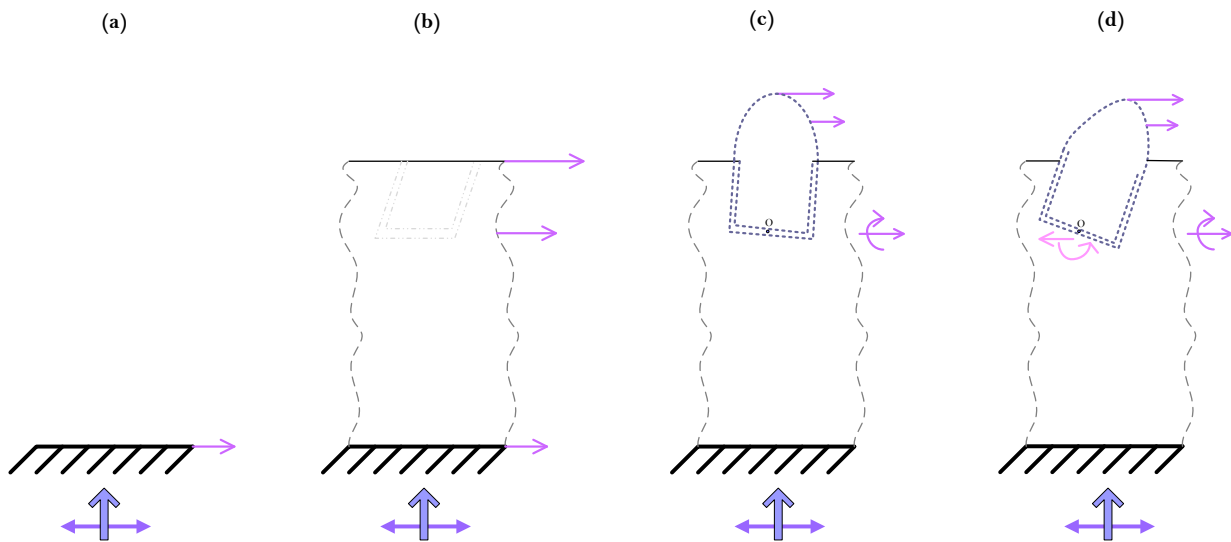
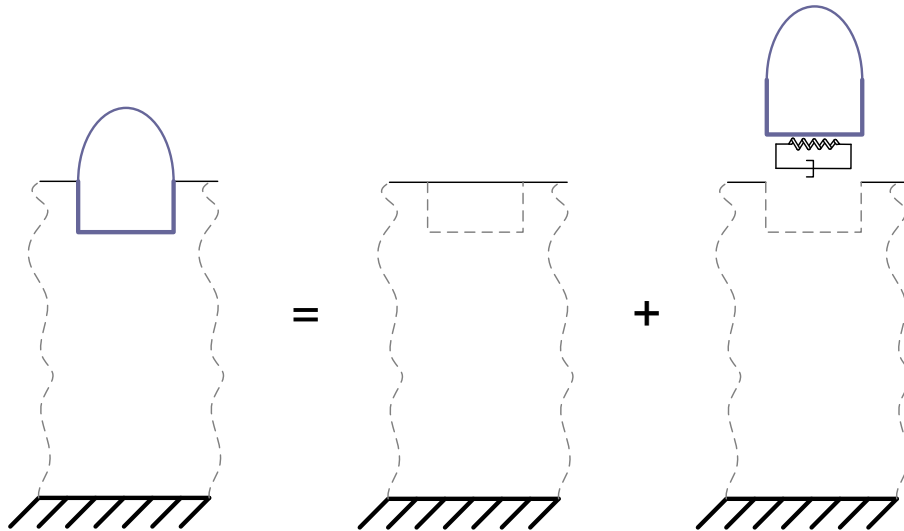


Figure 2. Seismic response of a structure resting on soil which lays on rock: (a) rock, (b) free field motion, (c) kinematic interaction, (d) inertial interaction.

Considering all the above information, it is mandatory to highlight that the final seismic performance of the structure is also depending on the characteristics of the superstructure. The inertial loads will cause additional moments and displacements at the superstructure that are going to interact with the soil, through the foundation. This state is known as *inertial interaction* (see Figure 2, d). The characteristics of the kinematic and inertial response are those who determine whether the soil structure interaction

will be beneficial or detrimental for the whole structure. In other words, depending on the type and profile of the foundation, of the soil and the seismic energy that will be introduced to the system, the result may be either beneficial or detrimental.

In order to clarify the impact of the SSI effects through the aforementioned *inertial interaction* of the superstructure, a hypothetical structure laying on rock is introduced. For the structure on the rock, the horizontal input motion of the bedrock can be directly applied to the base of the structure, due to the large stiffness of the rock that leads to zero amplification of the excitation. The inertial response of the system's base is constant throughout its height. Thus, the developed overturning moment and shear force will lead the base to no additional deformations but for the seismic motion's. As a result, no rocking component will appear. The performance of the structure depends only from its own characteristics.



**Figure 3. Substructure method of dealing with soil structure interaction.**

For the structure on the soft soil, things are different. In general, the input motion is amplified (the frequency content controls this part) as the seismic waves travel towards the surface of the site and result in larger accelerations and deformations (see *Figure 2*). The presence of the structure's rigid base will also change the seismic wave scenery and thus it will suffer different inertial responses through its height. The equilibrium demands a rocking moment to appear and additional deformations at the soil. Although in this chapter only a rough idea is given concerning the effects of the soil structure interaction, it is enough to understand the substructure method of analysis. For the structure of *Figure 3*, the method proceeds as follows. After the calculation of the free field response, which is the same as the control motion for this

study, it is used as input motion for the soil dynamic subsystem. The stiffnesses of the discontinuing line that is in contact with the rigid base are estimated. The soil can be modeled as a spring – dashpot system, which characteristics can be evaluated. Then the superstructure’s model can be subjected also to the free field motion through the spring – dashpot system.

It is obvious that in order to study the effects of the soil - structure interaction, many realistic and acceptable simplifications should be done. The need for approximate results was the main reason for not implementing the Finite Element Method in this study. FEM would effectively model the whole system and develop an accurate analysis, but this would be extremely time and money consuming. The superstructure was chosen to be modeled with the help of the so-called “stick model”. Stick models are widely employed in the dynamic analysis of bridges when approximate results are desired or when detailed models are difficult to construct. Its simplicity and relative accuracy makes it a satisfactory solution for modeling. With the appropriate masses and stiffnesses the stick model may be representative of one span or the whole bridge system.

The complicated SSI phenomenon has now become clearer. Interaction between the soil and the foundation subjected to an earthquake is distorting the expected response in a not easy predictable way. In the case where the superstructure behaves in a nonlinear way, the parameters of examination are more. All the aforementioned statements have been examined before by many researchers, after considering quite representative models for soil, foundations and superstructures. Spyrakos (1990, 1992) used simple linear elastic models and concluded that the soil-structure interaction effects make structures more flexible and less seismically affected. In another study, Mylonakis and Gazetas (2000) used another simplified elastoplastic model for a bridge and its foundation, which was subjected to a set of actual acceleration time histories recorded on soft soil. Though the lengthening of the period made the structure more flexible, the SSI phenomenon played detrimental role on the seismic performance of the bridge. In fact, damage in structures associated with SSI effects has been proven or suspected in many cases in the past. For instance, the Mexico City earthquake of 1985 was particularly destructive to 10 to 12-story buildings (founded on soft clay) whose period increased from about 1.0 sec (for the fixed-base structure) to nearly 2.0 seconds due to SSI (Resendiz & Roesset 1985). Other evidence for a detrimental role of SSI has been presented by Meymand (1998), Gazetas & Mylonakis (1998), and Celebi (1998). According to these findings and many other researches on this issue, the conclusion is that SSI may have either beneficial or detrimental effects on the structure, depending on its characteristics and those of the soil and earthquake motion.



# 2

## Soil-Foundation-Bridge System Modeling

### 2.1. Soil - Foundation System

After years of design experience with structures on, with, or within the soil, engineers, although it is not possible to model all details of geometry and material of a real problem, consider the following essential features in soil-foundation modeling: a) the soil consists of horizontal layers resting on a half space, both consisting of isotropic viscoelastic material with hysteretic damping, b) the properties vary with depth but remain constant within the individual layers, c) when the foundation interaction is taken into account, its behavior is influenced by the geometry, mass, and the type of the foundation, e.g. for pile foundation the number, the location of the piles, as well as their dimensions influence the behavior. Considering the simplest case of dynamic excitation, a harmonic oscillation, the dynamic response of the foundation may be easily computed once the “dynamic impedance” at the top of the foundation is known for each particular frequency of interest,  $\omega$ .

It is generally accepted, especially for the layers closer to the surface, that soil experiences nonlinear behavior when excited by the strong seismic motions such as the ones of interest to structural engineers. However, one can list a few reasons which can be called to advocate the practice of accepting linear behavior for the soil - foundation systems in modeling:

- 1) Currently available foundation design codes do not allow soil-foundation systems to respond in the inelastic range (no damage or plastic hinging of any kind is allowed). Thus the soil and foundations are designed, and expected, to respond in the elastic range.
- 2) With the currently available computational tools and power the cost and the time of performing nonlinear soil-foundation analyses are quite high.

- 3) The substructure method for soil-structure interaction analysis implicitly assumes the superposition principle to be valid. The total solution, when the structure is inserted into the seismic environment of the free field, is the sum of the free field and kinematic interaction parts of the response. Even when determining the free-field site response starting from the motion in the control point, superposition is used. This means that a linear behavior of the system is actually calculated.
- 4) Considering that soil and/or foundation behave in a nonlinear hysteretic manner increases the number of parameters required to capture this behavior on top of the geometric complexity required to model variability/randomness of soil strata. Such large number of parameters might render the nonlinear analysis of soil and foundation not only impractical but also highly unreliable since it is very difficult to evaluate these parameters.

In lieu of the above, before moving towards performing nonlinear soil analysis it is rather “mandatory” to fully clarify potential SSI effects caused in a linear soil environment. Therefore, one of the most important simplifications of the soil-foundation models considered by engineers, the linearity of the soil as well as the linearity of the foundation is also adopted in the present study.

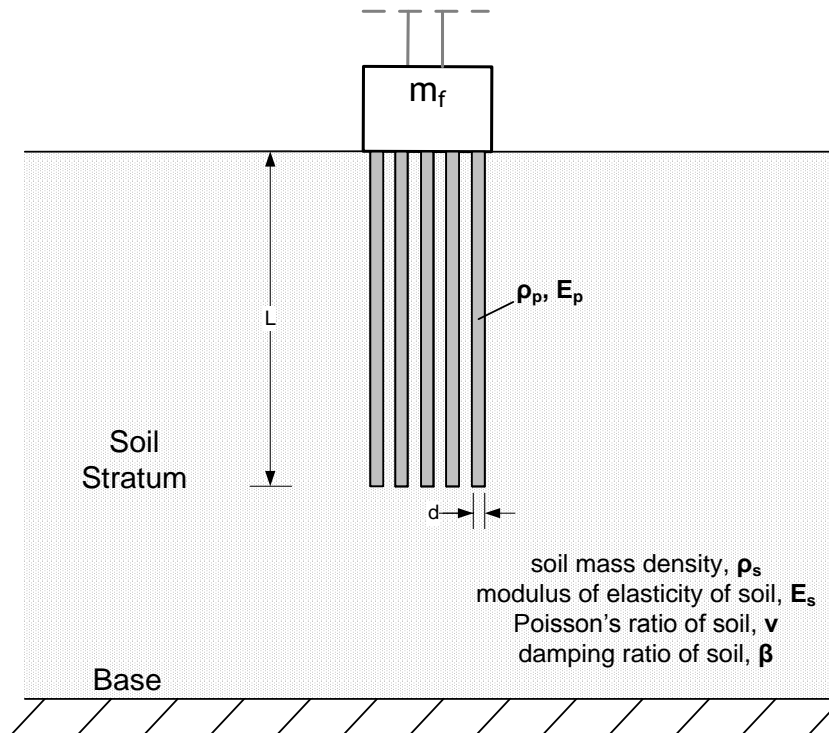


Figure 4. Constrained-head pile group floating in a homogeneous soil stratum.

*Figure 4* shows the soil-foundation system considered in this study. A group of circular floating piles of diameter  $d$  and length  $L$  is embedded in a homogeneous soil profile underlying by rigid bedrock. Each pile is treated as a linear elastic beam having constant Young's modulus,  $E_p$  and mass density,  $\rho_p$ . The soil is assumed to be a linear nonliquefiable hysteretic medium, with a constant mass density  $\rho_s$ , a constant Poisson's ratio  $\nu$ , and a constant Young's modulus  $E_s$ . All piles are rigidly connected to a pile cap, on the top of the pile group, which is also the base of the superstructure. The values of these parameters, which are summarized in Table 1, are representative of the real soil profile which exists in the vicinity of the Meloland Road Overcrossings in California, according to the California Division of Mines and Geology (Kampas and Makris, 2011).

### 2.1.1. Dynamic impedances of pile groups

The harmonic response of pile groups is substantially affected by the dynamic interaction between the soil and the piles and between the individual piles. The dynamic impedance of soil-foundation systems is evaluated as function of the frequency of oscillations under harmonic excitations. Following the early numerical studies by Wolf, Von Arx and Nogami, several researchers have developed a variety of computational (rigorous and simplified) methods for assessing the pile-soil-pile interaction and computing the dynamic impedances of pile groups. Under lateral loading, the impedances of the foundation being exposed to an earthquake motion are related to: bending ( $K_{xx}$ ), rocking ( $K_{rr}$ ) and coupled bending-rocking effects ( $K_{xr}$ ). For each sinusoidal excitation with a frequency  $\omega$ , dynamic impedance is defined as the ratio between the magnitudes of excitation and of the resulting displacement or rotation at the pile head:

$$K_{xx} = \frac{P_o e^{i\omega t}}{u_o e^{i(\omega t + \phi)}} \quad (1)$$

Such a definition is widely known from the simple Hooke's law,  $F=Ku$ . The horizontal dynamic force is described as  $F=P_o e^{i\omega t}$  and the resulting horizontal

displacement as  $u = u_0 e^{i(\omega t + \phi)}$ . The angle  $\phi$  represents the phase-difference between the input and the output, on account of the total damping the system experiences. Part of this energy dissipation (damping) takes place through the hysteretic action of the soil (internal/inherent material damping) and another part through the scattered wave fields that the piles generate themselves (radiation damping). The three dynamic impedances that take part in a seismic event are defined in a simple cantilever model in *Figure 5*. It is preferable to express the dynamic impedances as:

$$K_{xx} = K_{xx} + i\omega C_{xx}, \quad (2)$$

where,  $K_{xx}$  is the “spring” coefficient modeling the soil and the foundation,  $C_{xx}$  is the “dashpot” coefficient,  $\omega$  is the frequency of the harmonic input (under free interpretation the *seismic event*) (rad/sec) and  $i = (-1)^{1/2}$ .

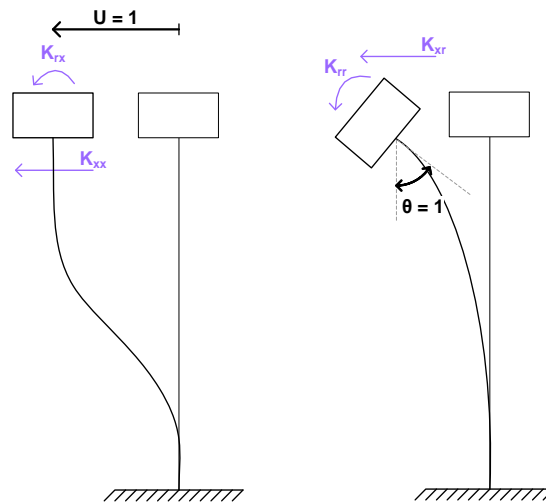


**Figure 5. Definition of the bending, rocking and coupled bending-rocking impedances.**

Physically,  $K_{xx}$  represents the stiffness and inertia characteristics, while  $C_{xx}$  the energy loss due to both hysteretic and radiation damping. Obviously, the total stiffness,  $K_{xx}$ , is strongly frequency sensitive, a fact that makes difficult the prediction of their behavior during a specific seismic excitation. Similarly, the dynamic impedances related with rocking and coupled bending-rocking are expressed as:

$$K_{rr} = K_{rr} + i\omega C_{rr} \quad (3)$$

$$Krx = K_{rx} + i\omega C_{rx} \quad (4)$$

Pile foundations, sometimes referred to as deep foundations, have been a subject of considerable research by engineers. The majority of the studies have focused on short and long-term static pile behavior, estimation of lateral deflection and load capacity. In the last 20 years though, many powerful techniques have been developed for computing foundation dynamic impedances. The codes that have been developed are a useful tool in the hands of engineers, but at the same time they can make the problem more unreliable. Gazetas, Dorby, Beredugo, Novak, Veletsos, are some of the engineers who looked through the problem of soil-structure interaction and ended up with more simple and also accurate ways of estimating the foundation dynamic impedances, without even the help of a computer (Gazetas, 1984; Gazetas and Dorby, 1984 a, b; Gazetas and Tassoulas, 1987a, b).

The dynamic stiffnesses of a pile group, in any vibration mode, can be computed using the dynamic stiffnesses of a single pile in conjunction with the use of superposition principle, originally developed for static loads by Poulos (1968), and later extended for dynamic loads by Kaynia and Kausel (1982), Sanchez-Salinerio (1983) and Roesset (1984). It can be used with confidence at least for groups with less than 50 piles. Dynamic interaction factors for various modes of loading are available in the form of non-dimensional graphs (Gazetas et al., 1991) and in some cases, closed form expressions derived from a beam on winkler foundation model in conjunction with simplified wave-propagation theory (Dobry and Gazetas, 1988; Makris and Gazetas, 1992). Depending on the foundation type and its soil-support condition, the procedures currently being used in evaluating SSI effects on bridges can broadly be classified into two main methods, namely, the so-called *elastodynamic* method that has been developed and practiced in the nuclear power industry for large foundations, and the so-called empirical *p-y method* that has been developed and practiced in the offshore oil industry for pile foundations.

In this study, for the estimation of the dynamic impedances of pile groups, the boundary element program **PILES** (Kaynia, 1989) was utilized. This software uses the elastodynamic method which is based on a frequency domain solution of the closed-form Green's function for both the soil and the piles, whose displacements have to be compatible. The term "displacements" includes not only translations but also rotations and likewise the term "response" both forces and moments. The software assumes that the behavior of the piles and the ground is linear elastic, while the pile cap is considered rigid and not in contact with the ground. The ground is assumed to be horizontally layered and resting either on rigid bedrock or viscoelastic halfspace. The piles are characterized by their radius, mass per unit length, bending and axial rigidities and

Poisson's ratio. Although it is made for circular piles, any type of cross section may be analyzed with an equivalent radius of its area. The most important results that **PILES** computes are the dynamic foundation stiffnesses of a specific pile group, after having interacted with the soil profile. The results are used in this study so as to be the data for an algebraic formula that predicts the impedances at different frequencies. *Table 1* summarizes the input used in **PILES** to model the soil profile of the problem studied.

**Table 1. Properties of the soil profile to be studied.**

<b>Number of layers (input PILES)</b>	70 ( max )	
<b>Total Thickness ( m )</b>	21.5	
<b>Homogeneous / Inhomogeneous</b>	Homogeneous	
<b>Halfspace / Rigid Base</b>	Halfspace	
<b>Shear Wave Velocity, <math>V_s</math> ( m/sec )</b>	110	<b><math>G = \rho_s V_s^2 = 22 \text{ MPa}</math></b>
<b>Mass Density, <math>\rho_s</math> ( kg/m<sup>3</sup> )</b>	1800	
<b>Damping Ratio, <math>\xi</math></b>	0.10	<b><math>E_s = 2(1+\nu)G = 0.062 \text{ GPa}</math></b>
<b>Poisson's Ratio, <math>\nu</math></b>	0.40	

*Figure 6* presents the 5x5 pile group of the 2 bridge models considered in this study. The number and characteristics of piles was chosen based on the real foundation image of the Meloland road overcrossing bridges. In order to examine the effect of the number of piles on the overall seismic response of the structure, 2 more pile groups were considered: one 3x3 and one 2x2 pile group, with the same material characteristics and equivalent pile diameters so as to represent the same foundation area and result in approximately the same static impedances ( $\omega=0$ ). As the number of piles decreases, the interaction is expected to be less between them because the distance between them is greater. Apparently the different pile groups lead to different impedance functions as functions of  $\omega$ . The 3 equivalent pile groups are also examined for the second bridge, where the diameters are greater due to the superstructure being larger. *Table 2* presents

the material and geometrical properties of the piles in the considered pile groups. The properties of the pile groups are identical for the two directions x and y due to the symmetric geometry. The bridge models are analytically presented in §2.3.

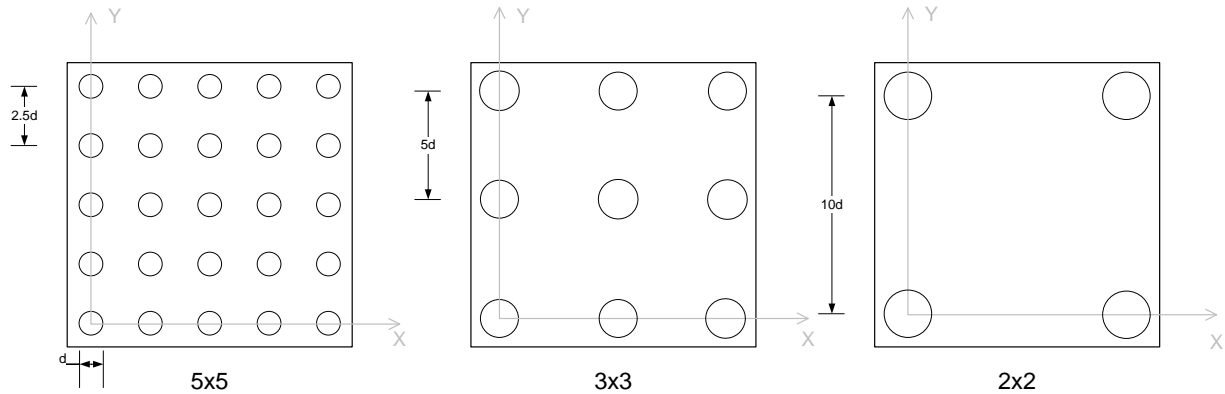


Figure 6. Geometry of 5x5 and equivalent 3x3 and 2x2 pile groups (for both bridges).

Table 2. Properties of the 3 equivalent pile groups of study.

Pile Group Label	Bridge I			Bridge II		
	5x5	3x3	2x2	5x5	3x3	2x2
Number of piles, N	25	9	4	25	9	4
Diameter, d ( m )	0.43	0.7	1	1.8	3	4.5
Length, L ( m )	21.5	21.5	21.5	21.5	21.5	21.5
Distance, S, from pile to pile ( m )	1.08	3.5	10	4.5	9	18
Mass Density, $\rho_p$ ( kg/m <sup>3</sup> )	2500	2500	2500	2500	2500	2500
Modulus of Elasticity, $E_p$ ( GPa )	18.5	18.5	18.5	18.5	18.5	18.5
L/d	50	31	21	12	7	5

The considered analyses with the PILES software are: 2 pile groups (one for each bridge) and 3 sets of pile configurations per group, 5x5, 3x3, 2x2, (same soil profile, with  $E_p/E_s = 300$ ,  $\rho_s/\rho_p = 0.7$  and  $s/d = 2.5, 5$  and  $10$ .) Figures 7, 8, and 9 present the dynamic impedances of Bridge I for the three sets of pile configuration. The stiffnesses are presented as functions of the dimensionless frequency of excitation  $a_o = \omega d/V_s$ , where  $\omega$  is the frequency of the harmonic excitation (or of the seismic event),  $d$  is the diameter of each pile and  $V_s$  is the S-wave velocity of the soil profile. The parameters  $K_{xx}$  and  $\omega C_{xx}$  are respectively the real and the imaginary parts of the horizontal dynamic stiffness of the pile group,  $K_{xx}$ , which are related to bending.

The values of the parameter  $a_o$  were picked so as to be representative of the range of interest. Specifically, for a range of excitation's periods  $T = 0.25 - 2$  secs and a mean value of shear wave velocity  $V_s = 200$  m/sec and diameter  $d = 1$  m, the  $a_o$  parameter takes the value of 0.25. This study focuses to values up to 1, which is considered as an upper limit of the values of interest.

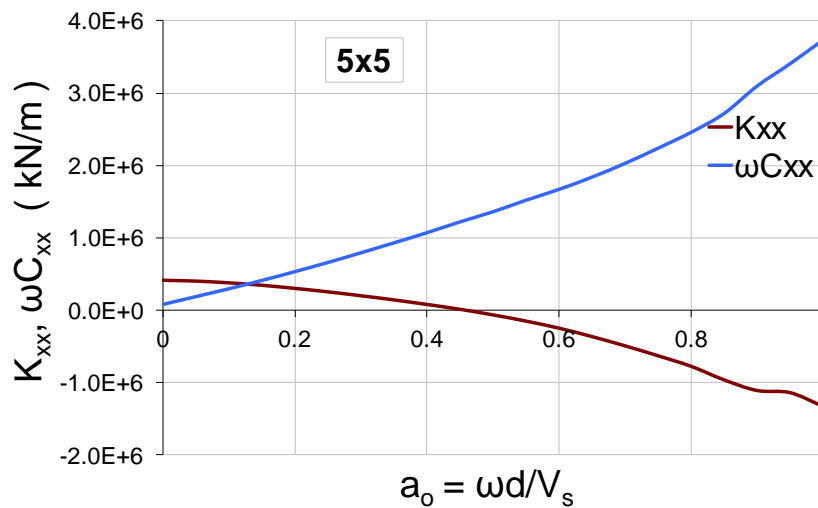


Figure 7.  $K_{xx}$ , of the 5x5 pile group, Bridge I.

As the number of the piles decreases, the horizontal dynamic stiffnesses tend to appear less variation through the frequency range. Specifically, the real part that corresponds to spring stiffnesses is getting smaller values as the frequency of the excitation moves towards  $a_o=1$  ( $a_o=1 \rightarrow \omega = 110 - 260$  rad/sec  $\rightarrow T = 0.05 - 0.02$  sec, depending on  $d$ ). The opposite is happening at the imaginary part, which represents the damping of the system.

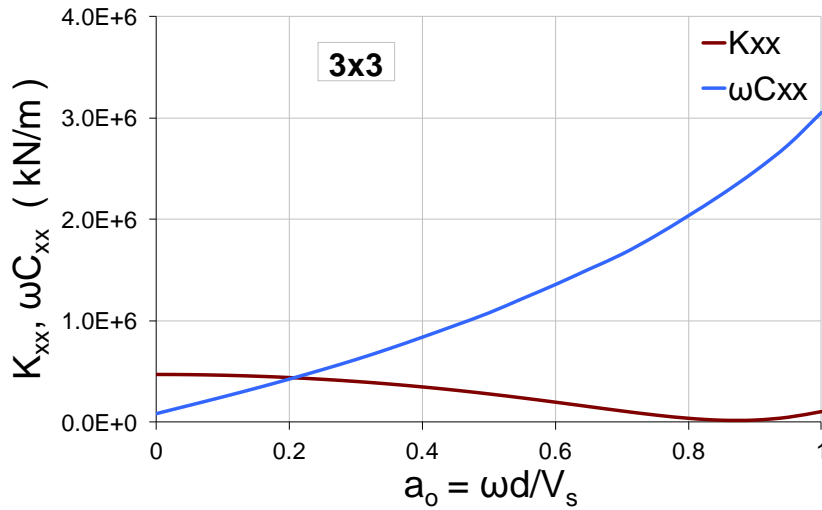


Figure 8.  $K_{xx}$ , of an equivalent to the 5x5 pile group in Figure 7, 3x3 pile group, Bridge I.

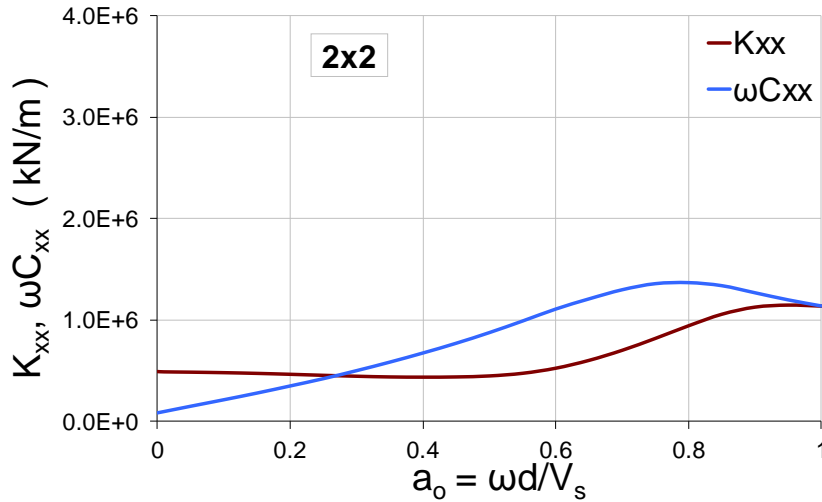


Figure 9.  $K_{xx}$ , of an equivalent to the 5x5 pile group in Figure 20, 2x2 pile group, Bridge I.

Figures 10 and 11 are comparing the impedances of the 3 pile groups. It is useful to observe the above conclusions in dimensionless figures, where the dynamic stiffnesses of the groups are compared with the static stiffnesses of the single piles:

$$\frac{K_{xx}}{N * K_{x,single}(a_o = 0)} \tag{5}$$

$$\frac{\omega C_{xx}}{N * K_{x,single}(a_o = 0)} \tag{6}$$

where  $K_{xx}$ ,  $\omega C_{xx}$  are the two parts of the bending dynamic stiffnesses,  $N$  is the number of the piles and  $K_{x, \text{single}}$  is the static bending stiffness of the single pile (see *Table 3*). *Figures 12* and *13* are showing the dimensionless impedances of *Figures 9* and *10*. The imaginary part is additionally divided by dimensionless coefficient  $a_o$ .

**Table 3. Single pile static stiffnesses.**

$E_p=18.50$ GPa	Bridge I			Bridge II		
Pile Group Label	5x5 (d=0.43m)	3x3 (d=0.70m)	2x2 (d=1m)	5x5 (d=1.8m)	3x3 (d=3m)	2x2 (d=4.5m)
Single Pile Static Stiffness (kN/m)	$9.02 \times 10^4$	$1.46 \times 10^5$	$2.08 \times 10^5$	$3.77 \times 10^5$	$6.22 \times 10^5$	$9.06 \times 10^5$

Concerning the rocking dynamic impedances,  $K_{rr}$  and  $\omega C_{rr}$  (real and the imaginary parts of the rotational dynamic stiffness of the pile group,  $K_{rr}$ ), are presented in *Figures 14, 15 and 16*, while *Figures 17 and 18* compare the values of  $K_{rr}$  and  $\omega C_{rr}$  for the three pile group configurations for the Bridge I. Presenting the same results for dimensionless rocking impedances, in *Figures 18 and 19*, the normalization follows the Equations (7) and (8).

$$\frac{K_{rr}}{N * \sum(x_i^2 * K_{x, \text{single}}(a_o = 0))} \tag{7}$$

$$\frac{\omega C_{rr}}{N * \sum(x_i^2 * K_{x, \text{single}}(a_o = 0))} \tag{8}$$

where  $N$  is the number of piles,  $x_i$  is the horizontal distance of each pile from the basic coordinate system of the pile group and  $K_{x, \text{single}}$  is the static stiffness related with bending of each pile (see *Table 3*).

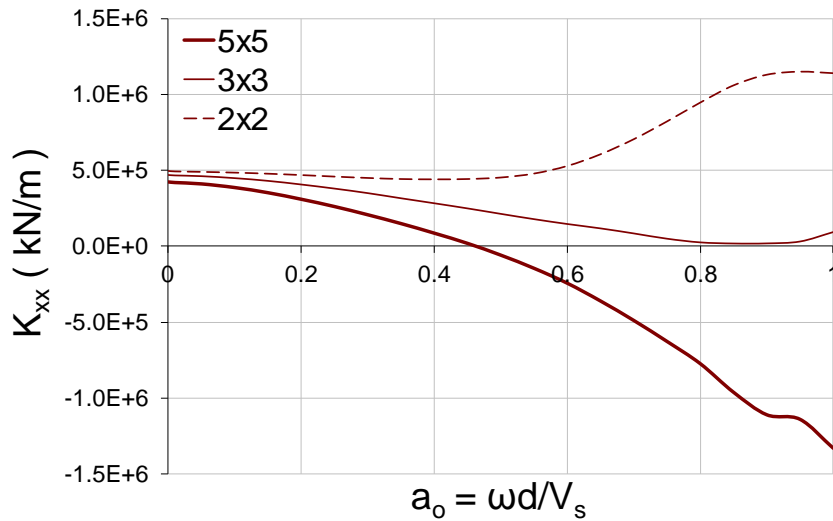


Figure 10. Comparison of the stiffnesses,  $K_{xx}(\omega)$ , of 5x5, 3x3 and 2x2 pile groups, Bridge I.

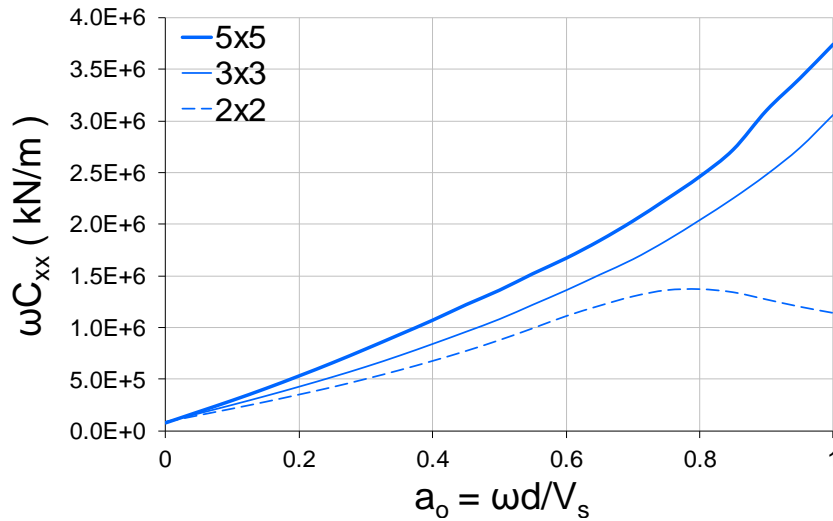


Figure 11. Comparison of the dampings,  $\omega C_{xx}(\omega)$ , of 5x5, 3x3 and 2x2 pile groups, Bridge I.

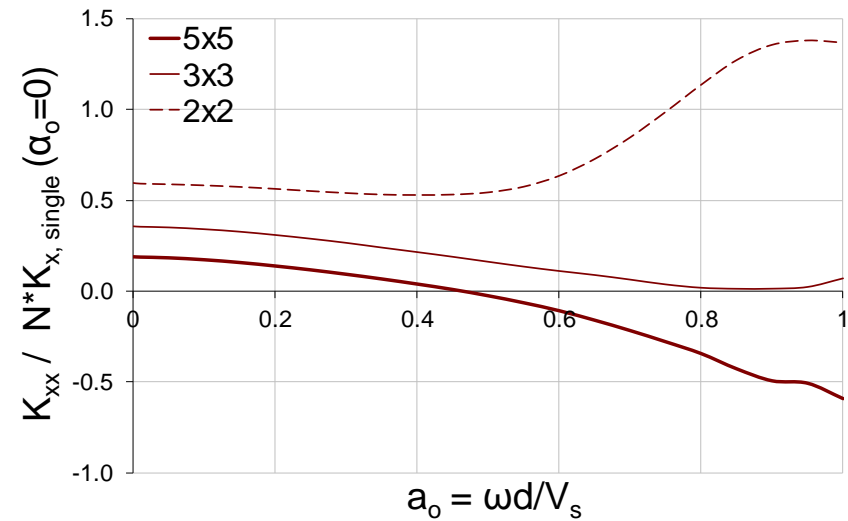


Figure 12. Dimensionless real parts of the bending dynamic impedances,  $K_{xx}(\omega)$ , Bridge I.

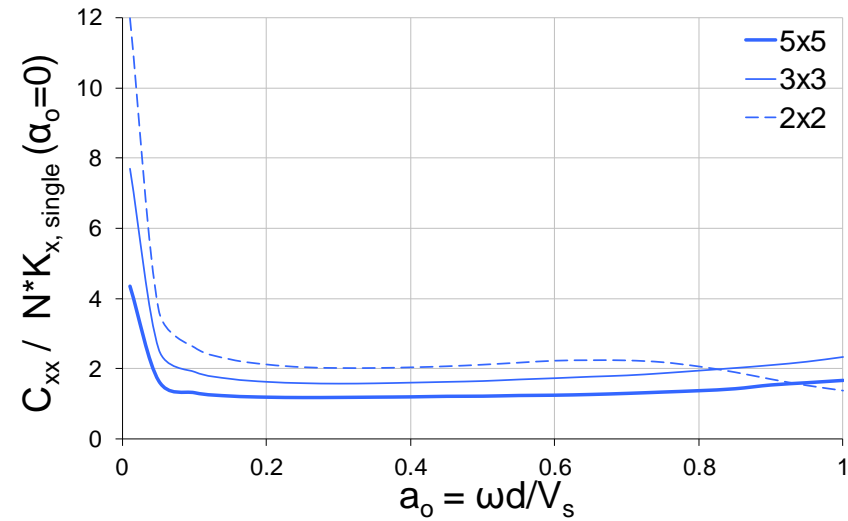


Figure 13. Dimensionless imaginary parts of the bending dynamic impedances,  $\omega C_{xx}(\omega)$ , additionally divided by  $a_0$ , Bridge I.

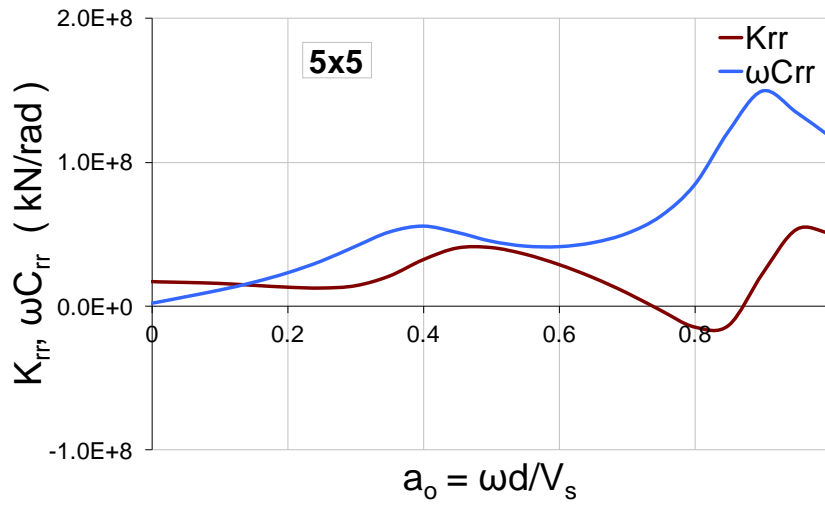


Figure 14.  $K_{rr}$ , of the 5x5 pile group, Bridge I.

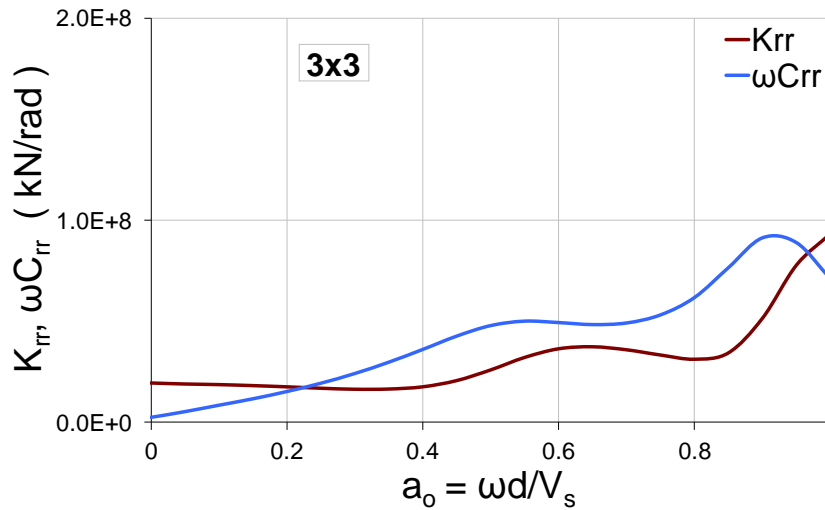


Figure 15.  $K_{rr}$ , of an equivalent to the 5x5 pile group in Figure 14, 3x3 pile group, Bridge I.

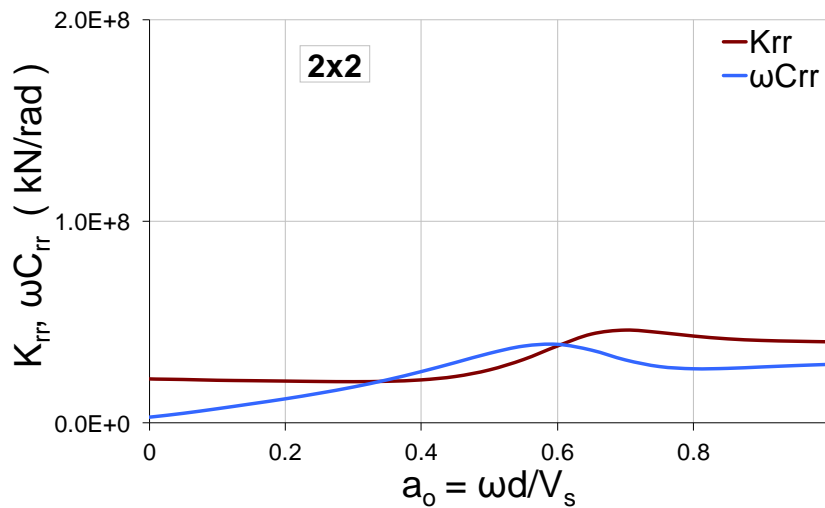


Figure 16.  $K_{rr}$ , of an equivalent to the 5x5 pile group in Figure 14, 2x2 pile group, Bridge I.

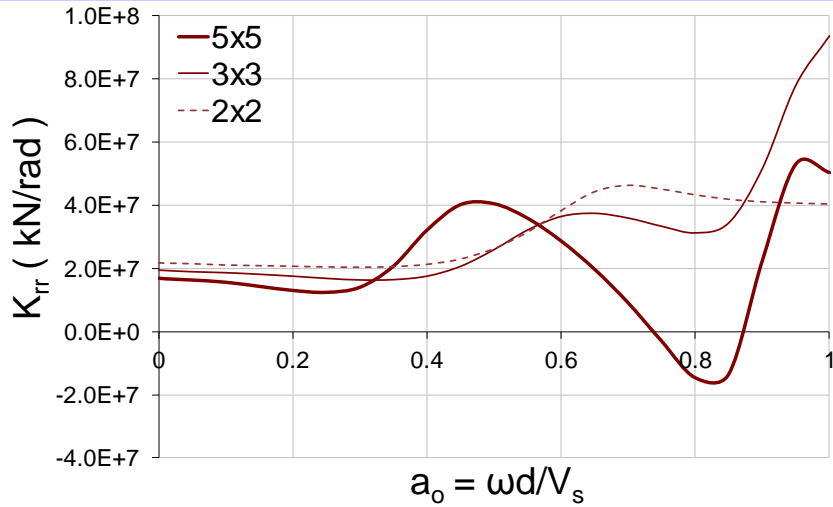


Figure 17. Comparison of the stiffnesses,  $K_{rr}(\omega)$ , of 5x5, 3x3 and 2x2 pile groups, Bridge I.

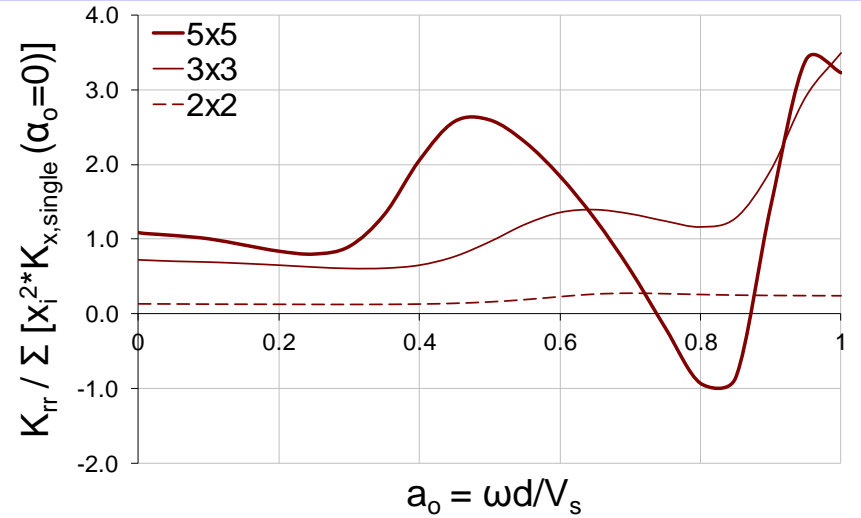


Figure 19. Dimensionless real parts of the rocking dynamic impedances,  $K_{rr}(\omega)$ , Bridge I.

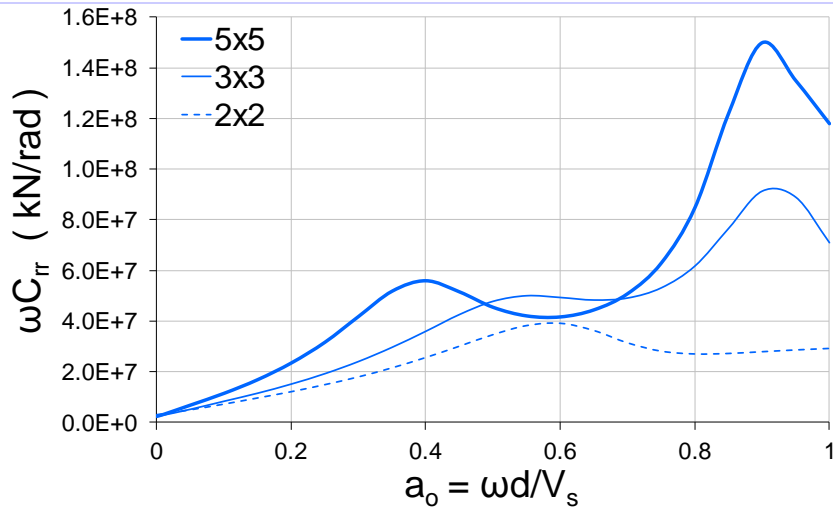


Figure 18. Comparison of the dynamic impedances,  $\omega C_{rr}(\omega)$ , of 5x5, 3x3 and 2x2 pile groups, Bridge I.

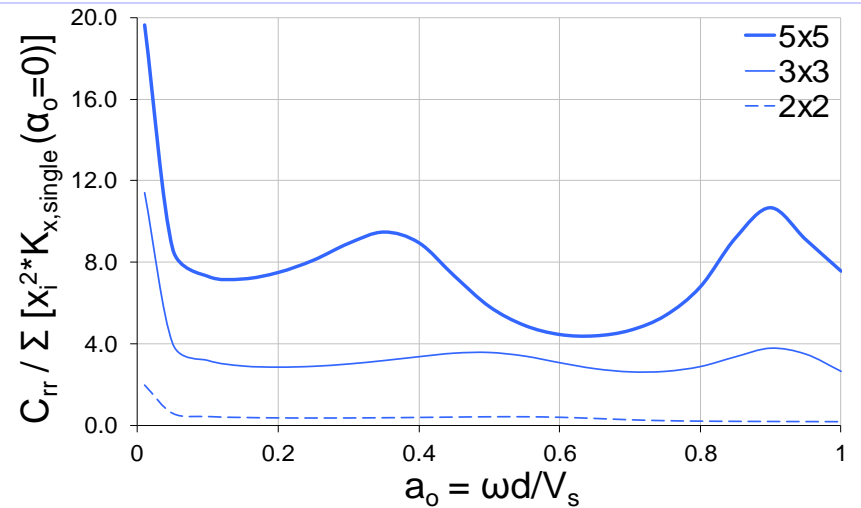


Figure 20. Dimensionless imaginary parts of the rocking dynamic impedances,  $\omega C_{rr}(\omega)$ , additionally divided by  $a_0$ , Bridge I.

Rocking oscillations are not in general independent of the bending response. Considering the effect of the coupling is beyond the scope of this study, however they coupling stiffnesses are presented here in for completeness. The coupled bending-rocking impedances ( $K_{rx}$ ,  $\omega C_{rx}$ ) are also obtained from PILES and are presented in the next figures.

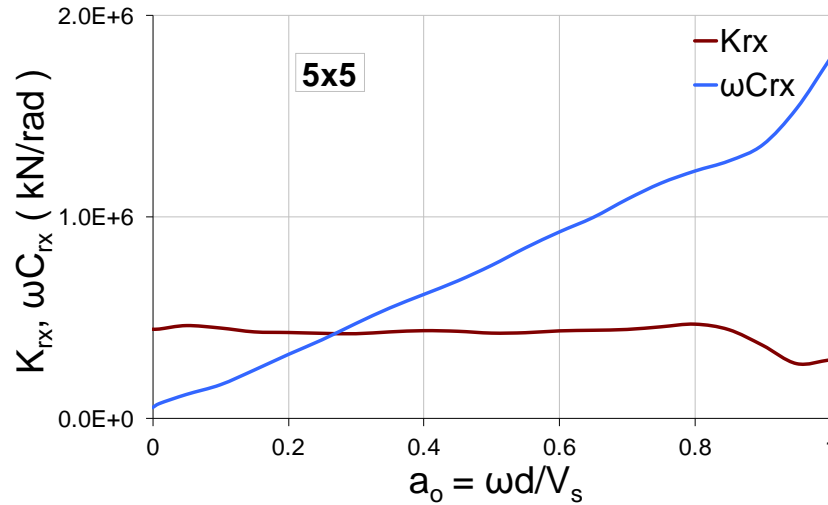


Figure 21.  $K_{rx}$ , of the 5x5 pile group, Bridge I.

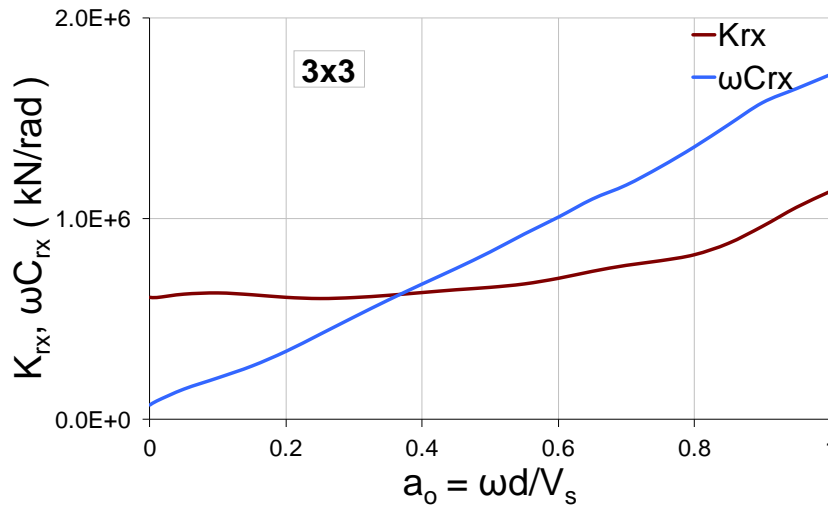


Figure 22.  $K_{rx}$ , of an equivalent to the 5x5 pile group in Figure 20, 3x3 pile group, Bridge I.

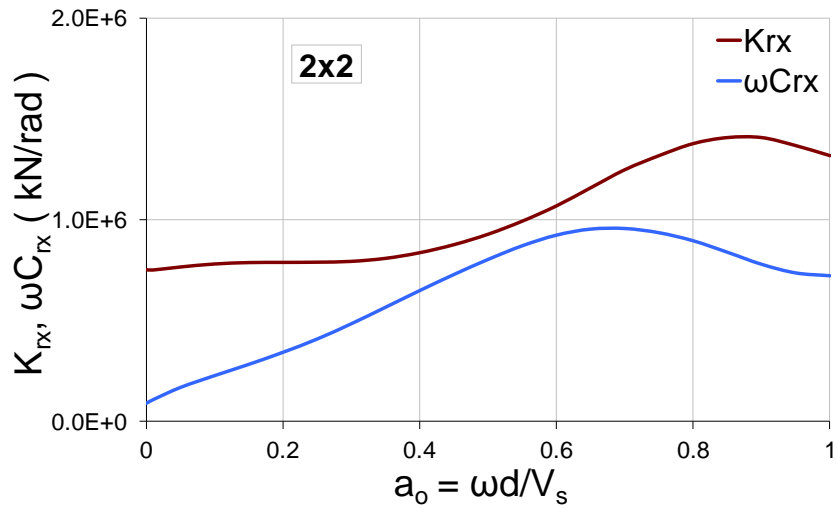


Figure 23.  $K_{rx}$ , of an equivalent to the 5x5 pile group in Figure 20, 2x2 pile group, Bridge I.

A general but significant comment applicable to all the presented figures above is that the values of the stiffness and damping of the soil-foundation systems considered here in, may greatly differ depending on the frequency of the (seismic) excitation. The next figures (Figures 24-30) present the dynamic impedances of the considered pile groups for Bridge II. The impedances are expected to reach larger values and may vary much more through the frequency range of interest.

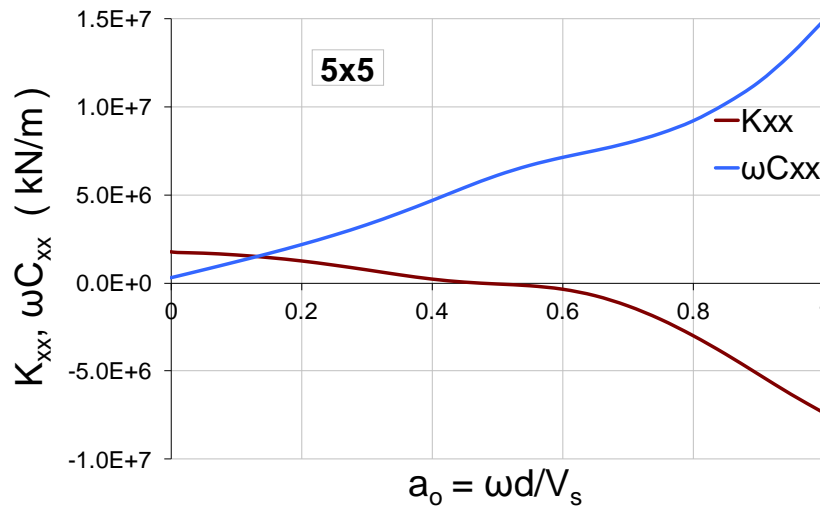


Figure 24.  $K_{xx}$ , of the 5x5 pile group, Bridge II.

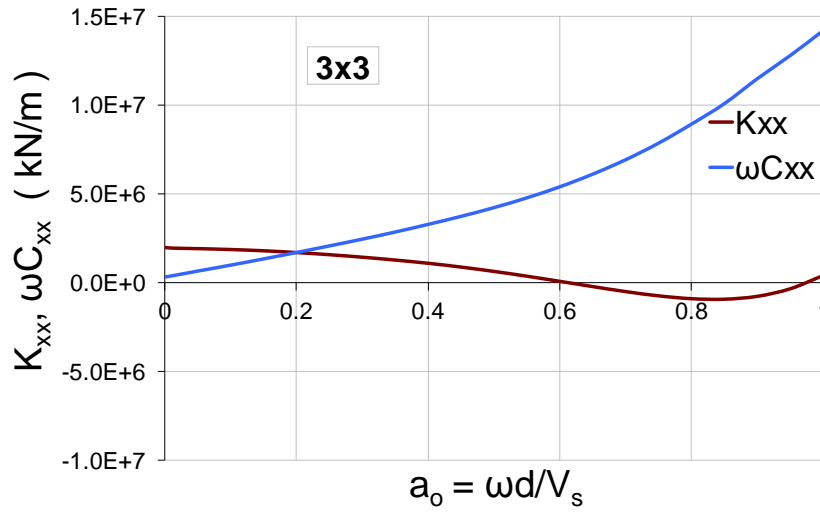


Figure 25.  $K_{xx}$ , of an equivalent to the 5x5 pile group in Figure 24, 3x3 pile group, Bridge II.

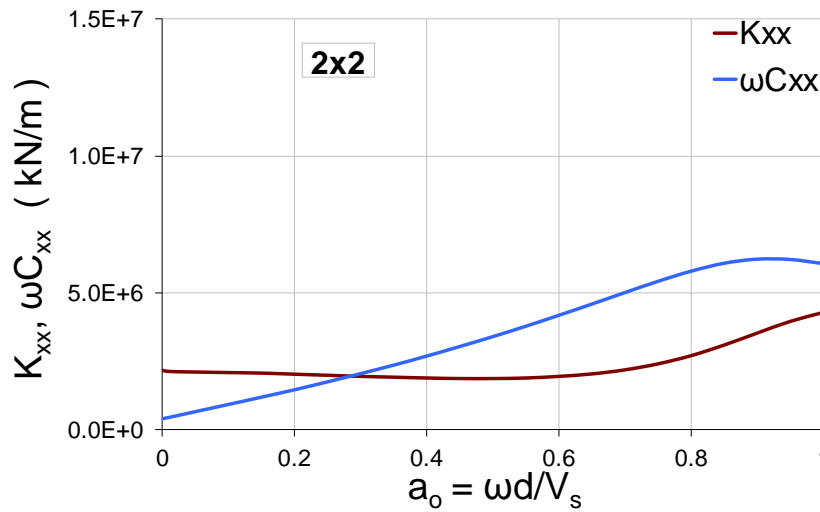


Figure 26.  $K_{xx}$ , of an equivalent to the 5x5 pile group in Figure 23, 2x2 pile group, Bridge II.

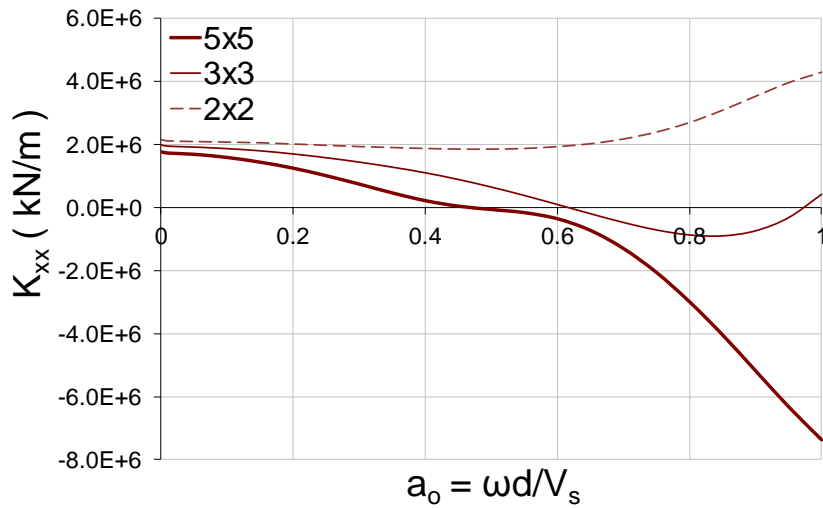


Figure 27. Comparison of the stiffnesses,  $K_{xx}(\omega)$ , of 5x5, 3x3 and 2x2 pile groups, Bridge II.

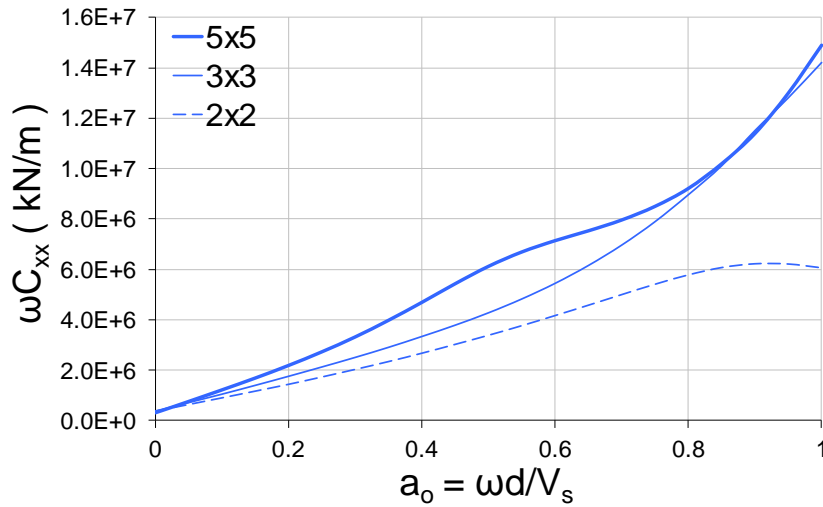


Figure 28. Comparison of the dampings,  $\omega C_{xx}(\omega)$ , of 5x5, 3x3 and 2x2 pile groups, Bridge II.

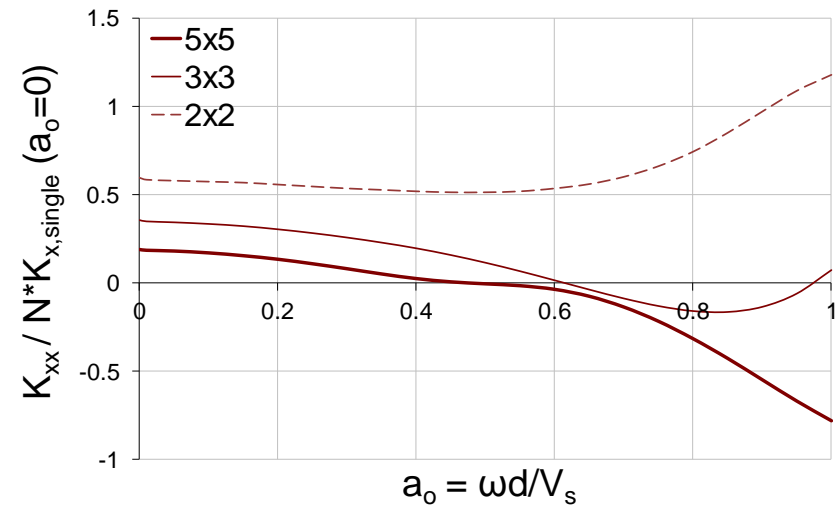


Figure 29. Dimensionless real parts of the bending dynamic impedances,  $K_{xx}(\omega)$ , Bridge II.

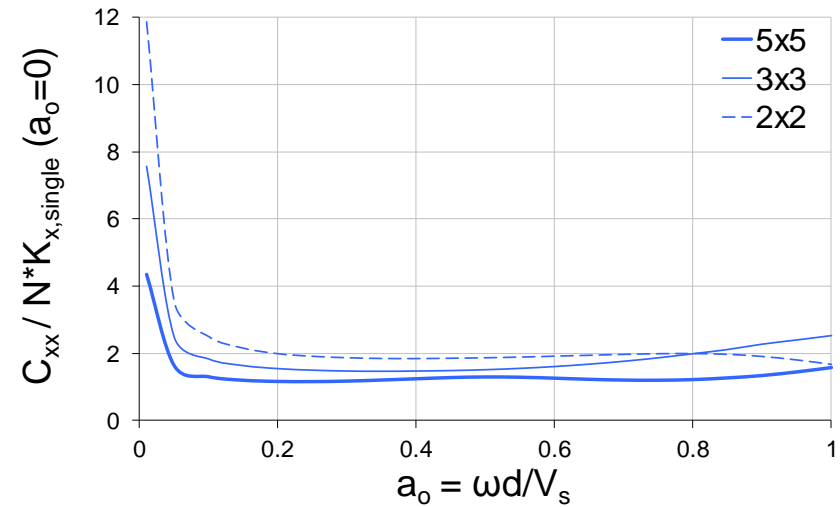


Figure 30. Dimensionless imaginary parts of the rocking dynamic impedances,  $\omega C_{xx}(\omega)$ , additionally divided by  $a_0$ , Bridge II.

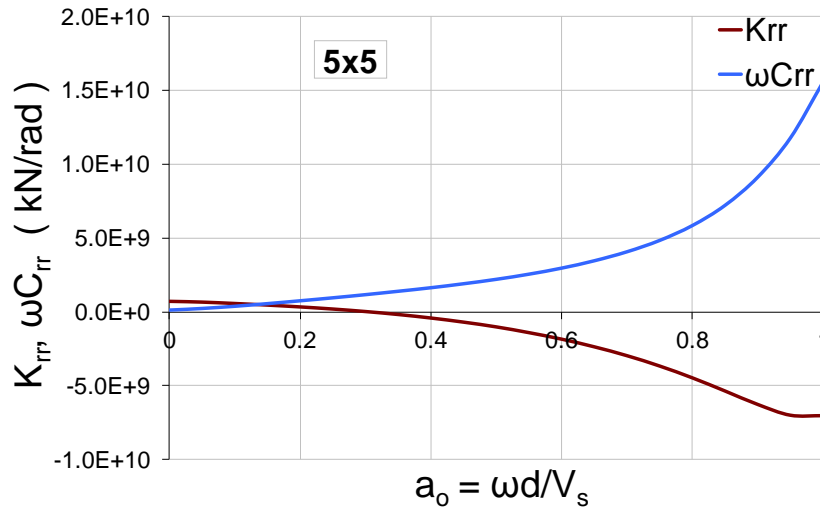


Figure 31.  $K_{rr}$ , of the 5x5 pile group, Bridge II.

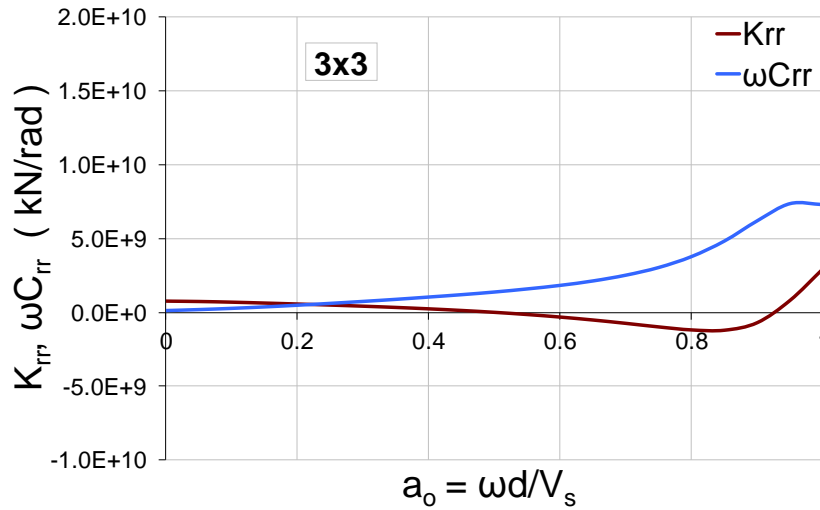


Figure 32.  $K_{rr}$ , of an equivalent to the 5x5 pile group in Figure 31, 3x3 pile group, Bridge II.

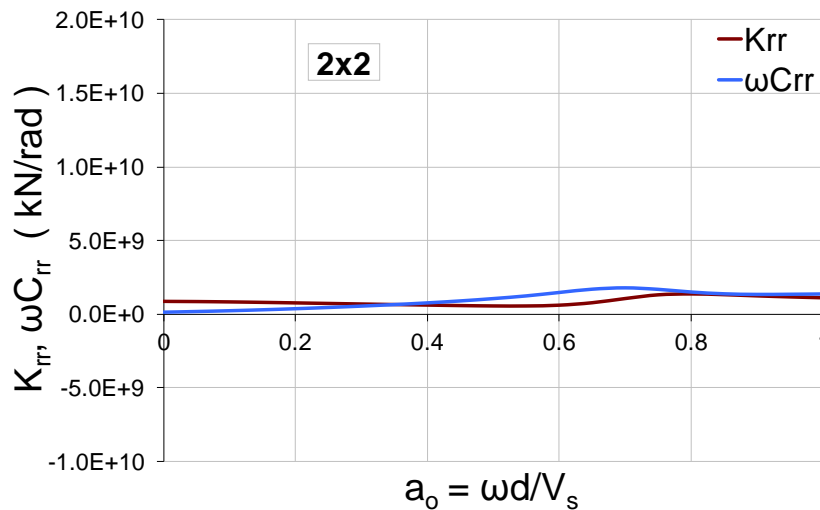


Figure 33.  $K_{rr}$ , of an equivalent to the 5x5 pile group in Figure 31, 2x2 pile group, Bridge II.

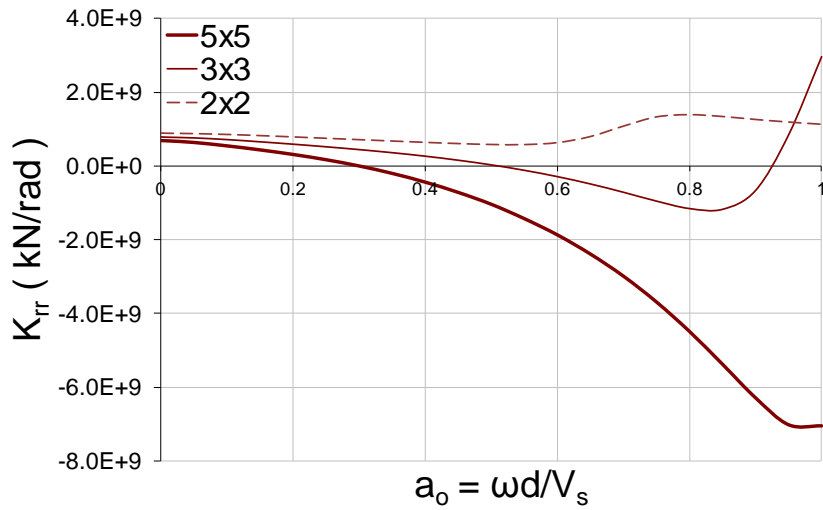


Figure 34. Comparison of the stiffnesses,  $K_{rr}(\omega)$ , of 5x5, 3x3 and 2x2 pile groups, Bridge II.

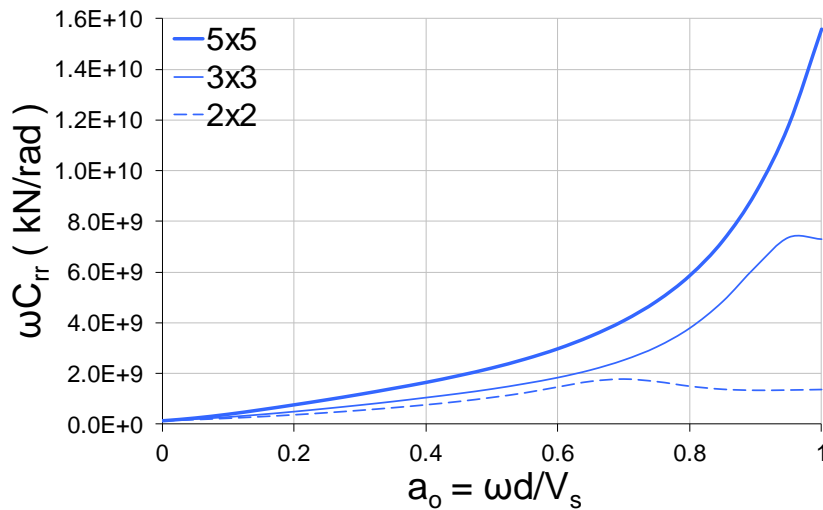


Figure 35. Comparison of the dynamic impedances,  $\omega C_{rr}$ , of 5x5, 3x3 and 2x2 pile groups, Bridge II.

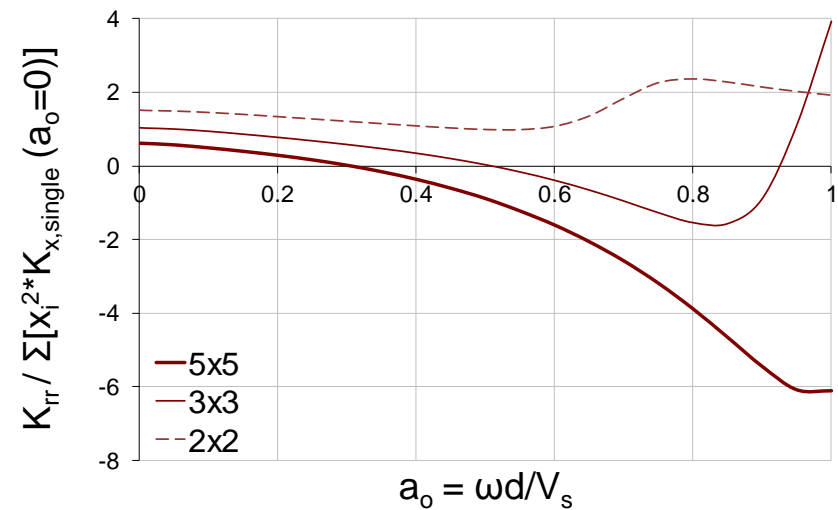


Figure 36. Dimensionless real parts of the rocking dynamic impedances,  $K_{rr}(\omega)$ , Bridge II.

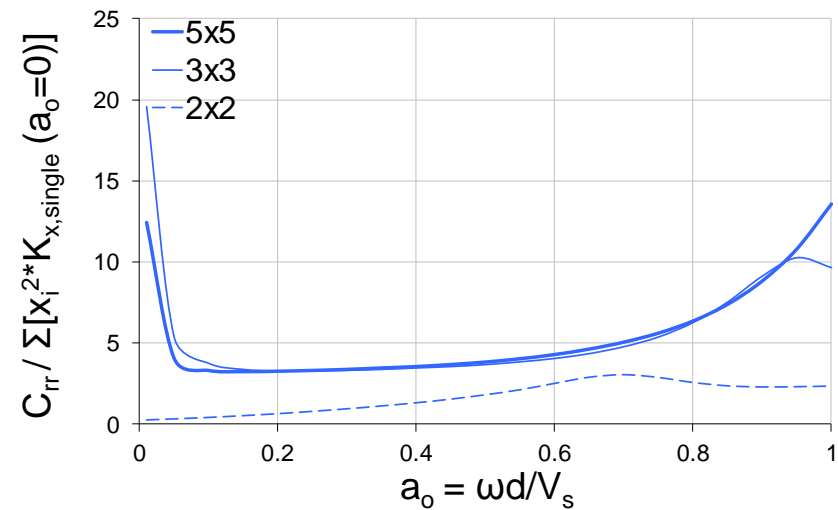


Figure 37. Dimensionless imaginary parts of the rocking dynamic impedances,  $\omega C_{rr}(\omega)$ , additionally divided by  $a_o$ , Bridge II.

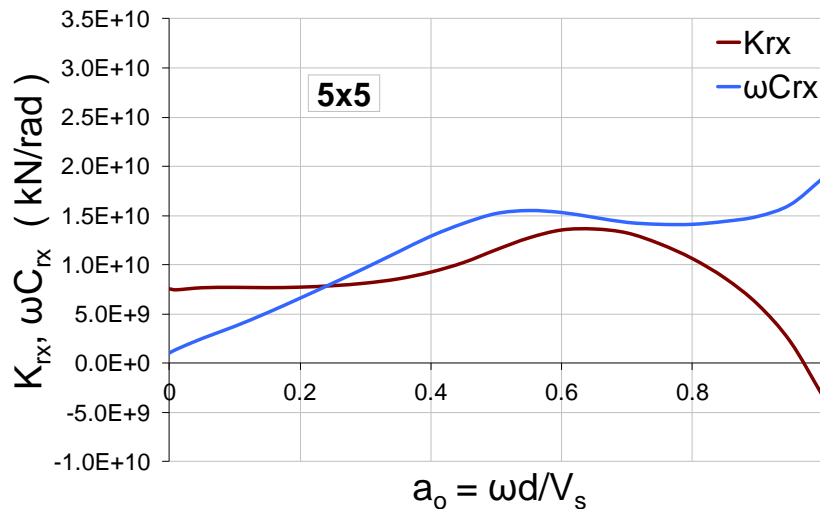


Figure 38.  $K_{rx}$ , of the 5x5 pile group, Bridge II.

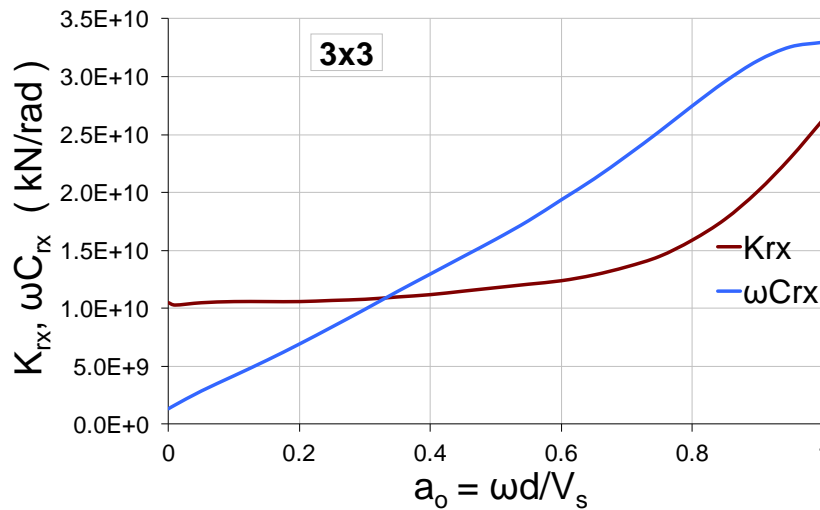


Figure 39.  $K_{rx}$ , of an equivalent to the 5x5 pile group in Figure 38, 3x3 pile group, Bridge II.

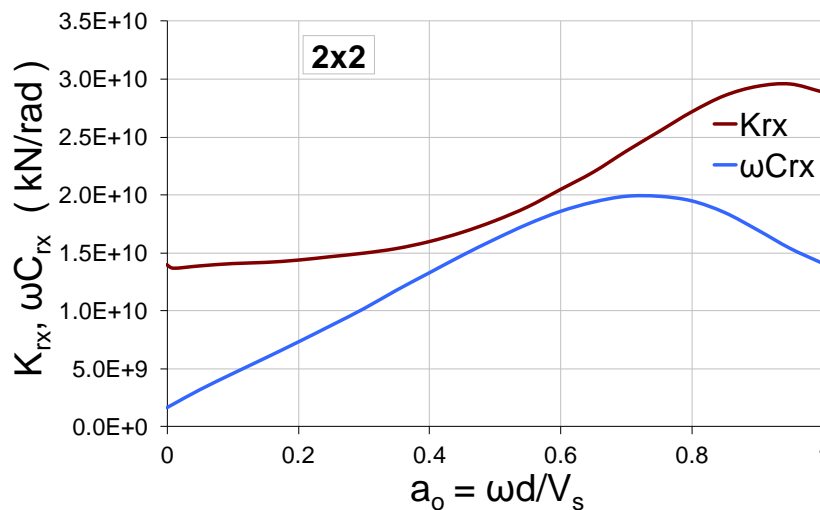
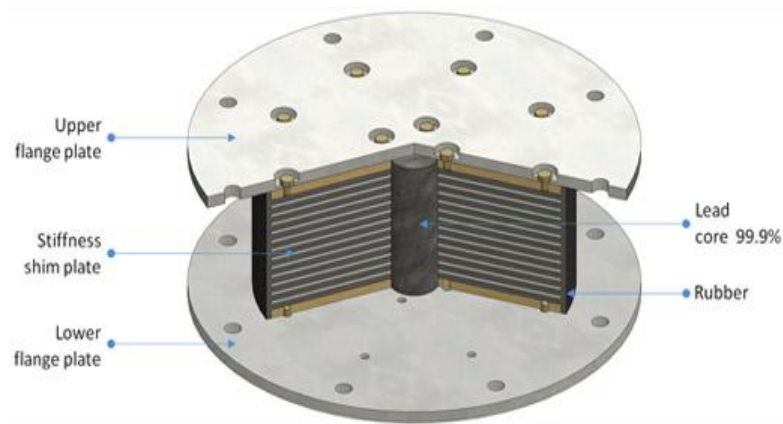


Figure 40.  $K_{rx}$ , of an equivalent to the 5x5 pile group in Figure 38, 2x2 pile group, Bridge II.

## 2.2. Seismic Isolation System

Seismic isolation is a powerful “technique” of mitigating earthquake hazard. It is meant to enable a building or non-building structure to survive a potentially devastating seismic event with minimal or no damage. In other words the isolation system which stands instead of a monolithic connection between the deck and the pier, decouples them and offers a kind of movement independency. As a result the seismic forces who “travel” through the foundation to the pier never reach the deck with their initial strength and characteristics, due to the energy reflection at the point of the isolation system and dissipation that takes place through the travel path.

The seismic isolation system of this study is considered to behave as a bilinear hysteretic spring with smooth elastic to post yielding transition. Such a behavior could be representative of typical lead rubber bearings, as well as of sliding bearings with metallic yielding devices or restoring force capability.



**Figure 41. Typical lead rubber bearing's components.**

Lead Rubber Bearing or LRB is a type of system which is employing heavy damping. It was invented in New Zealand (Robinson et al. 1974). *Figure 41* demonstrates the components of a typical LRB. Heavy damping mechanism incorporated in vibration control technologies and, particularly, in base isolation devices, is often considered a valuable source of suppressing vibrations thus enhancing a building's seismic performance.

Seismic isolation using sliding bearings has been recognized as one of practical and effective technologies for seismic protection of structural systems. In practice, a typical

sliding isolator usually consists of a sliding interface to uncouple the ground motion from the structure, and also a restoring force mechanism to reduce the residual isolator displacement.



Figure 42. Lead Rubber Bearing (LRB).

A friction pendulum system (FPS) is one of widely used sliding isolation systems and has been implemented in many existing structures. For a FPS isolator, the shape of the sliding interface is made spherical, so that the structure gravitational load applied on the slider will provide a restoring stiffness for the isolated structure to return to its original position after an earthquake (*Figure 43*).

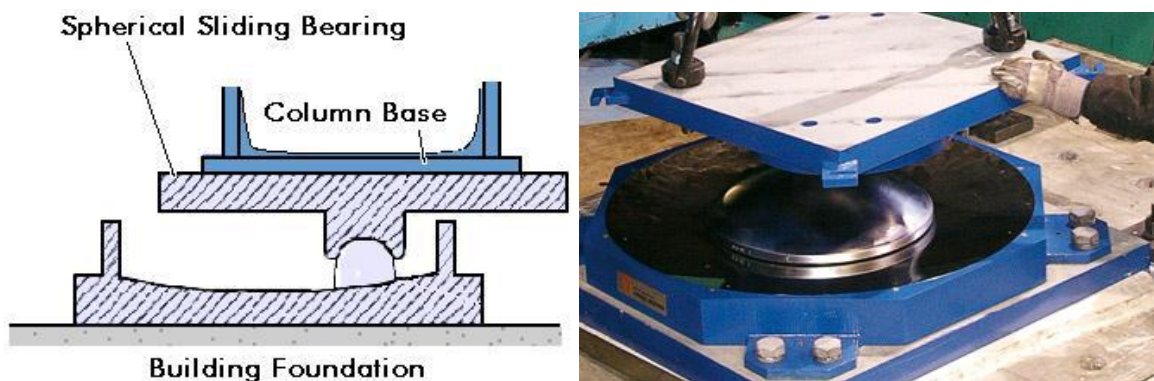


Figure 43. Friction Pendulum sliding bearing.

The friction pendulum system (FPS) has been implemented in many structures around the world. For an FPS isolator, the shape of the sliding interface is made

spherical, so that the structure gravitational load applied on the slider will provide a restoring force (stiffness) for the isolated structure to return to its original position after an earthquake (Figure 43). However, this stiffness will inevitably introduce an extra natural frequency, called isolation frequency, to the structural system. The isolation frequency of an FPS system depends on the radius of curvature of the spherical sliding surface. Therefore, FPS systems become sensitive to the frequency content of ground excitations in the vicinity to the isolation system frequency. Some studies have shown that when a structure isolated by an FPS is subjected to a ground motion with near-fault characteristics, the base displacement and the structural acceleration may be considerably amplified due to the long-period pulse - like wave component possessed in most near-fault earthquakes

In this study the isolation system is placed between the deck and the pier and not the foundation from the superstructure. Its nonlinear hysteretic behavior was modeled using a model proposed by Ozdemir (1976). Ozdemir's model suggests that a Maxwell model can be generalized with a nonlinear dashpot, which in the limit leads to an elastoplastic model (Figure 44). This is achieved by expressing mathematically the behavior of a viscoplastic system, after determining the equation of motion of Maxwell's model, with a back stress to control the postyielding behavior. The variables that particularly control the system are the yield strength ( $F_y$ ), the elastic stiffness ( $K_e$ ) and the postyielding stiffness ( $K_b$ ). The values of these parameters are those who determine the final performance of the isolation system which influences the whole structure. There are design philosophies which call for large  $K_b$  stiffness, in order to limit the displacement response, while others call for low so as to protect the bridge piers from large shear forces. The values used in this study are defined at the next paragraph.

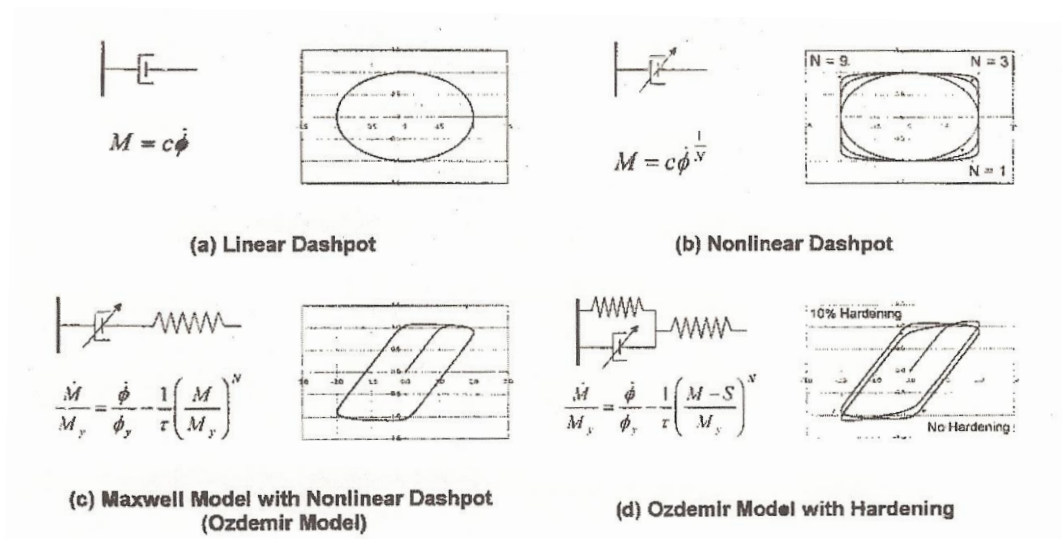


Figure 44. Development of Ozdemir's model.

### 2.3. Bridge Systems

Two bridge structures are considered in this study. The first (**Bridge I**) is representative of a typical highway overcrossing with a stiff short pier, while the second one (**Bridge II**) could be part of a long multispan bridge with flexible tall piers. *Figure 45* depicts the geometric characteristics of each bridge. The dynamic impedances of the 5x5 pile groups for both bridges were presented in §2.1.

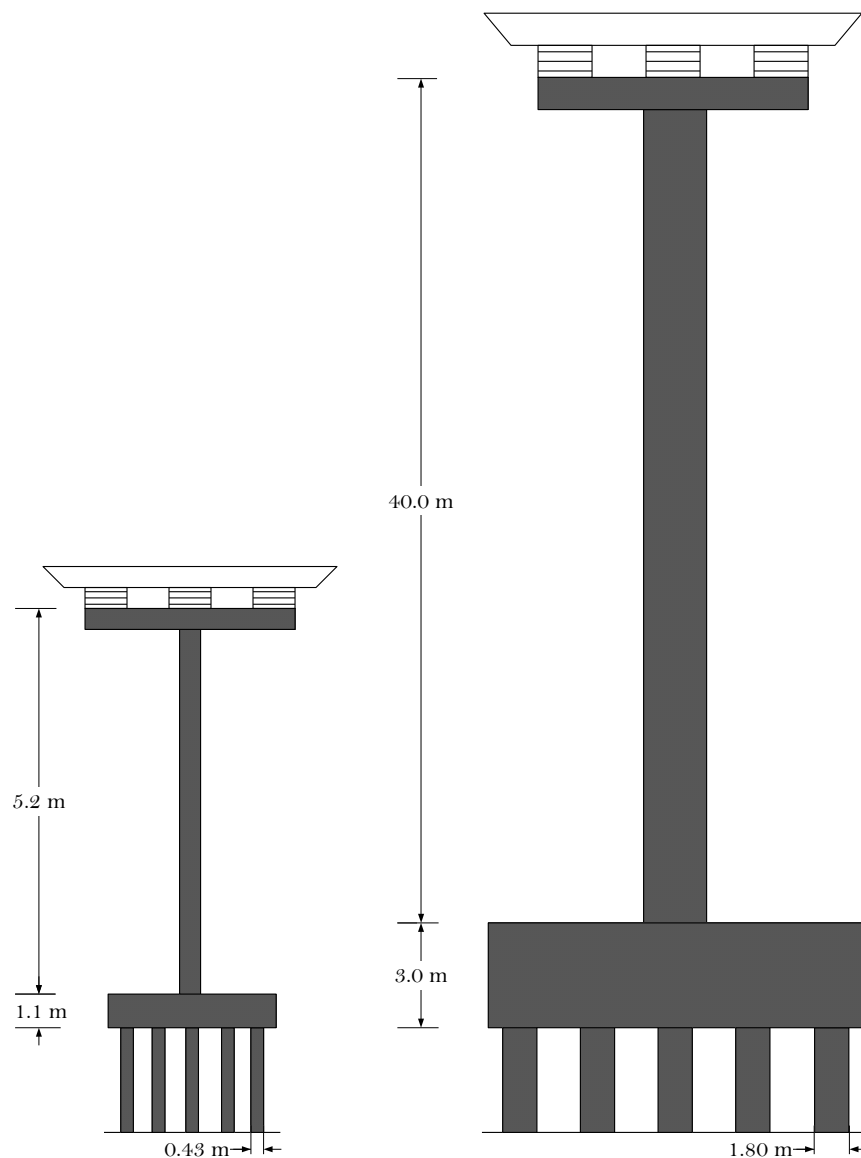
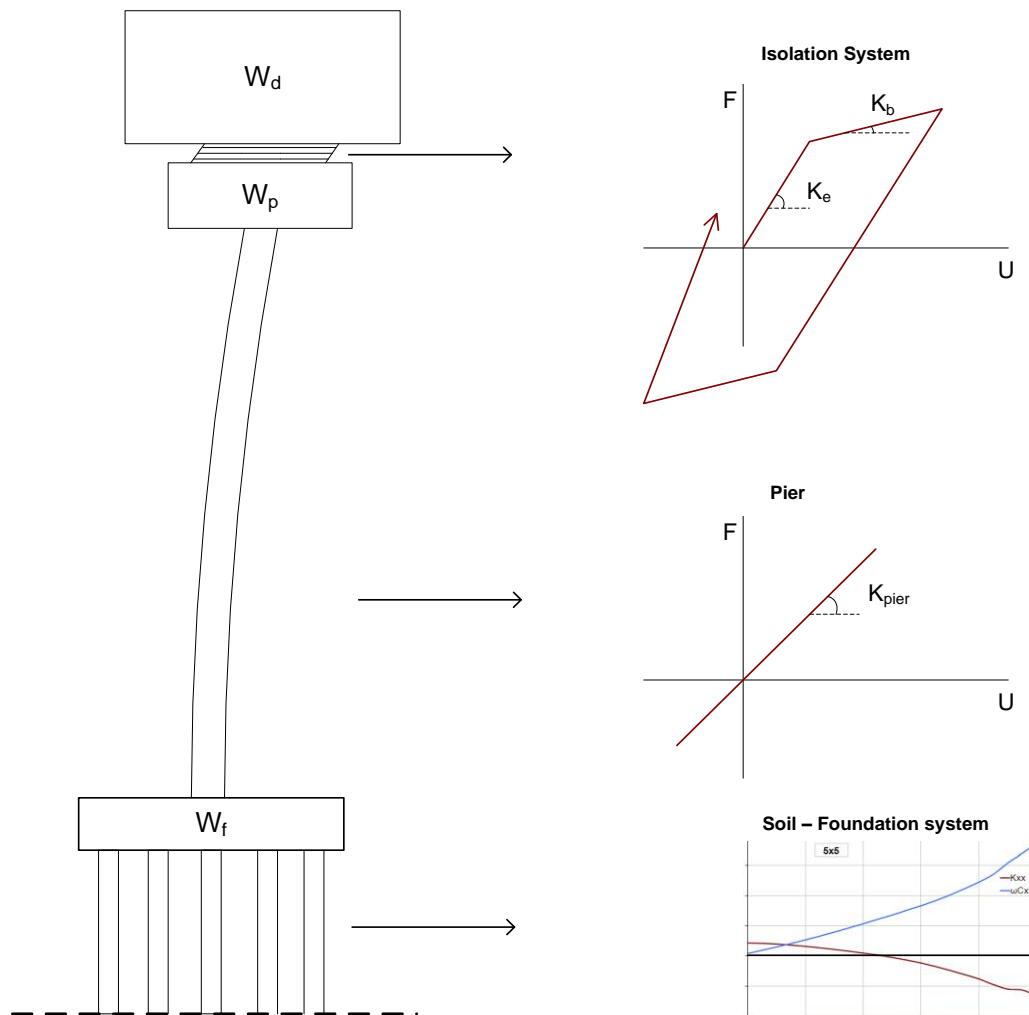


Figure 45. Geometrical representation of Bridge I and Bridge II.

The bridge models consist of a single linear pier (no yield considered), at the top of which the bilinear isolation system carries the deck's weight. At the bottom, the pier is monolithically connected to the pile group cap. The mass of the deck, the pier and the foundation are considered concentrated at a point on their top. The above assumptions get on well with the conventional design methods of large structures including seismic isolation, according to the Eurocode 2 and other codes provisions. The aforementioned characteristics are schematically presented in *Figure 46*.



**Figure 46. Stick model and the behavior of its parts.**

The pile caps are supported by a 5x5 pile group (in this figure), with pile spacing ( $S$ ) 2.5 times the pile diameter ( $d$ ) (see also *Figure 5*). The pile diameters were considered different for the two bridges, due to the different dimensions of the superstructures ( $d_1 = 0.43$  m,  $d_2 = 1.80$  m). The models are also analyzed with the

equivalent  $2 \times 2$  and  $3 \times 3$  pile groups which were presented previously. The diameter of each pile in the groups is adjusted in such a way as the total area of the pile groups ( $m^2$ ) to be the same in all three cases,  $5 \times 5$ ,  $3 \times 3$ , and  $2 \times 2$  in an attempt to retain approximately the same stiffness and damping constants for zero frequency in all three cases.

The non linear time history analyses for both bridges were performed without considering any cracked section (reduction of cross sectional area). Such consideration doesn't represent the real condition of a constructed bridge, but was chosen herein since this is a parametric study looking at the possible effects of SSI on seismic isolated bridges and not the analysis and design of a particular structure. *Table 4* presents the characteristics of the bridge models considered in the analyses.

**Table 4. Properties of the bridge models considered.**

Bridge model	Bridge I	Bridge II
Deck seismic weight, $m_d$ ( Mg )	265	1440
Isolation system period, $T_b$ ( sec )	2	4.5
Isolation strength ratio ( $F_y / W_d$ )	0.12	0.04
Pier seismic weight, $m_p$ ( Mg )	38.5	620
Pier weight/ Deck weight	0.15	0.43
Pier height, $h$ ( m )	5.2	40
Pier elastic stiffness, $k_p$ ( kN/m )	1.24E5	1.09E5
Pier damping ratio, $\xi$	5%	5%
Foundation seismic weight, $m_f$ ( Mg )	84	4248
Foundation moment of inertia, $I_f$ ( Mg $m^2$ )	173	126200
Pile cup height, $H_f$ ( m )	1.1	3

# 3

## Computational modeling

### 3.1. Computational Modeling of the Soil-Structure Interaction Problem

#### 3.1.1. Spring-Mass-Damper Models to account for SSI

Soil - structure interaction (SSI) problems have been studied for over half a century and as a result engineers have developed a plethora of close-form impedance functions for various soil-foundation systems. Although the analysis of the interaction problem treats the soil-foundation-structure system as many separate subsystems, the compatibility conditions at the interfaces are those guarantee its continuity. In the current work the analyses have developed frequency dependent impedance functions.

The nonlinear behavior of the isolation system prohibits the use of frequency domain analysis techniques to treat the SSI problem. In order to overcome this incompatibility between the frequency dependence of the soil-foundation springs and the requirement for nonlinear time history analysis, it is customary to introduce an approximation omitting the frequency dependency of the soil-foundation system considering that the springs and dashpots have constant, frequency – independent, values corresponding to the values that the impedances take for  $a_0=0$ . This assumption, in the present study is not unreasonable considering the fact that the isolation period, which is fairly large, is expected to dominate the overall seismic response of the bridge. These low excitation frequencies correspond to a range of  $a_0$  between 0 and 0.1 thus effectively the “static” values of the spring and damping coefficients.

The simple **Voigt model**, consisting of a spring and a dashpot, connected to the foundation mass, is the easy solution for modeling the impedance functions, under the aforementioned simplifications. *Figure 47* presents a Voigt model. Although it may be

widely used by engineers simulating SSI effects due to its simplicity, the constant values of its elements make it hard to adjust to frequency-sensitive impedances. *Figure 48* demonstrates the bridge model and the attached Voigt models for horizontal and rotational DOFs. The vertical degree of freedom is not depicted in the picture and will be neglected in this study.

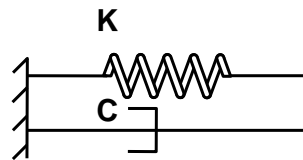


**Figure 47. Voigt model**

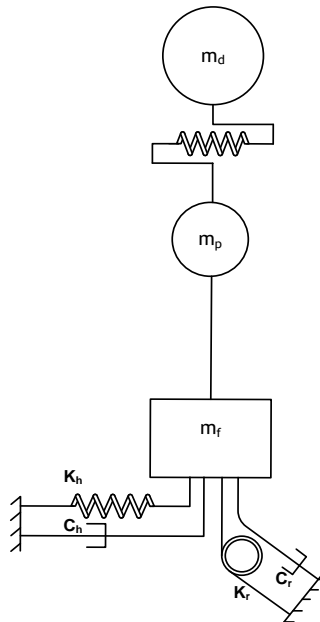


**Figure 48. Bridge model with two Voigt models; one translational and one rotational.**

The constant values of the springs and dashpots in a Voigt models make the analysis easier but are not representing the real behavior of the dynamic impedances (*Figures 7 to 40*). A closer examination of their behavior reveals that they resemble the dynamic stiffness of a simple spring-mass-dashpot system. By introducing a frequency-independent artificial mass, a spring and a dashpot in a foundation system, the time history nonlinear analyses can be easily performed. This is the basis of the procedure used by De Barros and Luco (1990) and Wolf and Somani (1986) where they introduced a spring-mass-damper secondary subsystem attached to the foundation mass with appropriately calibrated parameters to account for the frequency dependent behavior of

the soil-foundation system. Furthermore, more than one such systems could be used, particularly in cases of complicated dynamic impedance functions which have to be modeled. However, such systems alter the dynamics of the soil-foundation-structure system because the additional mass of the secondary system contributes to the inertial forces and moments of the system thus altering the actual input (right hand side of the equations of motion) to the system.

### 3.1.2. The concept of GYROMASS

For the mathematical modeling of the complicated behavior of the soil-foundation interacting with the structure, researchers had to think of a system which would predict precisely the result of such an interaction in the frequency domain while at the same time it can be utilized in time domain analysis without revoking any approximations as with the Voigt system discussed previously. Saitoh (2007) presented a system of basic mechanical elements (springs and dashpots) together with an element named “gyromass” capable of representing frequency dependent impedance functions while eliminating the shortcomings of the models introduced by Luco and others.

The gyromass is a frequency-independent mechanical element which has the same dimension as mass. It is defined as an independent unit generating a reaction force due to the relative acceleration of the nodes between which the gyromass is placed. The mechanical analogy of the gyromass (Figure 49-b) corresponds to a rotational disk and a rod attached to the disk with gears. The mass of the rod is considered negligible. The rod experiences an external force  $F$  and the disk rotates with rotational acceleration  $\ddot{\theta}$ . The relative acceleration of the rod  $\ddot{u}$  with respect to the fixed node at the right hand side is geometrically related to the rotational acceleration  $\ddot{\theta}$ .

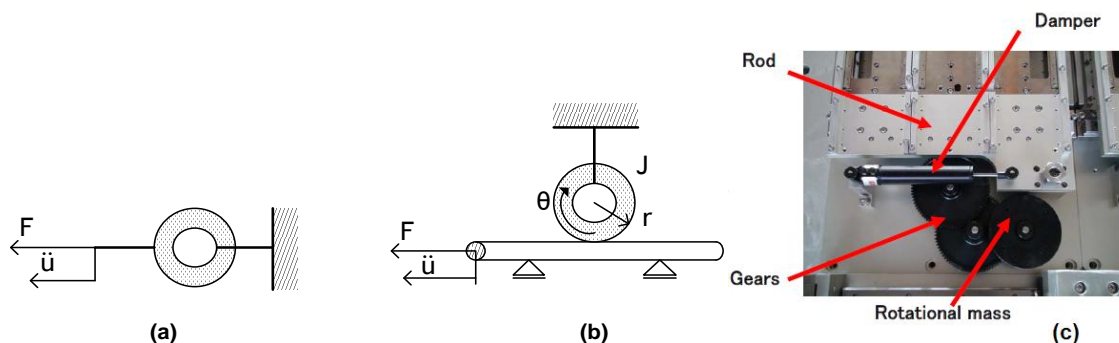


Figure 49. (a) Gyromass system; (b) mechanical analogy ; (c) mechanical system of gyromass.

As a result, the following relation between the external force  $F$  and the relative acceleration  $\ddot{u}$  is obtained:

$$F = \dot{m}\ddot{u} \quad (9)$$

$$\dot{m} = \frac{J}{r^2} \quad (10)$$

where,

$r$  = distance from the center of the disk to the point where the rod is attached,

$J$  = mass moment of inertia of the disk and

$\dot{m}$  = equivalent mass generated by the rotation of the disk.

Thus, the reaction force  $F$  is identical to the product of the equivalent mass  $\dot{m}$  and the relative acceleration  $\ddot{u}$ . The mass  $\dot{m}$  is the aforementioned “gyromass” so as to be distinguished from ordinary masses. The advantage of such an element focuses on its independence from the frequency  $\omega$ .

The model introduced by Saitoh containing springs, dashpots, and gyromasses to achieve better fitting of the dynamic impedances in the frequency domain is the **Type II model** (Figure 50). Type II model evolved from the simpler Type I model (Saitoh, 2007). The Type II model consists of one *base system*, where the spring-dashpot unit and the gyromass are connected in parallel and from two *core systems* where the spring-dashpot unit and the gyromass are connected in series as depicted in *Figure 50*.

The Type II model is a specific combination of base and core systems and is capable of fitting impedance functions with many variables and highly non-linear behavior. Undoubtedly, the Type II model can be generalized, with combinations of three or more core systems so as to optimize the fitting to impedance functions. In this study, the parametric analyses were carried using three different models for the simulation of the SSI effects. These are the:

- a) Voigt model for both translational and rotational degrees of freedom,
- b) Type II model for both translational and rotational DOF (see *Figure 51a*), and
- c) simple Type II model, for only the lateral DOF (see *Figure 52b*).

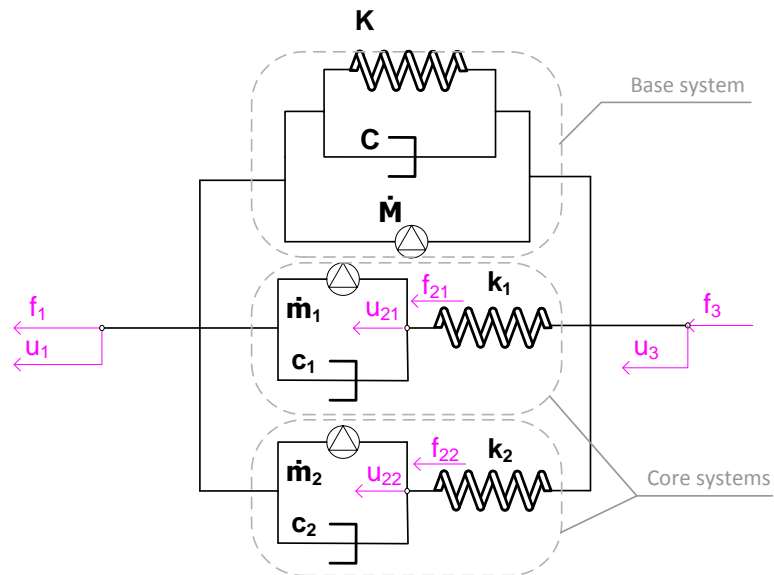


Figure 50. Saitoh's Type II model.

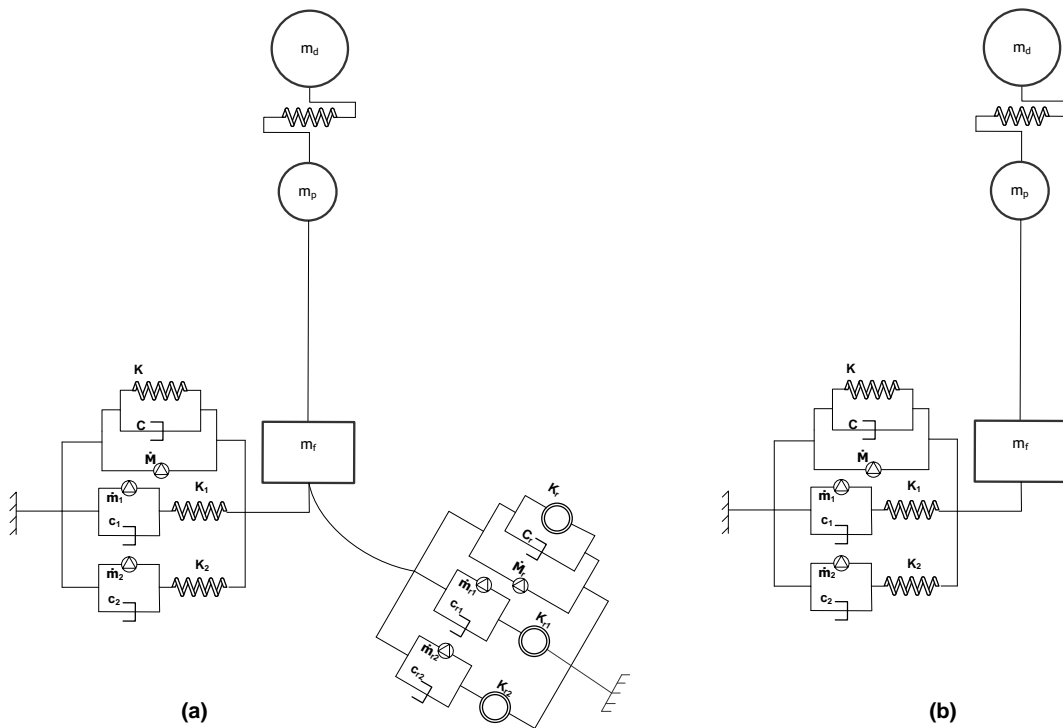


Figure 51. Bridge model with (a) a Type II system on translational and rotational DOFs and (b) simple Type II system (no rotational dof).

The equilibrium equation of a generalized Type II model, for the horizontal dof is:

$$\begin{aligned}
 F_{\text{TYPE II}} = F(a_o) = K \left\{ 1 + \sum_{i=1}^N \frac{\beta_i [\mu_i a_o^2 (\mu_i a_o^2 - 1) + \gamma_i a_o^2]}{(1 - \mu_i a_o^2)^2 + \gamma_i^2 a_o^2} - \mu_o a_o^2 + \right. \\
 \left. + i a_o \left[ \sum_{i=1}^N \frac{\beta_i \gamma_i}{(1 - \mu_i a_o^2)^2 + \gamma_i^2 a_o^2} + \gamma_o \right] \right\} u(a_o)
 \end{aligned} \tag{11}$$

where:

$N$ , the total number of core systems

$a_o = \frac{\omega d}{V_s}$ , the dimensionless frequency of excitation,

$\gamma_o = \frac{C V_s}{d K}$ , the dimensionless damping coefficient of the base system,

$\gamma_i = \frac{c_i V_s}{d k_i}$ , the dimensionless damping coefficient in each core system,

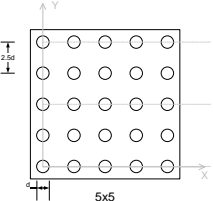
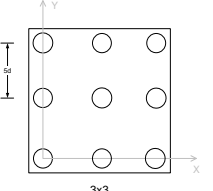
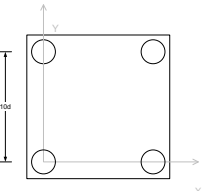
$\mu_o = \frac{M V_s^2}{d^2 K}$ , the dimensionless mass coefficient of the base system,

$\mu_i = \frac{m_i V_s^2}{d^2 k_i}$ , the dimensionless mass coefficient in each core system,

$\beta_i = \frac{k_i}{K}$ , the relative stiffness of each core and base system,

Equation (11) relates the displacements of the foundation with the forces developed, in the frequency domain. The values of the coefficients are those who determine the total dynamic stiffness. A similar equation with a similar set of variables is utilized for the rotational degree of freedom (Type II model) and relates the rotation of the system with the corresponding moment developed. *Tables 5* presents the initial values of the horizontal and rotational impedances ( $a_o=0$ ), of the three different pile configurations considered ( 5x5, 3x3 and 2x2) for the two bridges, as they were estimated by the software PILES. The values match all the 3 modeling approaches, Voigt, Type II and simple Type II system (only for the lateral impedances) and correspond to the static values of the impedances.

Table 5. Foundation system properties ( $a_0=0$ ) of a 5x5 pile group for the three modeling approaches.

Parameters for $a_0=0$ of all the three models (Type II, Voigt, simple Type II)	Bridge I				Bridge II			
	$K_{xx}$ (GN/m)	$K_{rr}$ (GN/rad)	$C_{xx}$ (GNs/m)	$C_{rr}$ (GNm s/rad)	$K_{xx}$ (GN/m)	$K_{rr}$ (GN/rad)	$C_{xx}$ (GNs/m)	$C_{rr}$ (GNm s/rad)
	0.42	17	0.008	0.35	1.78	700	0.14	8.4
	0.47	19.4	0.010	0.35	2	787	0.18	36.2
	0.50	21.9	0.011	0.35	2	787	0.20	8.1

The table summarizes the similarities and differences of the three models. In general, as the piles are getting fewer and their distances larger, the static dynamic impedances are becoming greater. A simple explanation for this is that when the piles are distant they have enough space to develop the frictional and lateral forces that are generated due to the earthquake excitation and soil-structure interaction.

## 3.2. Calibrating GYROMASS Models

### 3.2.1. Levenberg Marquadt Method

Apart from the static values of the problem, the dynamic group behavior is also known, as it was presented in Chapter 2. In order the three soil-foundation models (Type II, simple Type II, Voigt) to represent the estimated dynamic behaviors, the values of their parameters have to be evaluated/calibrated properly. For the complex relation of the Type II model (11), the problem now is a mathematical curve fitting one. The fitting was accomplished with a method applicable to non-linear least squares problems, the **Levenberg Marquadt method**.

A least squares problem comes up when a parametrical function has to adjust to a number of data, with the least possible error between the real data and those that the function estimates. Non linearity appears when the function which has to be adjusted is non-linear concerning its parameters. The method is based on an iterative correction of the values of the parameters so as to minimize the sum of the squares of the discrepancies with the real data. In reality, the method is a combination of two other methods: the *gradient descent method* and of *Gauss-Newton method*. The gradient descent method minimizes the sum of the squares of the aforementioned errors/discrepancies by adjusting the values of the parameters to the maximum least square objective. The Gauss-Newton method minimizes the sum of the squares of the discrepancies with the assumption that the function of the sum is locally squared and so the minimum of the square is found. Practically, when the values of the parameters are far from the optimum solution the Levenberg Marquadt method is working as the gradient descent method and when they are close to the optimum value, as the Gauss-Newton method.

When adjusting a function  $\hat{y}(t, p)$ , with  $t$  the independent variable, and  $p$  a string of parameters, in a data series  $(t_i, y_i)$  it is convenient enough to minimize the sum of the weighted squares of the estimated discrepancies between the estimated data  $y(t_i)$  and the values of the curve fitting function  $\hat{y}(t_i, p)$ . This is the error criterion,  $x^2$ .

$$\begin{aligned}
 x^2(p) &= \frac{1}{2} \sum_{i=1}^N \left[ \frac{y(t_i) - \hat{y}(t_i, p)}{w_i} \right]^2 = \\
 &= \frac{1}{2} (y - \hat{y}(p))^T W (y - \hat{y}(p)) = \\
 &= \frac{1}{2} y^T W y - y^T W \hat{y} + \frac{1}{2} \hat{y}^T W \hat{y}
 \end{aligned} \tag{12}$$

The parameter  $w_i$  is the estimation of the discrepancy of the value of  $y(t_i)$ . The weighted matrix  $W$  is diagonal with  $W_{ii} = \frac{1}{w_i^2}$ . If the function  $\hat{y}(t_i, p)$  is non-linear, then the minimization of  $w^2$  has to be completed with an iterative procedure. In each iteration the parameter of perturbation  $h$ , of the parameters  $p$  has to be evaluated.

### ○ Gradient descent method

The gradient descent method is a generalized method of minimization, which adjusts the parametric values at an opposite direction of that of the objection function's gradient. For big scale problems, with thousands of parameters the gradient descent method is the unique way of curve fitting. The gradient of function  $x^2$  with respect to the parameters is:

$$\begin{aligned} \frac{\partial}{\partial p} x^2 &= (y - \hat{y}(p))^T W \frac{\partial}{\partial p} (y - \hat{y}(p)) = \\ &= -(y - \hat{y}(p))^T W \left[ \frac{\partial \hat{y}(p)}{\partial p} \right] = \\ &= -(y - \hat{y}(p))^T W J \end{aligned} \quad (13)$$

where the  $m \times n$  Jacobean matrix  $\partial \hat{y} / \partial p$  represents the local sensitivity of the function  $\hat{y}$  to the changes of the values of the parameters  $p$ . In order to simplify things,  $J$  will be used instead of  $\partial \hat{y} / \partial p$ . The perturbation  $h$  that leads the parameters to the direction of the maximum descent is:

$$h_{gd} = \alpha J^T W (y - \hat{y}) \quad (14)$$

where  $\alpha$  is the positive coefficient that controls the size of the step towards the maximum descent.

### ○ Gauss-Newton method

The Gauss Newton method is a tool for the minimization of the sum of the discrepancies' squares. It assumes that the objective function is almost squared with respect to its parameters, near the optimum solution. For ordinary problems the Gauss Newton method is converging much faster than the gradient descent method

The function evaluated with the perturbed parameters model can locally be expressed by the 1<sup>st</sup> order Taylor series:

$$\hat{y}(p+h) \approx \hat{y}(p) + \left[ \frac{\partial \hat{y}}{\partial p} \right] = \hat{y} + Jh \quad (15)$$

and with the help of equation (12):

$$x^2(p+h) \approx \frac{1}{2}y^T W y + \frac{1}{2}\hat{y}^T W \hat{y} - \frac{1}{2}y^T W \hat{y} - (y - \hat{y})^T W J h + \frac{1}{2}h^T J^T W J \quad (16)$$

This proves that  $x^2$  is almost squared at the perturbation  $h$  and the Hessian matrix of the  $x^2$  criterion is  $J^T W J$ . The perturbation  $h$  that minimizes  $x^2$  is:

$$\begin{aligned} \frac{\partial(x^2(p+h))}{\partial h} &= 0 \Rightarrow \\ -(y - \hat{y})^T W J + h^T J^T W J &= 0 \Rightarrow \\ [J^T W J] h_{gn} &= J^T W (y - \hat{y})^T \end{aligned} \quad (17)$$

### o Levenberg Marquadt Method

The Levenberg Marquadt algorithm adjusts the changes of the parameters between the two aforementioned methods,

$$[J^T W J + \lambda I] h_{lm} = J^T W (y - \hat{y}) \quad (18)$$

where small changes of the value  $\lambda$  lead to the Gauss – Newton method and big changes of the value  $\lambda$  lead to the gradient descent method. At a great distance from the minimum function the gradient descent method is useful due to the stability and fast convergence that it serves. As the solution moves towards the minimum and the values of  $\lambda$  are adjustably getting smaller, the Levenberg Marquadt method becomes Gauss Newton and the solution converges rapidly to the local minimum. The relation that Marquadt used for the adjustment between the two methods is:

$$[J^T W J + \lambda \text{diag}(J^T W J)] h_{lm} = J^T W (y - \hat{y}) \quad (19)$$

### 3.2.2. Parameter calibration of Type II model

As it has become clear, the Voigt model is the only one that consists of spring-dashpot systems, without masses or gyromasses. At the case of Voigt model, the Levenberg-Marquadt method is not applicable, as there are no parameters to be evaluated apart from the dynamic impedances for  $a_0=0$ . On the other hand, the Type II model (and the simple Type II) has to be defined properly, for each case of studying. The calibration of its parameters (see Equation (11)) is accomplished with the help of Levenberg-Marguadt method, as it was presented at §3.2.1. The mathematical expression (Equation 11) is now fully defined and the values of its parameters, for the 5x5, 3x3, and 2x2 pile groups of bridges I and II, are presented in Table 5.

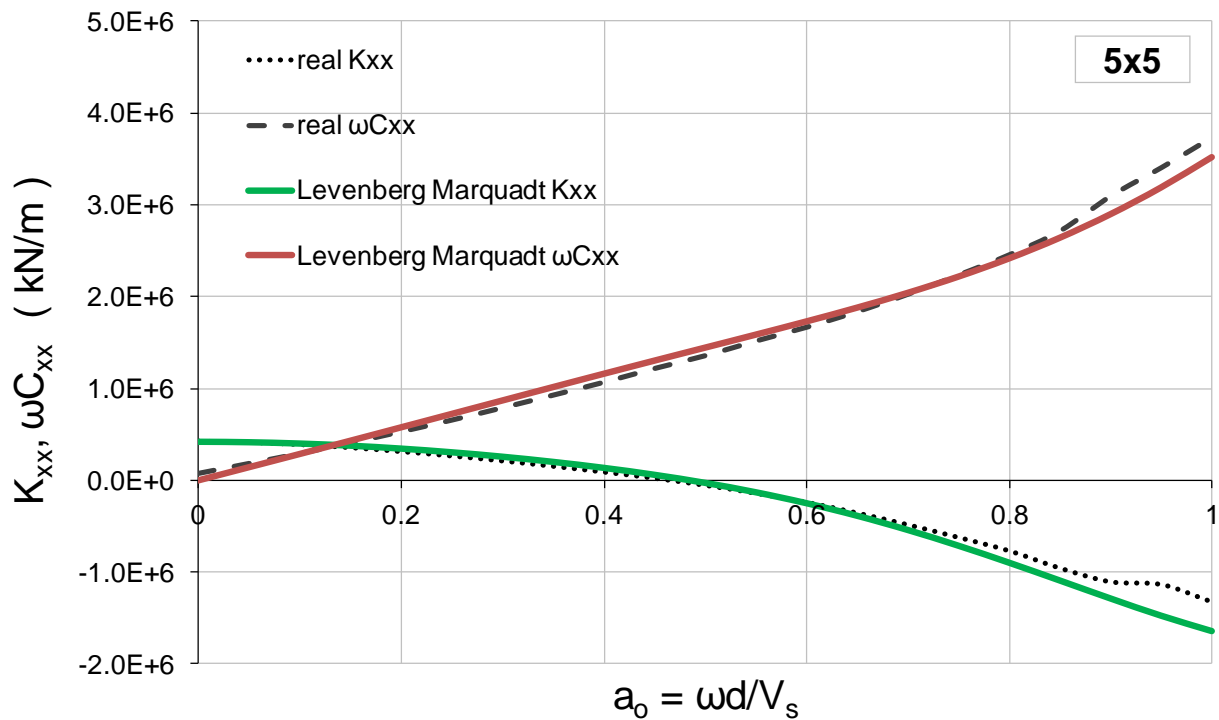


Figure 52. Real horizontal dynamic impedances of 5x5 pile group of Bridge I, in comparison with the fitted horizontal impedances by Levenberg Marquadt method.

Figure 52 compares actual and fitted data of the dynamic impedance of the 5x5 pile group for the Bridge I. The same algorithm was also used to estimate the parameters of the other cases of studying: the 3x3 and 2x2 equivalent pile groups for both Bridge I and Bridge II. There are many combinations of values that can describe satisfactorily the same curve. The algorithm ends up with those values that best fit the given

impedances. *Table 6* summarizes the values of the variables that are going to be used in this study, for the horizontal degree of freedom of the three equivalent pile groups. *Table 7* summarizes the same variables for the rotational degree of freedom.

**Table 6. Dimensionless coefficients of Type II model that calibrate horizontal impedance functions of 5x5, 3x3 and 2x2 pile groups.**

Coefficient	Bridge I			Bridge II		
	5x5	3x3	2x2	5x5	3x3	2x2
$K_{xx} / N * K_{x,single}$	0.19	0.36	0.60	0.19	0.36	0.60
$\gamma_0$	2	4.2	0.13	5	3	0.6
$\mu_0$	5	1.1	1.6	2.5	1.2	1.1
$\beta_1$	1.2	0.9	0.03	0.28	1	0.08
$\gamma_1$	2	0.5	10	0.8	0.55	5
$\mu_1$	1.9	0.82	2	3.4	0.8	0.1
$\beta_2$	6	0.14	2.5	2.7	1.22	2
$\gamma_2$	0.4	0.17	1.1	0.2	0.4	0.9
$\mu_2$	0.5	0.02	1.2	0.65	0.8	1

**Table 7. Dimensionless coefficients of Type II model that calibrate rotational impedance functions of 5x5, 3x3 and 2x2 pile groups.**

Coefficient	Bridge I			Bridge II		
	5x5	3x3	2x2	5x5	3x3	2x2
$K_{rr} / \Sigma (x_r^{2*} K_{x,\text{single}})$	1.09	0.72	0.13	0.61	1.04	1.52
$\nu_{ro}$	2.2	1.2	1.32	5.5	1.4	1.3
$\mu_{ro}$	2.5	0.5	0.2	3.3	0.6	0.8
$\beta_{r1}$	1.45	0.85	0.48	8	2.6	0.04
$\nu_{r1}$	0.23	0.27	1.8	0.01	0.33	2
$\mu_{r1}$	1.18	1.14	4.7	0.01	1.03	1.1
$\beta_{r2}$	1.65	1.3	0.23	6.7	0.2	0.55
$\nu_{r2}$	1.95	1.5	0.6	0.23	0.2	0.75
$\mu_{r2}$	6.5	3.1	3.2	0.79	0.2	2.4

The following figures (*Figures 53-64*) are demonstrating the curve fitting that the Type II and Voigt models are achieving to the actual impedances obtained from software PILES. Practically it is a graphic representation of the fitting that the models with the variable values of Tables 6 and 7 achieve.

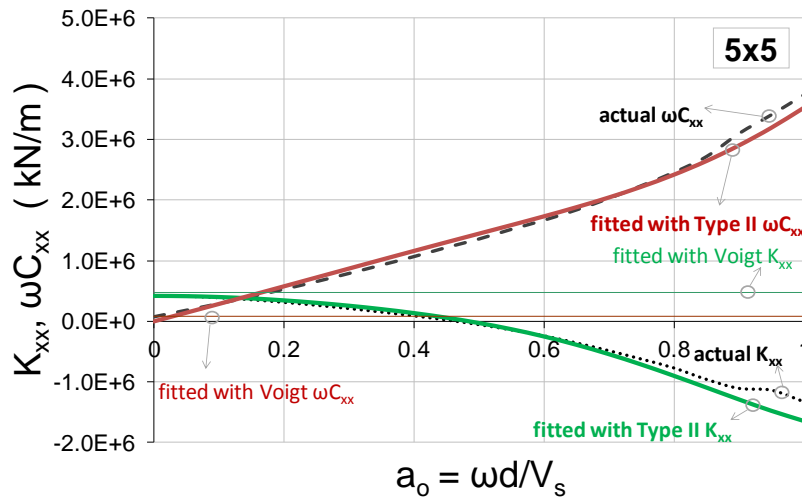


Figure 53. The actual and fitted horizontal impedances, of the 5x5 pile group, Bridge I.

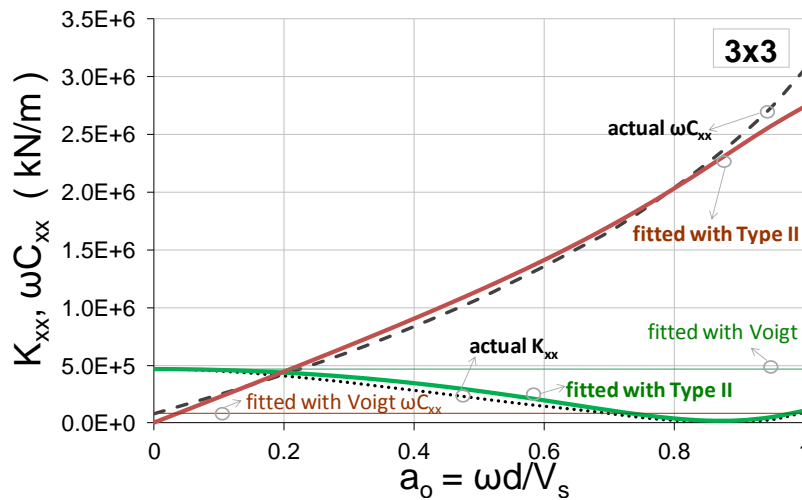


Figure 54. The actual and fitted horizontal impedances, of the 3x3 pile group, Bridge I.

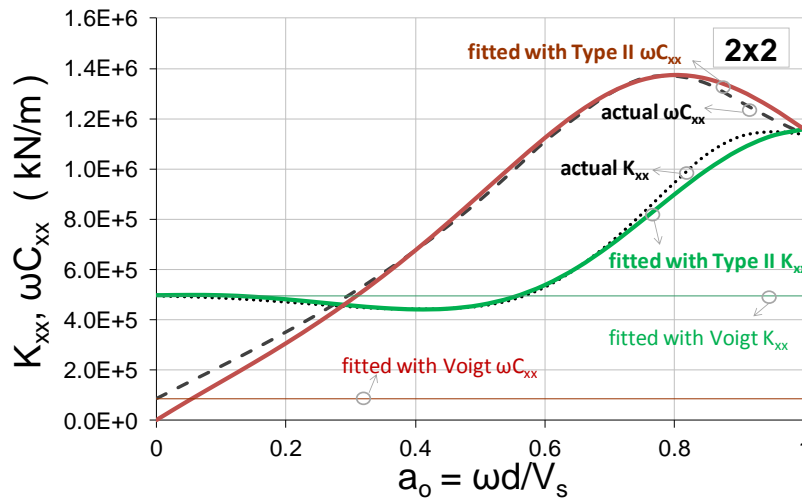


Figure 55. The actual and fitted horizontal impedances, of the 2x2 pile group, Bridge I.

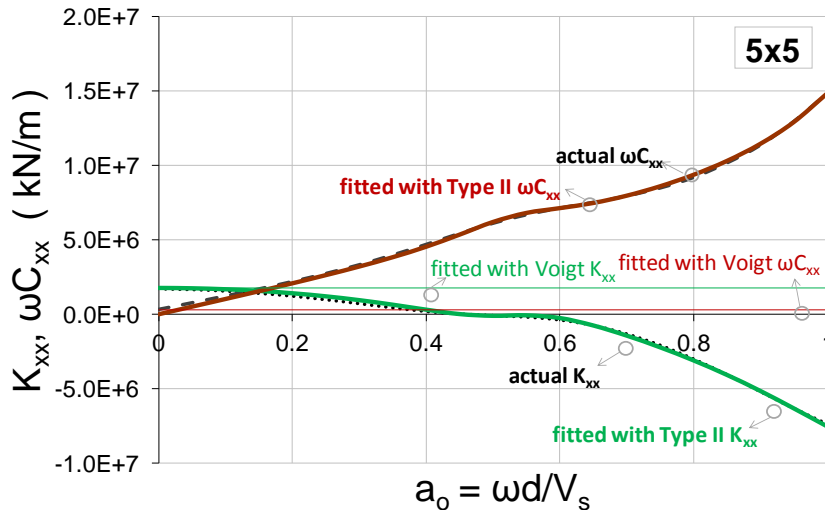


Figure 56. The actual and fitted horizontal impedances, of the 5x5 pile group, Bridge II.

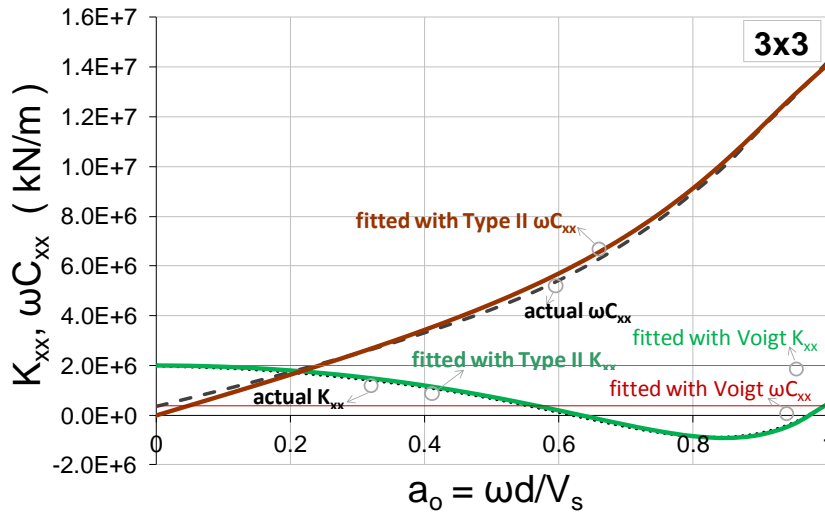


Figure 57. The actual and fitted horizontal impedances, of the 3x3 pile group, Bridge II.

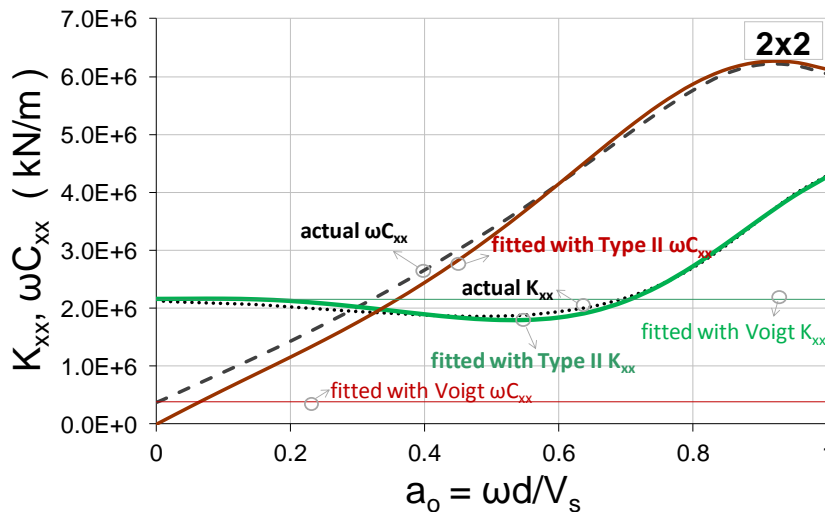


Figure 58. The actual and fitted horizontal impedances, of the 2x2 pile group, Bridge II.

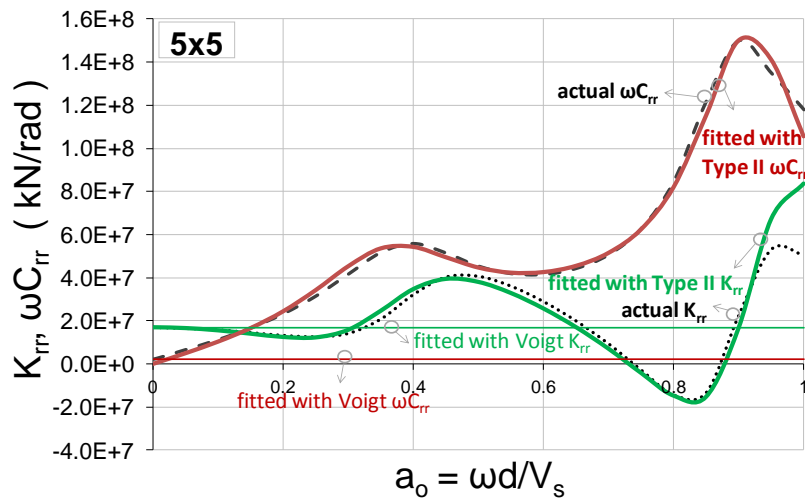


Figure 59. The actual and fitted rotational impedances, of the 5x5 pile group, Bridge I.

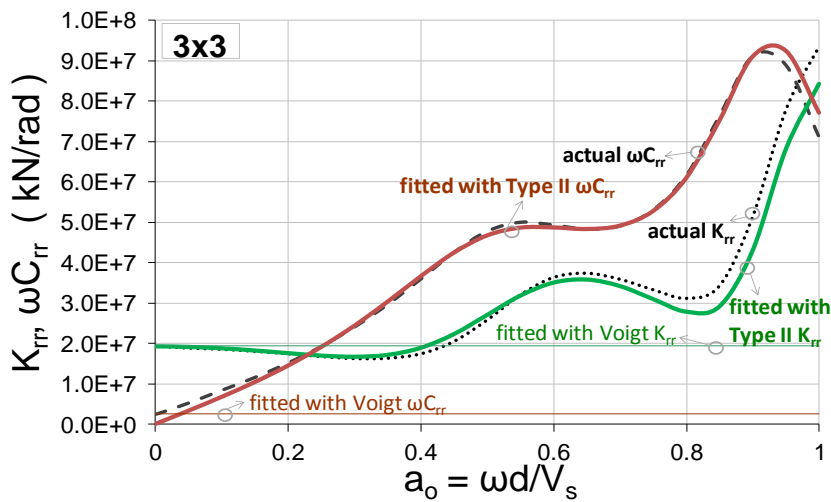


Figure 60. The actual and fitted rotational impedances, of the 3x3 pile group, Bridge I.

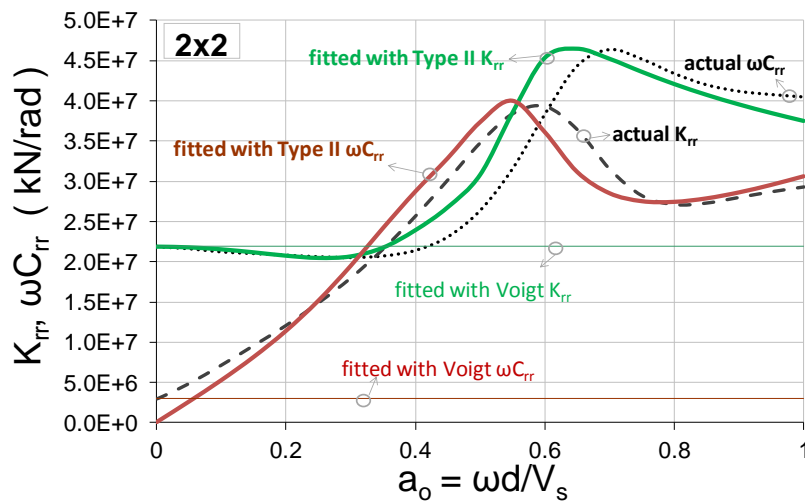


Figure 61. The actual and fitted rotational impedances, of the 2x2 pile group, Bridge I.

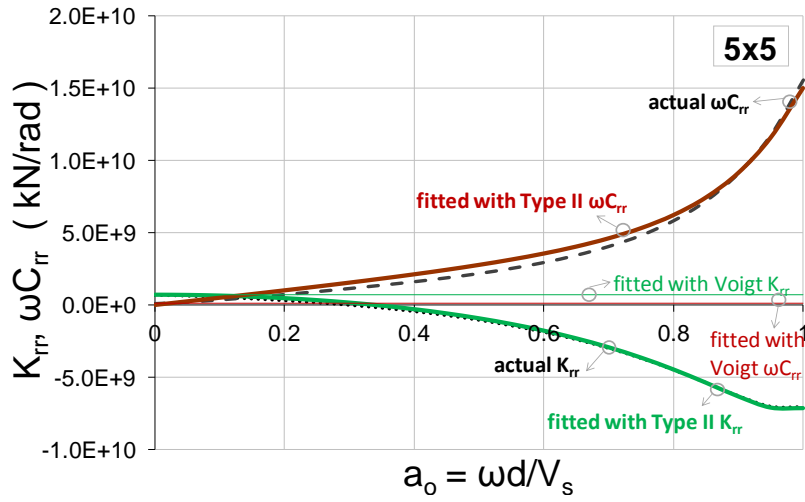


Figure 62. The actual and fitted rotational impedances, of the 5x5 pile group, Bridge II.

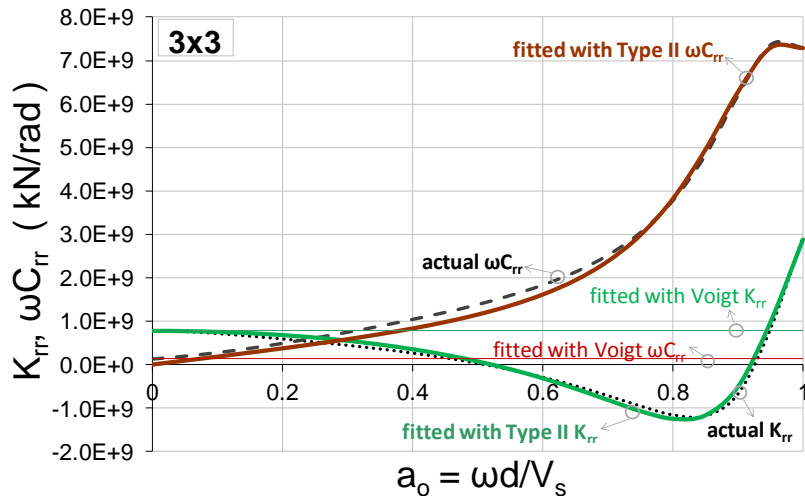


Figure 63. The actual and fitted rotational impedances, of the 3x3 pile group, Bridge II.

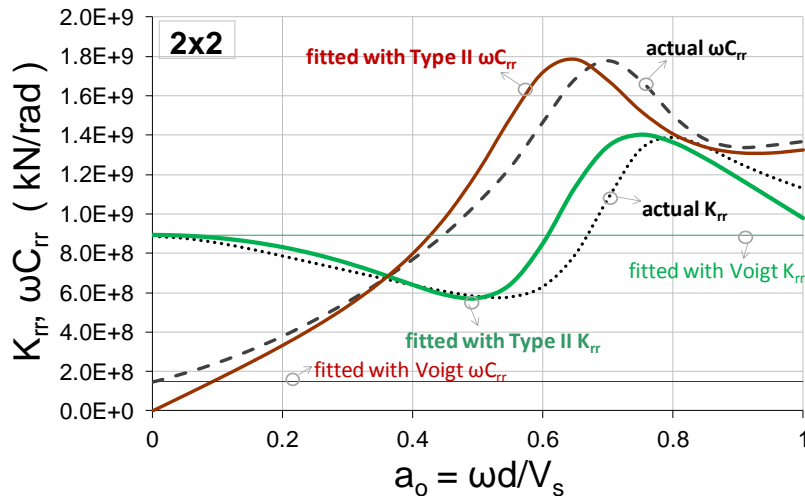


Figure 64. The actual and fitted rotational impedances, of the 2x2 pile group, Bridge II.



The system has 4 DOF, deck displacement w.r.t the pier or isolation system displacement, displacement of the pier w.r.t. its base, displacement of the foundation w.r.t. ground, and rotation of the foundation. The equations of dynamic equilibrium of the system are:

$$\begin{aligned} \Sigma F_{x_{\text{deck}}} = 0 &\Rightarrow m_d \cdot \ddot{u}_{d,\text{tot}} + m_d \cdot \ddot{u}_g + f_{\text{ISOL}} = 0 \Rightarrow \\ &m_d \cdot \ddot{u}_{d,\text{tot}} + m_d \cdot \ddot{u}_g + k_{\text{ISOL}} \cdot u_{\text{ISOL}} = 0 \end{aligned} \quad (20)$$

$$\begin{aligned} \Sigma F_{x_{\text{pier}}} = 0 &\Rightarrow m_p \cdot \ddot{u}_{p,\text{tot}} + m_p \cdot \ddot{u}_g + f_p - f_{\text{ISOL}} = 0 \Rightarrow \\ &m_p \cdot \ddot{u}_{p,\text{tot}} + m_p \cdot \ddot{u}_g + k_p \cdot u_p + c_p \cdot \dot{u}_p - k_{\text{ISOL}} \cdot u_{\text{ISOL}} = 0 \end{aligned} \quad (21)$$

$$\begin{aligned} \Sigma F_{x_{\text{foundation}}} = 0 &\Rightarrow m_f \cdot \ddot{u}_f + m_f \cdot \ddot{u}_g + f_{\text{VOIGT}} - f_p = 0 \Rightarrow \\ &m_f \cdot \ddot{u}_f + m_f \cdot \ddot{u}_g + K_h \cdot u_f + C_h \cdot \dot{u}_f - k_p \cdot u_p - c_p \cdot \dot{u}_p = 0 \end{aligned} \quad (22)$$

$$\begin{aligned} \Sigma M_{\text{foundation}} = 0 &\Rightarrow M_{\text{INERTIAL}} + M_{\text{VOIGT}} - f_{\text{VOIGT}} \cdot \frac{H_f}{2} - f_p \cdot \frac{H_f}{2} = 0 \Rightarrow \\ &I_f \ddot{\theta}_f + K_r \cdot \theta_f + C_r \cdot \dot{\theta}_f - K_h \cdot u_f \cdot \frac{H_f}{2} - C_h \cdot \dot{u}_f \cdot \frac{H_f}{2} - \\ &- k_p \cdot u_p \cdot \frac{H_f}{2} - c_p \cdot \dot{u}_p \cdot \frac{H_f}{2} = 0 \end{aligned} \quad (23)$$

where,  $\mathbf{u}_g$  is the ground displacement,  $\mathbf{u}_f$  is the foundation displacement,  $\mathbf{u}_{\text{ISOL}}$  is the isolation system displacement,  $\theta_f$  is the rotation of the foundation,  $m_d$  is the mass of deck,  $m_p$  is the mass of pier,  $m_f$  is the mass of foundation,  $\mathbf{k}_{\text{isol}}$  is the stiffness of the isolation system (the behavior of isolation is bilinear hysteretic and is modeled by Ozdemir's model),  $\mathbf{k}_p$  is the linear elastic stiffness of pier,  $\mathbf{c}_p$  is the damping coefficient of the pier,  $I_f$  is the mass moment of inertia of the pile group cap,  $H_f$  is the height of pile cap.

The values  $K_h$ ,  $C_h$ ,  $K_r$ ,  $C_r$  are the spring and damping constants of the Voigt models calculated previously from the foundation-soil impedances for  $a_0=0$  (see *Table 5*). The system of equations is transformed to state-space form, after reduction of order, and solved utilizing a predictor corrector scheme, based on 4<sup>th</sup> order Runge-Kutta algorithms, suitable for solving 1<sup>st</sup> order nonlinear ordinary differential equations.

### 3.3.2. Type II Model

Figure 66 presents the bridge system with the Type II models in the undeformed and deformed configurations. The system has the same 4 DOF in the structural system as before, however the presence of the Type II models increase the number of DOFs (two internal DOF per Type II model) to total 8.

$$\begin{aligned} \Sigma F_{x_{\text{deck}}} = 0 &\Rightarrow m_d \cdot \ddot{u}_{d,\text{tot}} + m_d \cdot \ddot{u}_g + f_{\text{ISOL}} = 0 \Rightarrow \\ &m_d \cdot \ddot{u}_{d,\text{tot}} + m_d \cdot \ddot{u}_g + k_{\text{ISOL}} \cdot u_{\text{ISOL}} = 0 \end{aligned} \quad (24)$$

$$\begin{aligned} \Sigma F_{x_{\text{pier}}} = 0 &\Rightarrow m_p \cdot \ddot{u}_{p,\text{tot}} + m_p \cdot \ddot{u}_g + f_p - f_{\text{ISOL}} = 0 \Rightarrow \\ &m_p \cdot \ddot{u}_{p,\text{tot}} + m_p \cdot \ddot{u}_g + k_p \cdot u_p + c_p \cdot \dot{u}_p - k_{\text{ISOL}} \cdot u_{\text{ISOL}} = 0 \end{aligned} \quad (25)$$

$$\begin{aligned} \Sigma F_{x_{\text{foundation}}} = 0 &\Rightarrow m_f \cdot \ddot{u}_f + m_f \cdot \ddot{u}_g + f_{\text{TYPE II}} - f_p = 0 \Rightarrow \\ &m_f \cdot \ddot{u}_f + m_f \cdot \ddot{u}_g + [f_{\text{base}} + f_{\text{core 1}} + f_{\text{core 2}}] - k_p \cdot u_p - c_p \cdot \dot{u}_p = 0 \end{aligned} \quad (26)$$

where,

$$f_{\text{base}} = \dot{M}\ddot{u}_f + K_h u_f + C_h \dot{u}_f \quad (27)$$

$$f_{\text{core 1}} = k_1(u_f - u_{21}) = \dot{m}_1 \ddot{u}_{21} + c_1 \dot{u}_{21} \quad (28)$$

$$f_{\text{core 2}} = k_2(u_f - u_{22}) = \dot{m}_2 \ddot{u}_{22} + c_2 \dot{u}_{22} \quad (29)$$

$$\begin{aligned} \Sigma M_{\text{foundation}} = 0 &\Rightarrow M_{\text{INERTIAL}} + M_{\text{TYPE II}} - f_{\text{TYPE II}} \cdot \frac{H_f}{2} - f_p \cdot \frac{H_f}{2} = 0 \Rightarrow \\ &I_f \ddot{\theta}_f + [M_{\text{base}} + M_{\text{core 1}} + M_{\text{core 2}}] - [f_{\text{base}} + f_{\text{core 1}} + f_{\text{core 2}}] \cdot \frac{H_f}{2} - \\ &\quad - [k_p \cdot u_p - c_p \cdot \dot{u}_p] \cdot \frac{H_f}{2} = 0 \end{aligned} \quad (30)$$

where,

$$M_{\text{base}} = \dot{M}_r \ddot{\theta}_f + K_r \theta_f + C_r \dot{\theta}_f \quad (31)$$

$$M_{\text{core 1}} = k_{r1}(\theta_f - \theta_{21}) = \dot{m}_{r1} \ddot{\theta}_{21} + c_{r1} \dot{\theta}_{21} \quad (32)$$

$$M_{\text{core 2}} = k_{r2}(\theta_f - \theta_{22}) = \dot{m}_{r2} \ddot{\theta}_{22} + c_{r2} \dot{\theta}_{22} \quad (33)$$

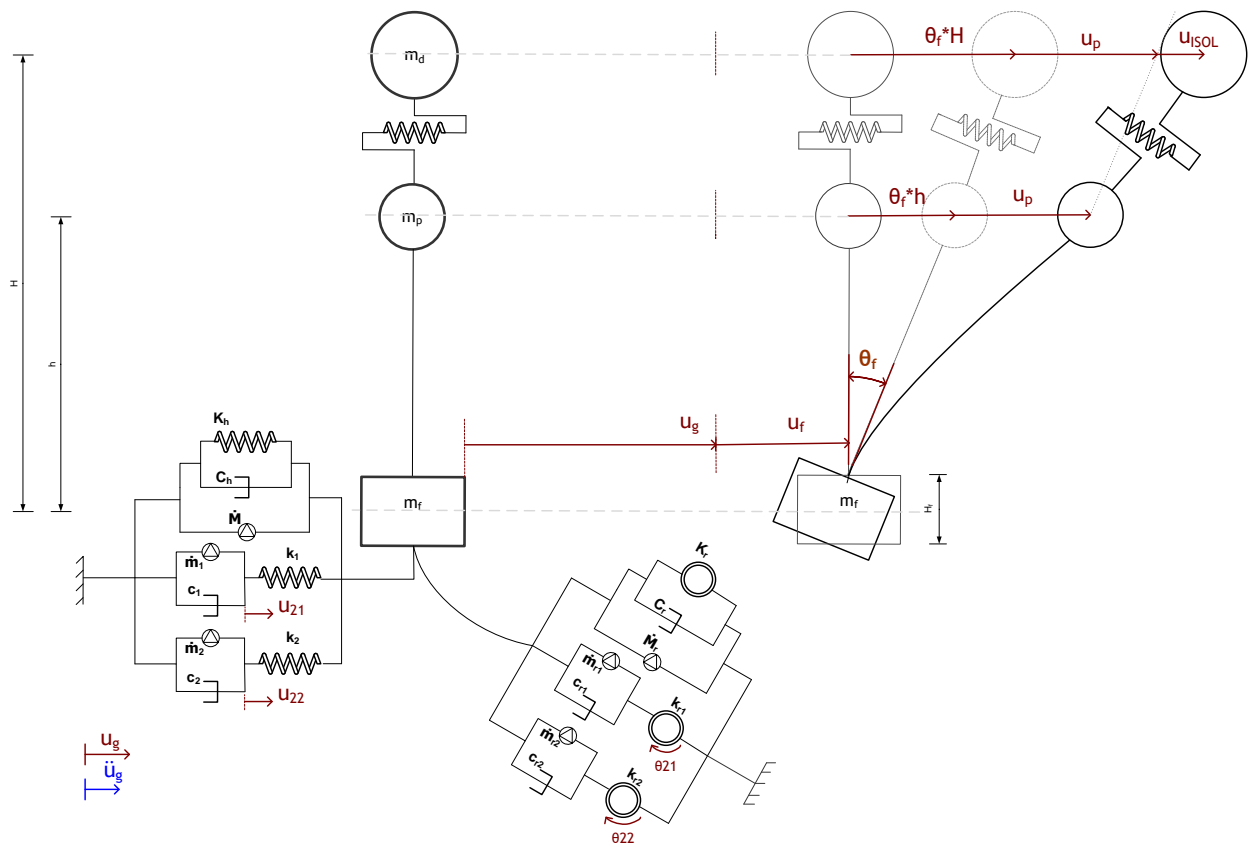


Figure 66. Undeformed and deformed configuration of the bridge system with Type II models.

### 3.3.3. Simple Type II Model

The Simple Type II model has the same set up with the Type II mechanism but only for the translational degree of freedom at the foundation level. The rotational DOF is omitted. The system has 3 DOF, (translation of deck, translation of the pier, translation of the foundation) and accordingly 3 equations of motion:

$$\begin{aligned} \Sigma F_{x_{deck}} = 0 &\Rightarrow m_d \cdot \ddot{u}_{d,tot} + m_d \cdot \ddot{u}_g + f_{ISOL} = 0 \Rightarrow \\ &m_d \cdot \ddot{u}_{d,tot} + m_d \cdot \ddot{u}_g + k_{ISOL} \cdot u_{ISOL} = 0 \end{aligned} \quad (34)$$

$$\begin{aligned} \Sigma F_{x_{pier}} = 0 \Rightarrow m_p \cdot \ddot{u}_{p,tot} + m_p \cdot \ddot{u}_g + f_p - f_{ISOL} = 0 \Rightarrow \\ m_p \cdot \ddot{u}_{p,tot} + m_p \cdot \ddot{u}_g + k_p \cdot u_p + c_p \cdot \dot{u}_p - k_{ISOL} \cdot u_{ISOL} = 0 \end{aligned} \quad (35)$$

$$\begin{aligned} \Sigma F_{x_{foundation}} = 0 \Rightarrow m_f \cdot \ddot{u}_f + m_f \cdot \ddot{u}_g + f_{TYPEII} - f_p = 0 \Rightarrow \\ m_f \cdot \ddot{u}_f + m_f \cdot \ddot{u}_g + [f_{base} + f_{core1} + f_{core2}] - k_p \cdot u_p - c_p \cdot \dot{u}_p = 0 \end{aligned} \quad (36)$$

where,

$$f_{base} = \dot{M}\ddot{u}_f + K_h u_f + C_h \dot{u}_f \quad (37)$$

$$f_{core1} = k_1(u_f - u_{21}) = \dot{m}_1 \ddot{u}_{21} + c_1 \dot{u}_{21} \quad (38)$$

$$f_{core2} = k_2(u_f - u_{22}) = \dot{m}_2 \ddot{u}_{22} + c_2 \dot{u}_{22} \quad (39)$$

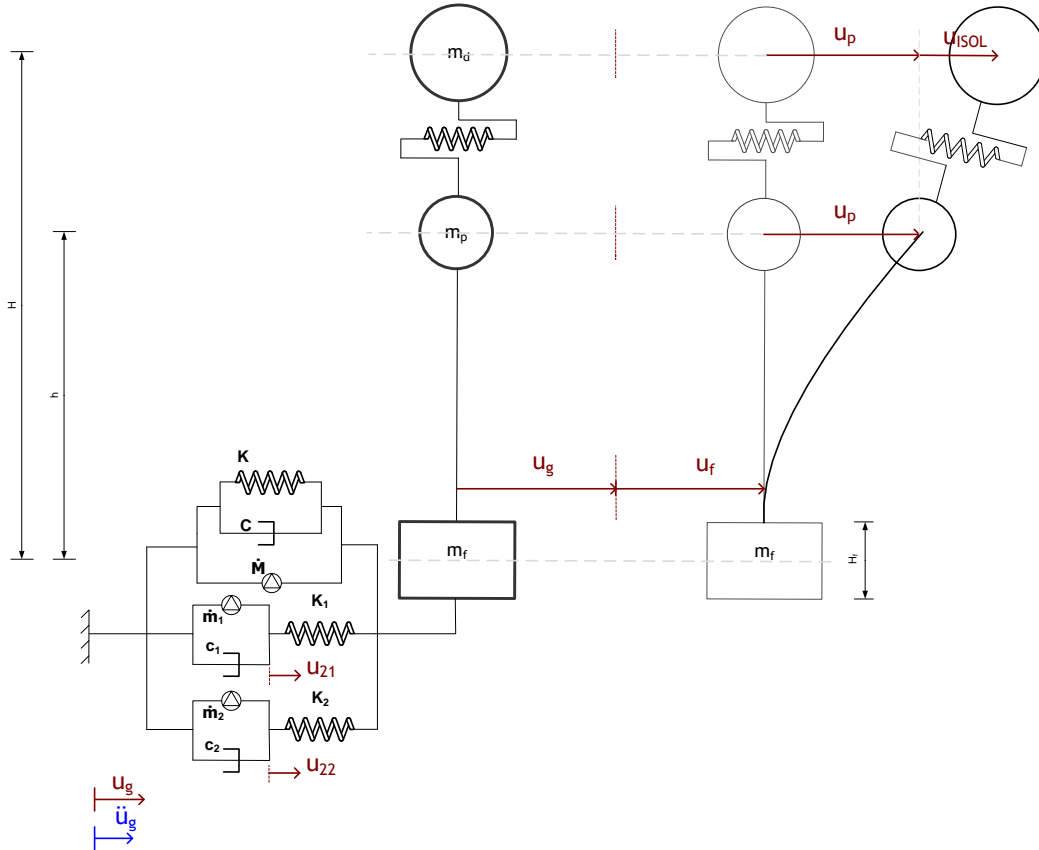


Figure 67. Undeformed and deformed configuration of the bridge system with Simple Type II model.

The advantage of the **gyromass** element is now clear. It contributes to the total force that the Type II system represents as an ordinary mass but it doesn't appear as an additional inertial force, as it is attached to the Type II model and is activated by the relative acceleration between the foundation and the ground.

### 3.4. Dynamic properties of the Soil-Foundation-Structure System (Eigenvalue Analysis)

Natural frequencies and mode shapes are functions of the structural properties and boundary conditions of a structural system. For example a cantilever beam has a set of natural frequencies and their associated mode shapes. In general, if the structural properties change, but not the boundary conditions, the frequencies and the mode shapes change also. However there are cases where the mode shapes do not change. If the boundary conditions change then both the frequencies and mode shapes of the cantilever have to change. The reason for computing these characteristics is to possibly identify how the input seismic energy will be directed in the structure. An earthquake's energy is distributed to frequency ranges and if those coincide with the "natural" frequencies of the structure might make the structural response/vibration much more intense and possibly lead to damage or even structural failure. Although this fact reveals the high possibilities of the resonance appearing, other parameters such as the duration of the vibration and the distance of the structure from the seismic epicenter, determine finally whether it will take place or not.

The eigenvalue analysis is carried out on a set of differential equations which describe the equilibrium of the whole system, from the soil to the deck. The state-space formulation of the equations of motion of the system is followed in this work and accordingly the eigenvalue analysis is carried on the state-space equations modeling the system. In general terms the  $2^{\text{nd}}$  order differential equations of motion are reduced to  $1^{\text{st}}$  order differential equations and take the form presented in the equations below.

$$\dot{\bar{x}}(t) = [A_c] \bar{x}(t) + [B_c] \dot{u}_g(t) \quad (40)$$

where,

$$\bar{x}(t) = \begin{bmatrix} \bar{u}(t)^T & \dot{\bar{u}}(t)^T \end{bmatrix}^T, \quad (41)$$

$$[A_c] = \begin{bmatrix} 0 & I \\ -M^{-1}K & -M^{-1}C_D \end{bmatrix}, \quad (42)$$

$$[B_c] = \begin{bmatrix} 0 \\ -M^{-1}B_f \end{bmatrix}, \quad (43)$$

M= mass matrix, K=stiffness matrix, C<sub>D</sub>= damping matrix and B<sub>f</sub>= influence matrix. Finally the eigenvalues of the system can be deduced from the common eigenvalue problem:

$$[Ac]\bar{p} = \gamma_i \bar{p} \quad (44)$$

where  $\bar{p}$  is the mode vector and  $\underline{\gamma}_i$  are the complex values of the system:

$$\gamma_i = -\xi_i \omega_i \pm i \omega_i \sqrt{1 - \xi_i^2} \quad (45)$$

$$\omega_i = \sqrt{\gamma_i \times \gamma_i^*}, \quad \xi_i = -\frac{\text{Re}(\gamma_i)}{\omega_i} \quad (46)$$

The limitation of the approach lies in the required linearity of the system equations. To this end, the nonlinear behavior of the isolator is replaced by an equivalent linear system, with stiffness and linear viscous damping appropriate to simulate the total dissipated energy of the nonlinear isolator. The stiffness of the equivalent linear isolator is chosen to take the value of the postyielding stiffness,  $K_b$  (see Table 4) of the actual isolator and the equivalent linear viscous damping coefficient to take the value of 10% of critical ( $\xi$ ). For Bridge I, when the foundation is modeled by Type II systems,  $A_c$  is a matrix of dimensions 16x16, due to the 16 1<sup>st</sup> order ordinary differential equations modeling the system (there are 8 degrees of freedom; 4 in the superstructure and 4 in the two Type II models; see Section 3.3.2). Of the total 16 eigenvalues 4 pairs determine the 4 mode shapes of the system.

After formulating the equations of motion according to the Equation (40) the matrices  $[Ac]$  and  $[Bc]$  are determined and the eigenvalue problem of Equation (44) solved. Table 8 presents the eigenvalues for Bridge I with Voigt and Type II models, while Table 9 for Bridge II. It should be pointed out here that the real bridge, is controlled by a bilinear behavior with two different periods, as it was presented in Table 4.

Small differences are observed between the Type's II and Voigt's eigenvalues, which is in complete accordance with the flexibility of the system when is modeled with Type II. What has to be highlighted once again is that the isolation's stiffness was considered constant for the needs of the eigenvalue analysis (resulting in  $T=2$ secs for Bridge I and  $T=4.5$ secs for Bridge II). The real isolation model though, is a bilinear one, with 2 different periods governing the behavior of the isolator (e.g. for Bridge I:  $K_e=26154$  kN/m  $\rightarrow T_e=0.63$ secs,  $K_b=2615.4$  kN/m  $\rightarrow T_b=2$  secs). Depending on the incoming motion the performing eigenperiod may be either the elastic one or a combination of both elastic and postyielding. These differences will be commented later

on, where the analysis results will be plotted. The characteristics of the system have now been revealed and can be compared with the features of different excitations. The non linear time history analysis is the tool.

**Table 8. Eigenvalues of Bridge I, with the 5x5 pile group.**

mode	Type II			Voigt		
	f (Hz)	T (sec)	$\xi$	f (Hz)	T (sec)	$\xi$
#1	0.49	2.028	9.62%	0.49	2.027	9.62%
#2	8.91	0.112	22.56%	8.26	0.121	22.70%
#3	9.39	0.106	67.20%	12.44	0.08	57.60%
#4	28.08	0.036	65.40%	309.	0.003	100%

**Table 9. Eigenvalues of Bridge II, for the 5x5 pile group.**

mode	Type II			Voigt		
	f (Hz)	T (sec)	$\xi$	f (Hz)	T (sec)	$\xi$
#1	0.22	4.561	9.62%	0.22	4.561	9.62%
#2	2.11	0.473	10.41%	2.08	0.480	9.69%
#3	2.59	0.385	73.63%	3.32	0.300	81.46%
#4	5.51	0.181	22.22%	11.91	0.084	44.43%

Before presenting the earthquake excitations that were used in this study for the time history analyses, it is important to compare the eigenvalues that were estimated analytically with those of the equivalent single degree of freedom problems. *Table 10* reveals the translational eigenperiod of the free standing pier assuming that it was a

cantilever, of the isolation system as it would behave alone and of the foundation system assuming that it was alone and had only  $K_x$  and  $K_r$  springs. The resemblance between the real eigenvalues and those of the single dof problems is great, especially for Bridge II. This is expected, as each mode shape there is always one predominant degree of freedom.

**Table 10. Eigenperiods (sec) of the single degree of freedom components of Bridge I and II.**

<b>SDOF system</b>	<b>Bridge I</b>	<b>Bridge I</b>
<b>Pier as a cantilever</b>	0.11	0.47
<b>Isolation system as a sdof system</b>	2.00	4.50
<b>Foundation as a sdof system (translational)</b>	0.09	0.31
<b>Foundation as a sdof system (rotational)</b>	0.02	0.08

### 3.5. Seismic Excitations

Two sets of ground motion time histories are used in this study and are introduced in both bridge models, for the three equivalent pile groups ( $5 \times 5$ ,  $3 \times 3$ ,  $2 \times 2$ ) and the three foundation modeling approaches of each pile group (Voigt, Type II, Simple Type II). The first set, referred as NF (near fault), consists of 20 ground motions, assembled by Somerville et al. (1997). The motions are recordings by National earthquake hazards Reduction Program (NEHRP), from earthquakes with multiple fault mechanisms, magnitude range of 6.7-7.4 and epicentral distances between 0 and 10 km. These recordings correspond to medium to soft soil (site class D conditions). *Table 11* presents the NF set of ground motions.

Table 11. List of the NF set of ground motions.

Record ID	Seismic event	Station	Component	Scale factor
1,2	1978 TABAS		N, P	1.00
3,4	1989 Loma Prieta	Los Gatos	N, P	1.00
5,6	1989 Loma Prieta	Lex Dam	N, P	1.00
7,8	1992 Cape Medocino	Petrolia	N, P	1.00
9,10	1992 Erzincan		N, P	1.00
11,12	1992 Landers	Lucerne	N, P	1.00
13,14	1994 Northridge	Rinaldi	N, P	1.00
15,16	1994 Northridge	Olive View	N, P	1.00
17,18	1995 Kobe	Kobe	N, P	1.00
19,20	1995 Kobe	Takatori	N, P	1.00

The second set, referred as FF (far field) is identical to the set used in Whittaker et al (1998) and Constantinou and Quarshie (1998). It consists of ten pairs of scaled acceleration time histories from six actual earthquakes with magnitudes larger than 6.5 and epicentral distances between 10 and 20 km. The recordings correspond to soft rock or stiff soil. The scale factors were chosen so as the average spectrum of all the response spectra from the 20 motions to match a target design spectrum, as presented in AASHTO, for soil type II,  $A=0.4$ . The procedure is described analytically in Tsopelas et al (1997). *Table 12* presents the FF set of ground motions. The two sets of motions of *Tables 8* and *9* are shown graphically in *Figure 68*. There is also their average spectrum, indicated with bold line.

Table 12. List of the FF set of ground motions.

Record ID	Seismic event	Station	Component	Scale factor
1,2	1992 Landers	Joshua ( CDMG )	90, 0	1.48
3,4		Yermo ( CDMG )	270, 360	1.28
5,6	1989 Loma Prieta	Gilroy 2 ( CDMG )	0, 90	1.46
7,8		Hollister ( CDMG )	0, 90	1.07
9,10	1994 Noorthridge	Century ( CDMG )	90, 360	2.27
11,12		Moorpark ( CDMG )	180, 90	2.61
13,14	1949 W. Washington	325 ( USGS )	N86E, N04W	2.74
15,16	1954 Eureka	022 ( USGS )	N79E, N11W	1.74
17,18	1971 San Fernando	241 ( USGS )	N00W, S90W	1.96
19,20		458 ( USGS )	S00W, S90W	2.22

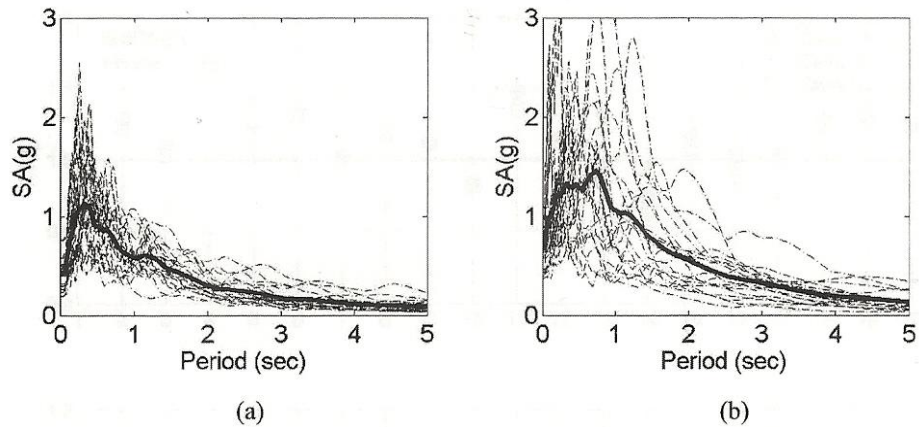


Figure 68. Response spectra (a) FF set of motions; (b) NF set of motions.

# 4

## Analyses Results and Discussion

### 4.1. Non Linear Time History Analyses and Results

Non-linear time history analyses of the two bridge models (Bridge I and Bridge II) with different foundations (2x2, 3x3, and 5x5 pile groups) utilizing three different soil-structure interactions models (Voigt, Type II for translation and rotation, and Simple Type II for translation only) subjected to both Far Field (FF) and Near Fault (NF) sets of seismic excitations are performed to evaluate and compare the superstructure and foundation responses in order to quantify the effects of the soil-structure interaction modeling on these structures. The bridge system responses in terms of displacements and forces in the superstructure and foundation are considered. The state-space formulation is utilized, where the second order differential equations of motion are transformed into a system of first order differential equations.

The critical response quantities for the design of a bridge structure are the isolation system displacement (isolation drift) and the shear force in the pier. In the present study the results of the parametric analyses are presented in terms of ratios as isolation drift ratio (IDR) and pier shear ratio (PSR). Since the objective of this study is to evaluate the effect of soil-structure–interaction modeling the analyses considering the Type II model/s are compared against the analyses with the Voigt model. Thus IDR and PSR are defined as follows:

$$\text{IDR} = \frac{\text{Isolation drift}_{\text{TYPEII}}}{\text{Isolation drift}_{\text{VOIGT}}} \quad (47)$$

$$\text{PSR} = \frac{\text{Pier shear}_{\text{TYPEII}}}{\text{Pier shear}_{\text{VOIGT}}} \quad (48)$$

## 4.2. Bridge I Analyses

*Figure 69* summarizes the results of the isolation drift ratio and *Figure 70* the pier shear ratio for Bridge I, when subjected to the FF set of seismic motions for all three pile groups considered (2x2, 3x3 and 5x5). The IDR is constant ( $\pm 1\%$  max deviation), around unity for all seismic excitations and for all three pile groups considered, indicating the insensitivity of the isolation system displacement on the SSI modeling in this particular case. It should be reminded (see also *Figures 10* and *21*) that the impedances for all three pile group do not show substantial variability between them for The variation around unity is now slightly larger, ranging between  $+2\%$  and  $-4\%$  between all the seismic excitations. The pier shear ratio is also more sensitive to the pile group. The 2x2 pile group results in higher response compared to the other two for every seismic excitation and with the max differences (in EQ 13) reaching almost 6% between the 2x2 and the 5x5 pile groups. The larger sensitivity of the PSR as compared to IDR is attributed to the higher frequency content of the pier shears relative to isolation system displacements; and because of this is rather expected.

*Figures 71* and *72* present the IDR and PSR for the NF seismic excitation set. Similar observations are made to the FF set of motions. For this set of seismic motions, also, the IDR is insensitive to the SSI modeling (Type II vs Voigt) and the pile group considered. The PSR although shows a slight sensitivity to both SSI modeling (2.5% max difference) and pile group considered (4% max difference between 2x2 and 5x5 pile groups), for all practical purposes it is also considered insensitive.

From the NF set of motions, NF12 (1992, Landers seismic event) shows the larger differences, although smaller than 4%, in IDR as well as the PSR compared to the other seismic events. *Figure 73* presents the acceleration time history of this motion (Table 11, §3.5). *Figure 74*, *75*, *76* and *77* show the isolation system displacement history, the isolation system force normalized by the deck weight vs isolation system drift, the pier shear force normalized by the carried weight vs pier drift and the foundation system shear vs foundation drift for the NF 12 respectively. These results of the nonlinear time history analysis were used to define some hidden characteristics of the models introduced. As it is already been discussed, the dynamic impedances are strongly frequency dependent parameters. *Figure 78* presents foundation system shear vs foundation drift or in other words the force vs displacement of the Voigt and the Type II models used to represent the SSI. An apparent stiffness can be obtained from these hysteretic loops (Type II and Voigt), estimated as the gradient of the shape, if its tangent is considered. In spite the differences shown between these two curves in *Figure 79*, the equivalent stiffness and damping will be very similar.

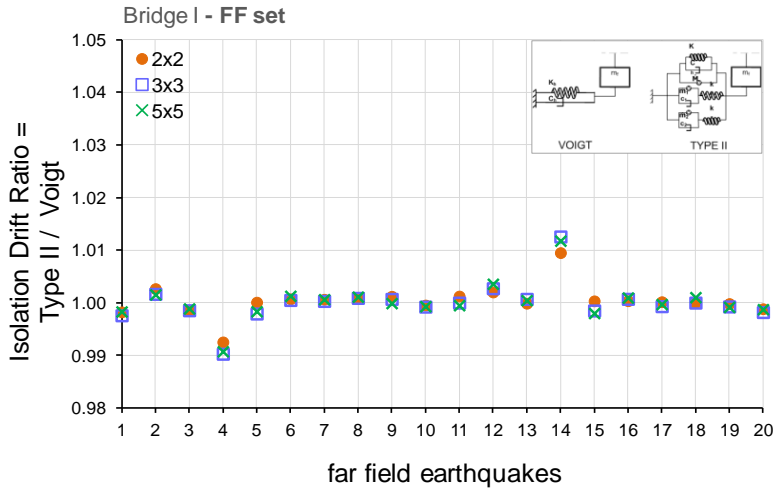


Figure 69. IDR for Bridge I and FF set.

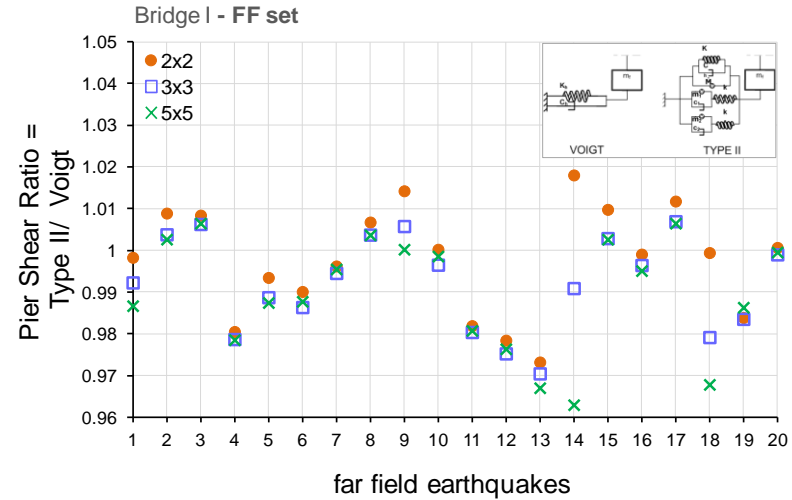


Figure 70. PSR for Bridge I and FF set.

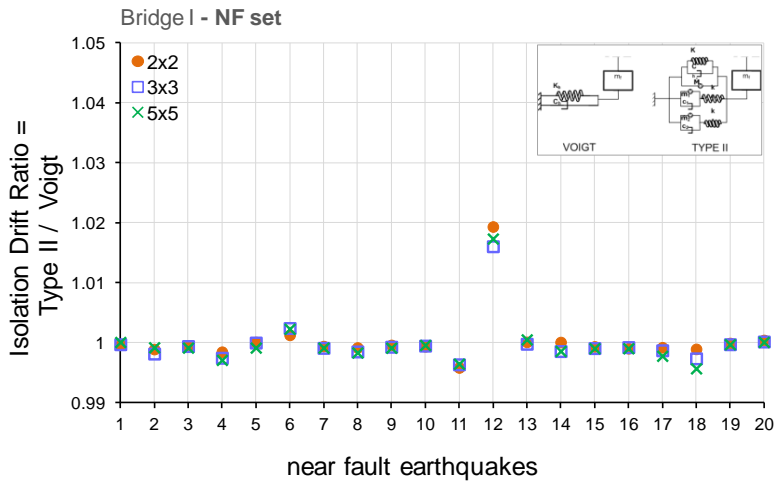


Figure 71. IDR for Bridge I and NF set.

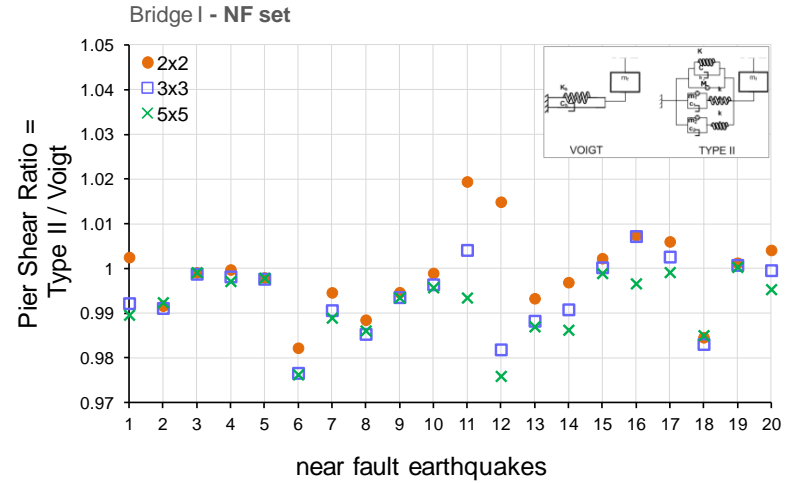


Figure 72. PSR for Bridge I and NF set.

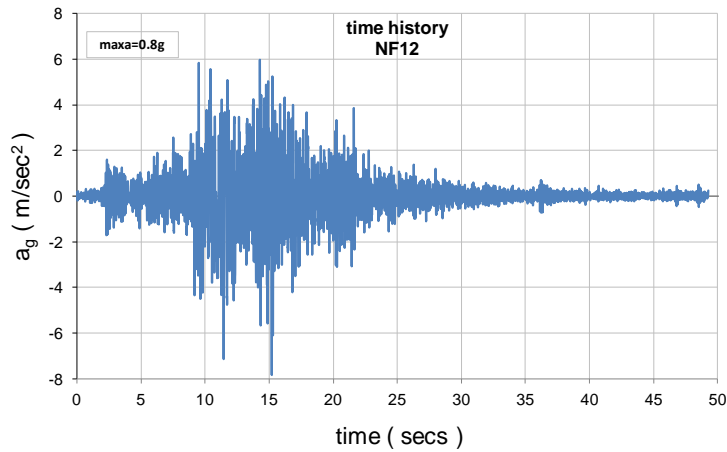


Figure 73. Acceleration time history of NF12 seismic event (1992, Landers).

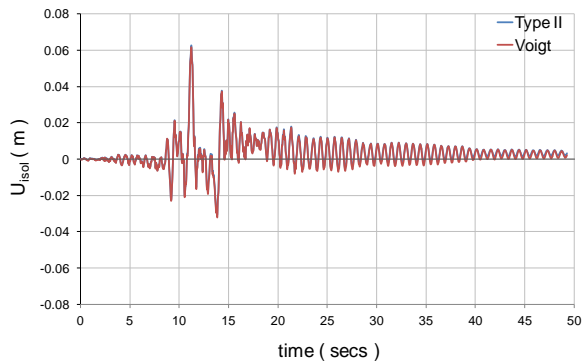


Figure 74. Isolation displacement for NF 12 (Bridge I, 5x5 pile group).

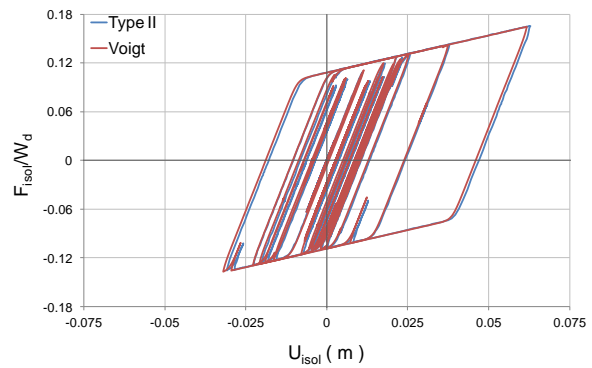


Figure 75. Isolation system loop for NF12 (Bridge I, 5x5 pile group).

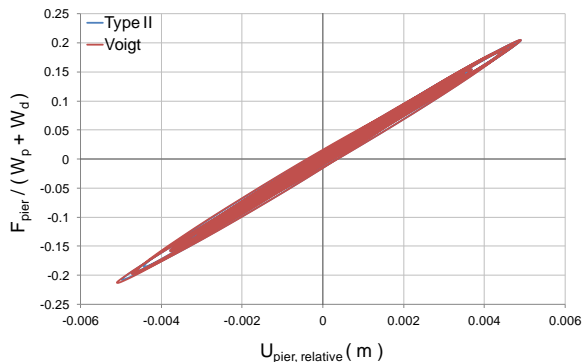


Figure 76. Pier shear vs pier drift for NF 12 (Bridge I, 5x5 pile group).

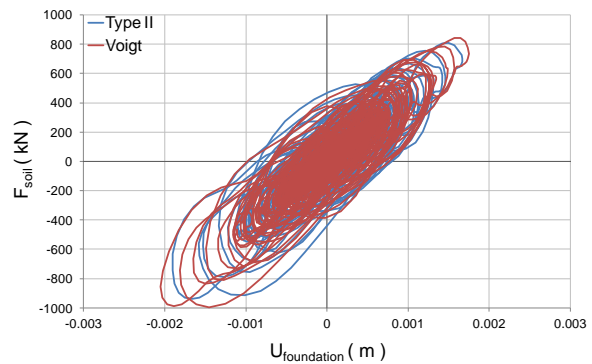


Figure 77. Foundation shear vs foundation drift for NF12 (Bridge I, 5x5 pile group).

Although the NF12 ground motion is the only near fault excitation which seems to influence the performance of Bridge I when the SSI effects are taken into account, the differences observed are very small. The discrepancies between the two models in terms

of isolation displacements reach the value of 2%, while in terms of pier's displacements the value of 3%. The same figures hold also for the pier's forces (Figure 69). Some larger discrepancies are observed at the soil-foundation displacements and forces; however, these are expected due to the nature of the two models, Voigt and Type II.

### 4.3. Bridge II Analyses

Figure 78 and 79 show the IDR and PSR for Bridge II and FF set of motions. The differences in the isolation drift between the Voigt model and the Type II range between -10% and +10% (-2% on the average over all motions), much larger when compared to the differences observed for Bridge I. The results for the three pile groups are also different than Bridge I; the 5x5 pile group, which could be characterized as the more "flexible" of the three (see Figure 27 and 28), experiences larger isolation drifts for three seismic motions where for the rest no significant differences are observed. Over all the isolation drift seem to be insensitive to the 3 pile groups considered but it is not insensitive to the SSI modeling since there are seismic motions, 5 out of 20, where the observed differences between Voigt and Type II model are larger than 5% absolute value and reach 10% maximum.

The PSR also shows larger differences than Bridge I, -16% maximum and -10% on the average over all seismic motions. This indicates that using a more accurate SSI model (Type II) than the simple Voigt the shear forces in the pier are on the average 10% smaller over this FF motion set. PSR is sensitive to the pile groups with differences between them ranging from 2% (motion # 3) to 10% (motion #9).

Figure 80 and 81 show the IDR and PSR for the NF set of motions. The IDR response of the Bridge II under the NF motions appears similar to the corresponding response for the Bridge I, where the IDR shows insensitivity between the 3 pile groups and the seismic motions (IDR in the range +1% and -2% for 19 out of the 20 motions). Only NF #16 motion (1994 Northridge, Olive View station, Fault Parallel component) shows difference between the Voigt and the Type II models for SSI reaching 8%. Over all the displacement ratio appears consistently lower (slightly though) than 1 indicating that the more accurate model for SSI results in slightly lower isolation system displacements. It is also interesting to observe that for the NF set, IDR for the 5x5 pile group, the "flexible" one, is consistently lower than the other 2 pile groups which is a behavior opposite from the one observed for the FF set of motions.

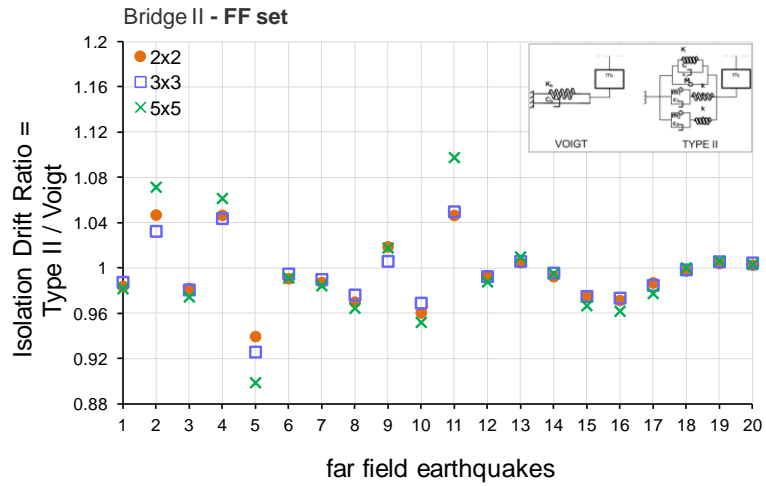


Figure 78. IDR for Bridge II and FF set.

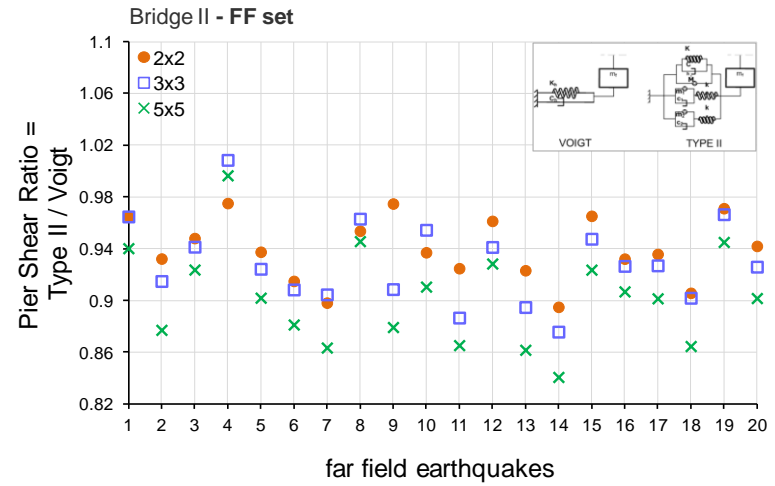


Figure 79. PSR for Bridge II and FF set.

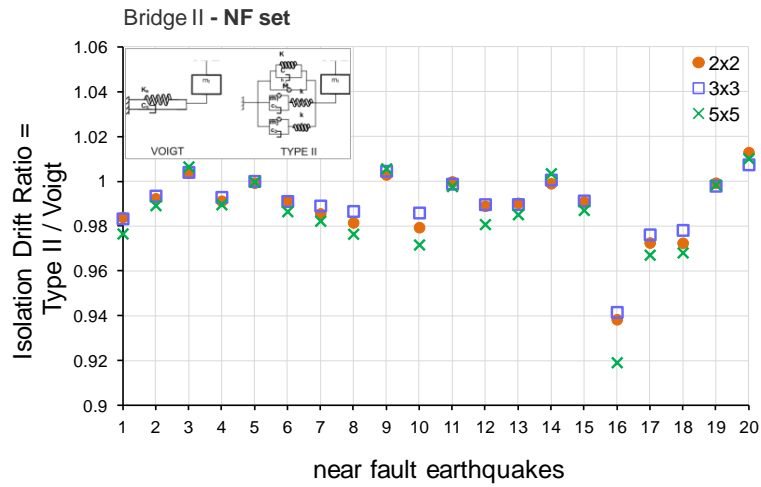


Figure 80. IDR for Bridge II and NF set.

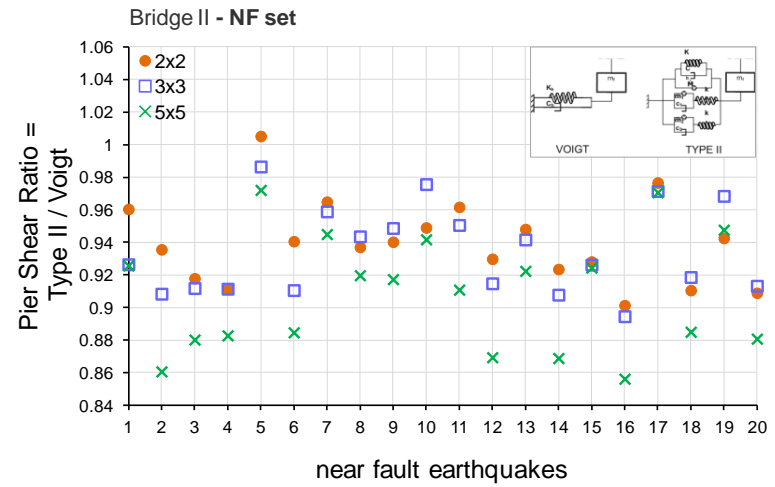
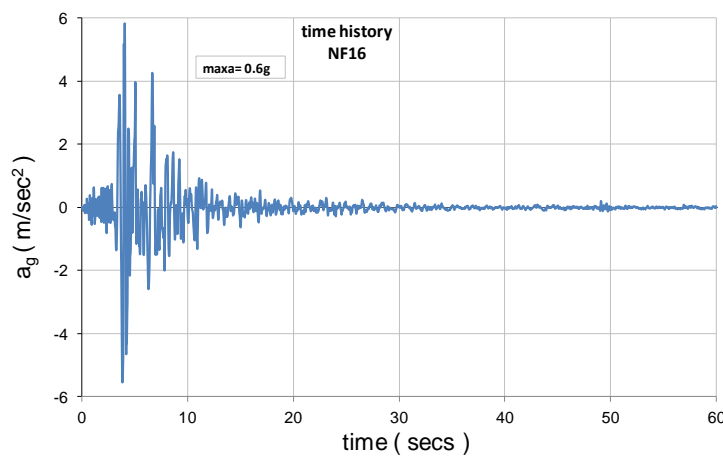


Figure 81. PSR for Bridge II and NF set.

The PSR shows similar behavior to the FF set of motions, -15% maximum and -8% on the average over all seismic motions. Again it indicates that using a more accurate SSI model (Type II) than the simple Voigt the shear forces in the pier are on the average 8% smaller over this FF motion set. PSR is sensitive to the pile group with differences between them ranging from 0% (motion # 17) to 8% (motion #2).

The NF16 excitation is the one which results in the larger differences for Bridge II. Therefore the time history responses of Bridge II will be presented and discussed next. *Figure 82* presents the time history of the NF16 seismic event (Olive View station) (see Table 9, §3.3).



**Figure 82. Acceleration time history of NF16 motion (Northridge 1994, Olive View station).**

*Figures 83, 84, 85, and 86* show the isolation system displacement history, the isolation system force normalized by the deck weight vs isolation system drift, the pier shear force normalized by the carried weight vs pier drift and the foundation system shear vs foundation drift for the NF16 respectively. There is only, approximately 10% difference in the isolation displacements between the Voigt and the Type II models as shown in *Figure 84*. Higher differences are observed in *Figures 85 and 86*. For the pier drift the difference reach 15% and for the pier shear forces are 17%. The higher values for all the responses occur for the simple SSI Voigt model. But the reasons for the differences occurring are investigated and presented, as analytically as possible.

After presenting the response of the two soil-foundation systems in *Figure 86*, it is obvious that there are differences between the Voigt and the Type II models concerning the maximum values of foundation's forces. The maximum foundation force for the Type II model is 13% less than the Voigt model. The same holds for the foundation's displacement. The main reason for this is the larger damping of the Type II model.

The comparison of the stiffnesses of the 3 pile groups highlights that the 5x5 group is the most “weak”, while the greater stiffness is performed by the 2x2 pile group. The same conclusion was also reached for Bridge I. The main reason for this is that the less the piles (and the greater the diameter) the smaller the interaction between them. Each pile has the space to develop the stresses and deformations, without interacting with another pile’s stress field.

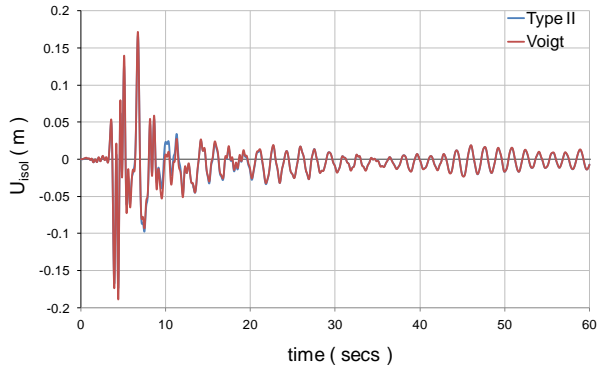


Figure 83. Isolation displacement for NF16 (Bridge II, 5x5 pile group).

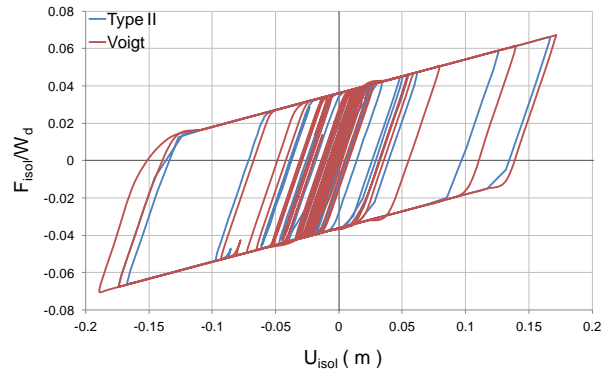


Figure 84. Isolation system loop for NF16 (Bridge II, 5x5 pile group).

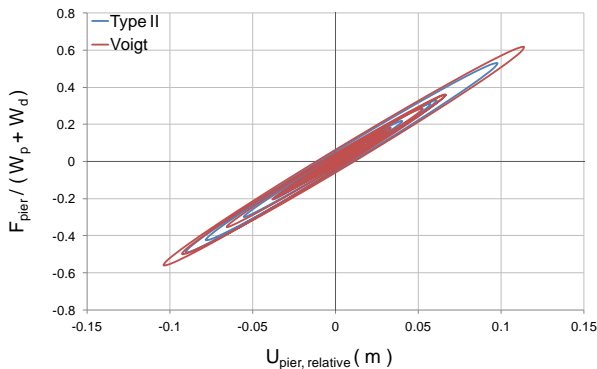


Figure 85. Pier shear vs pier drift for NF16 (Bridge II, 5x5 pile group).

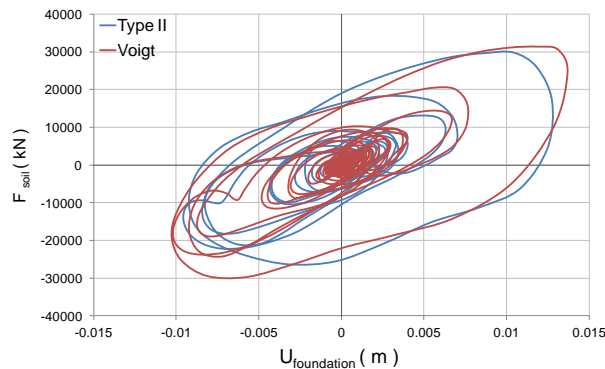


Figure 86. Foundation shear vs foundation drift for NF16 (Bridge II, 5x5 pile group).

Although the differences between the Type II and Voigt models reach the figure of 20%, neither of the 2 severe excitations (for Bridge I and for Bridge II) presented above correspond to larger displacements and forces when the Type II model utilized. Detailed responses of one more seismic motion, FF11 (Northridge 1994, Moopark station) are presented in Figures 80 to 84. Isolation system displacements for Type II model are 15% larger than the displacements from the Voigt model. However, the opposite is the case for the pier where the drift for the Voigt model is 16% larger and the pier shear is 19% larger.

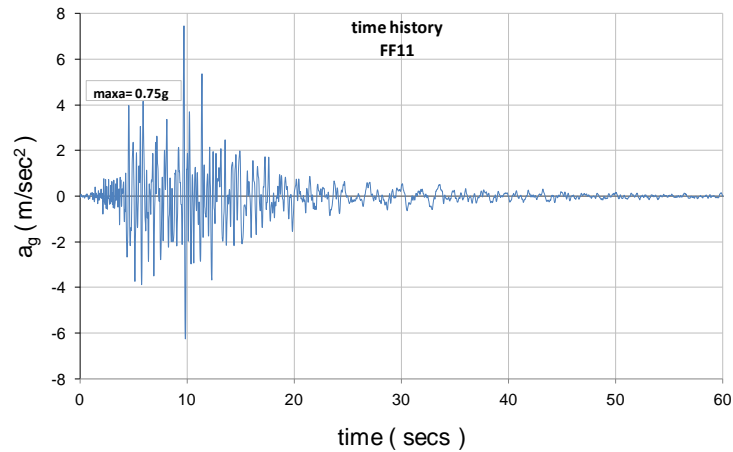


Figure 87. Acceleration time history of FF11 motion (Northridge 1994, Moopark station).

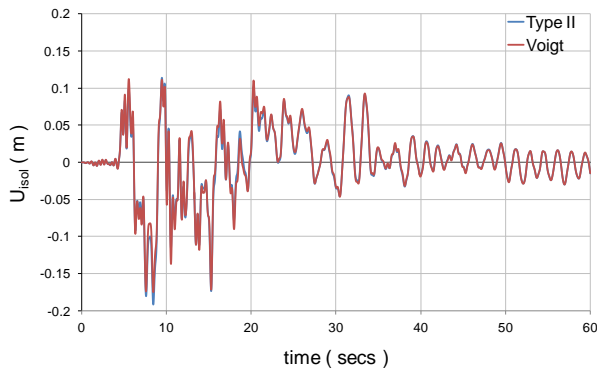


Figure 88. Isolation displacement for FF 11 (Bridge II, 5x5 pile group).

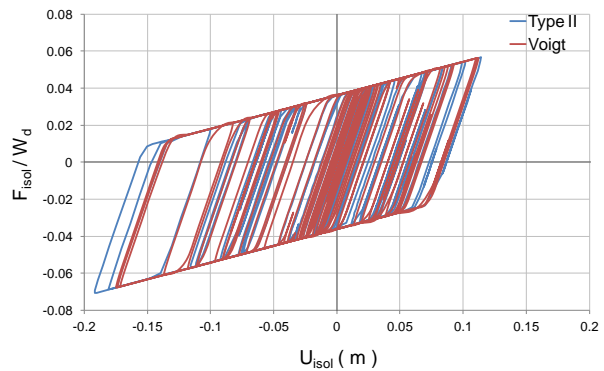


Figure 89. Isolation system loop for FF11 (Bridge II, 5x5 pile group).

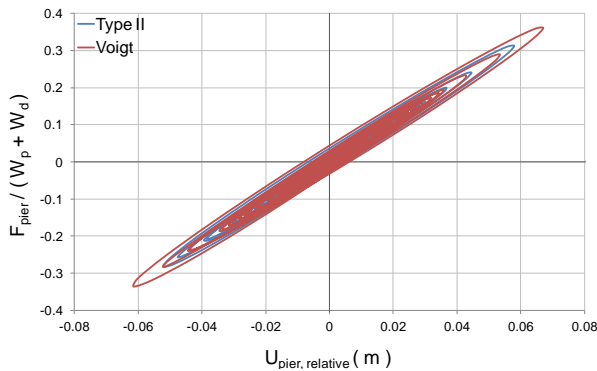


Figure 90. Pier shear vs pier drift for FF 11 (Bridge II, 5x5 pile group).

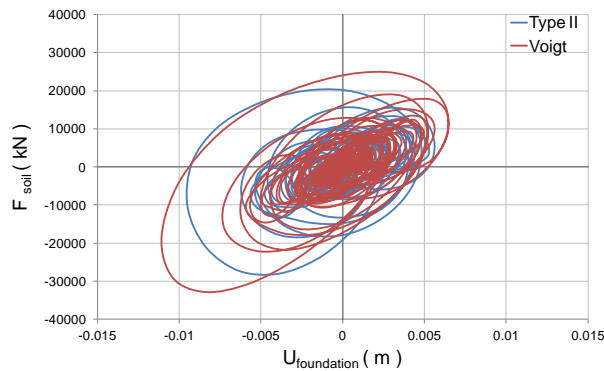


Figure 91. Foundation shear vs foundation drift for FF11 (Bridge II, 5x5 pile group).

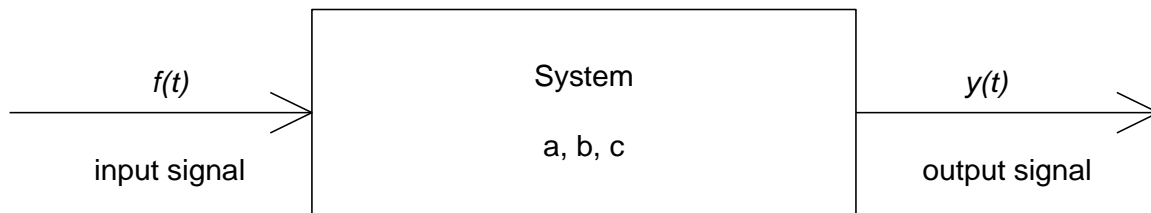
In general, the greatest discrepancies between the Type II and Voigt models appear for Bridge II, for both NF and FF sets of motions. Both bridge systems have also been examined to quantify the differences between the previously presented results of

the Voigt and the Type II systems with the third model (see §3.2), the so called *Simple Type II*. The comparison of the maximum values between this and the Type II model, for both bridges and sets of motion showed that the two systems behave almost identically. The rotational degree of freedom of the soil-foundation system doesn't seem to play a significant role in the specific seismic isolated models considered in this study. The maximum discrepancies observed hardly reached 5%. The model is going to be discussed again later in this study.

## 4.4. Qualitative Prediction of SSI Response

### 4.4.1. Transfer Function

In order to present the analysis results in a more comprehensive way, the concept of the *Transfer Function* is introduced. It will be helpful to develop a pictorial approach to the system modeling. To begin, we can imagine a differential equation as being a model of the engineering system which transforms the input signal  $f(t)$  into an output signal  $y(t)$  (the solution of the differential equation). The system is characterized by the values of the coefficients  $a$ ,  $b$ ,  $c$ , which are independent from the input signal. A different engineering system will be characterized by a different set of coefficients. This is easy to describe graphically:



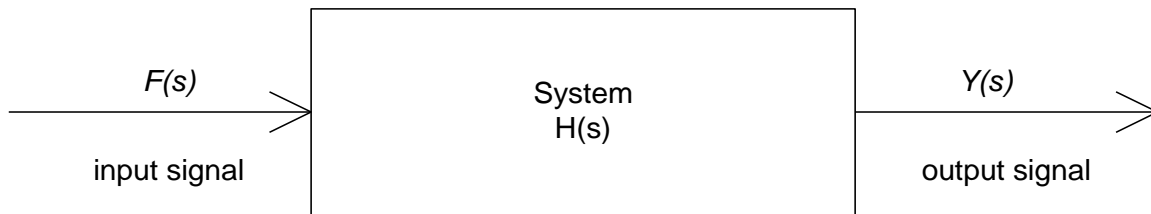
After the Laplace transform the differential equation is transformed into:

$$Y(s) = H(s)F(s), \quad H(s) = \frac{1}{as^2 + bs + c} \quad (42)$$

in which  $H(s)$  is the *Transfer Function*, which is nothing more than the ratio of the output to the input. In order the above to be obtained analytically, linearity and time-invariance are to be true/assumed for the system. Input is analyzed to an infinite sum of sinusoidal signals and output is formed as a sum of the responses to each sinusoidal function (linearity). The mathematical description of  $H$  can be defined in the time domain (differential equations), in the Laplace domain (transfer functions) and in the frequency domain (frequency response), with explicit relationships among the three counterparts. The following theorem can be put forward:

*The frequency response characteristics of a system can be determined from its Transfer Function, by substituting the Laplace variable  $s$  by  $j\omega$ , where  $\omega$  is the angular frequency (rad/sec).*

Finally, after the Laplace transformation the process can be graphically described as:



The TF provides an easy and efficient way of identifying the properties of a structure were the input and the response signals are recorded. The maximum values (peaks) of the TF indicate the eigenvalues (periods and corresponding damping). Eigenvalue analysis performed in §3.4 has resulted in the system properties. However, for this analysis to be performed the non-linear component of the system, the isolation system model, had to be replaced by an equivalent linear model and accordingly the results of the eigenvalue analysis are the properties of the equivalent linear system. Transfer Functions (ratio of the Fourier power spectra of the output to the input) are adopted in this study since they are not limited by the requirement for system linearity as is the eigenvalue analysis. The properties are obtained from the graphical representation of the TFs. The input signal is nothing more than the earthquake/input acceleration which filters through the structure. The output may be any quantity of the structure's response.

#### 4.4.2. White Noise or actual Seismic Motion as Input to the TF

As can be deduced from the above definitions, TF can be obtained independently of the characteristics of the input. Thus, one TF can be obtained from a seismic motion input into the system and another TF can be obtained from a white-noise acceleration as input. The “problem” with a real seismic event is that it can be decomposed to an infinite sum of sinusoidal signals with different frequencies, usually not uniformly distributed along the frequency range. The resonance may appear in structures that their periods are in accordance with the predominant period of the excitation. Thus, the TF of a real seismic event cannot present the accurate eigenvalues of the structure, as the governing frequency may suppress some eigen-periods which are really existing. For this purpose the TF from a “white noise” acceleration signal is used in this study. *White noise* is a random signal with a flat (constant) power spectral density. In other words, a signal that contains equal power within any frequency band with a fixed width. The TF of the artificial signal is expected to reveal all the eigenvalues of the structures studied.

#### 4.4.3. Structural System Properties

##### **Bridge I**

One important characteristic of nonlinear systems with plastic behavior is that their transfer functions show many peaks - with high amplitudes. This behavior is stronger the higher the strength of the system. These peaks are not necessarily located at the actual highest eigenperiod/s. When a white noise signal propagates through a structure it excites all the peaks (together with the ones due to plastic behavior) and thus makes the 4 eigenperiods of the system studied here hard to identify. The problem of identifying the periods of a system would be greater in the case where a real seismic event is the input to the system. A seismic input does not have uniform power spectrum (constant amplitude over the frequency domain) and as a result some periods/frequencies of the system might not be excited. To investigate the effect of the

isolation system strength on the Transfer Functions of the system, 3 analyses of the same system subjected to white noise were performed: where yield strength corresponds to:

- (i) 12% of the carried weight ( $F_y = 0.12 \cdot \text{deck weight}$ ),
- (ii) 3% of the carried weight ( $F_y = 0.03 \cdot \text{deck weight}$ ), and
- (iii) 0.5% of the carried weight ( $F_y = 0.005 \cdot \text{deck weight}$ )

The objective of this parametric analysis (varying the friction coefficient of the isolation system) is to unmask the period/s of the system which are hidden when the strength of the system takes relatively large values. *Figure 92* presents the white noise acceleration signal used in these analyses.

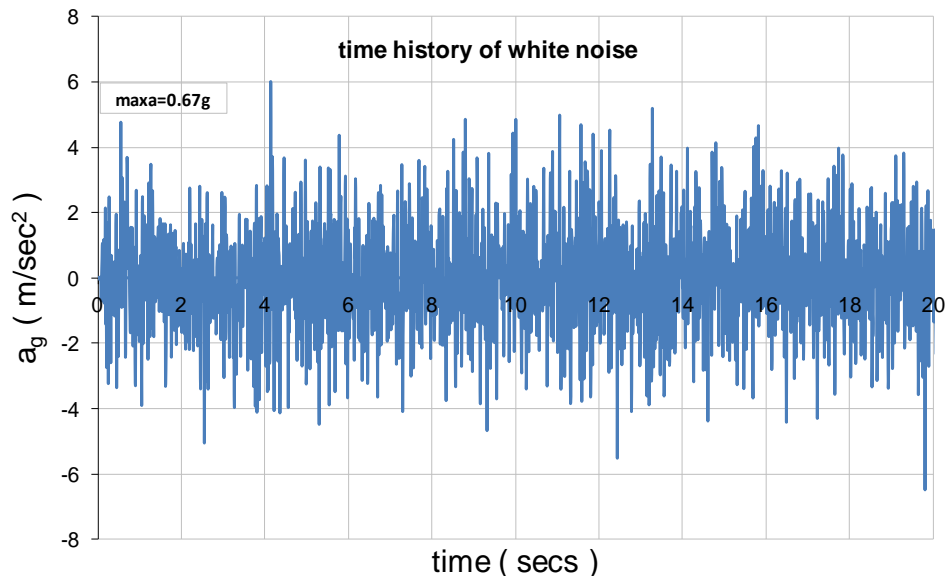


**Figure 92. White Noise signal: Acceleration vs time.**

*Figure 93* shows the TFs between the foundation acceleration (output) and the ground acceleration (input) of the 3 yield strength scenarios, as mentioned above. The specific TFs aim at identifying the periods of the system which correspond to the foundation oscillation modes (translational and rotational). Of course, any of the other periods may appear corresponding to the pier and/or the isolation mode. The smaller the strength (the less the friction) the clearer the resonances. It is evident that the curve corresponding to small friction is the smoother over all frequency range, where the TF for the system with 12% friction (green line) shows the more peaks.

When observing *Figure 94* it is evident that when the strength is very small (friction coefficient 0.5%) a peak at period of  $T \approx 2$  secs is very pronounced. This period matches the eigenvalue analysis results and is the isolation period of the system

considering the post yielding stiffness. It is obvious now, that large strength (friction coefficients) can suppress periods of the system. As it has already been mentioned the bilinear behavior of the isolator consists of 2 different periods (for Bridge I:  $K_e=26154$  kN/m  $\rightarrow T_e= 0.63$ secs,  $K_b= 0.1*K_e =2615.4$  kN/m  $\rightarrow T_b= 2$  secs). So, it wouldn't be wrong to say that the system finally performs with an effective period, depending on the maximum displacement of each cycle of the vibration. The peak that appears around 0.8secs in Figure 94 for  $F_y=12\%*W_d$ , is probably an effective period peak. The linearization of the isolator with a constant eigenperiod at  $T=2$ secs is not the real period based on a TF analysis but it's an upper limit of it.

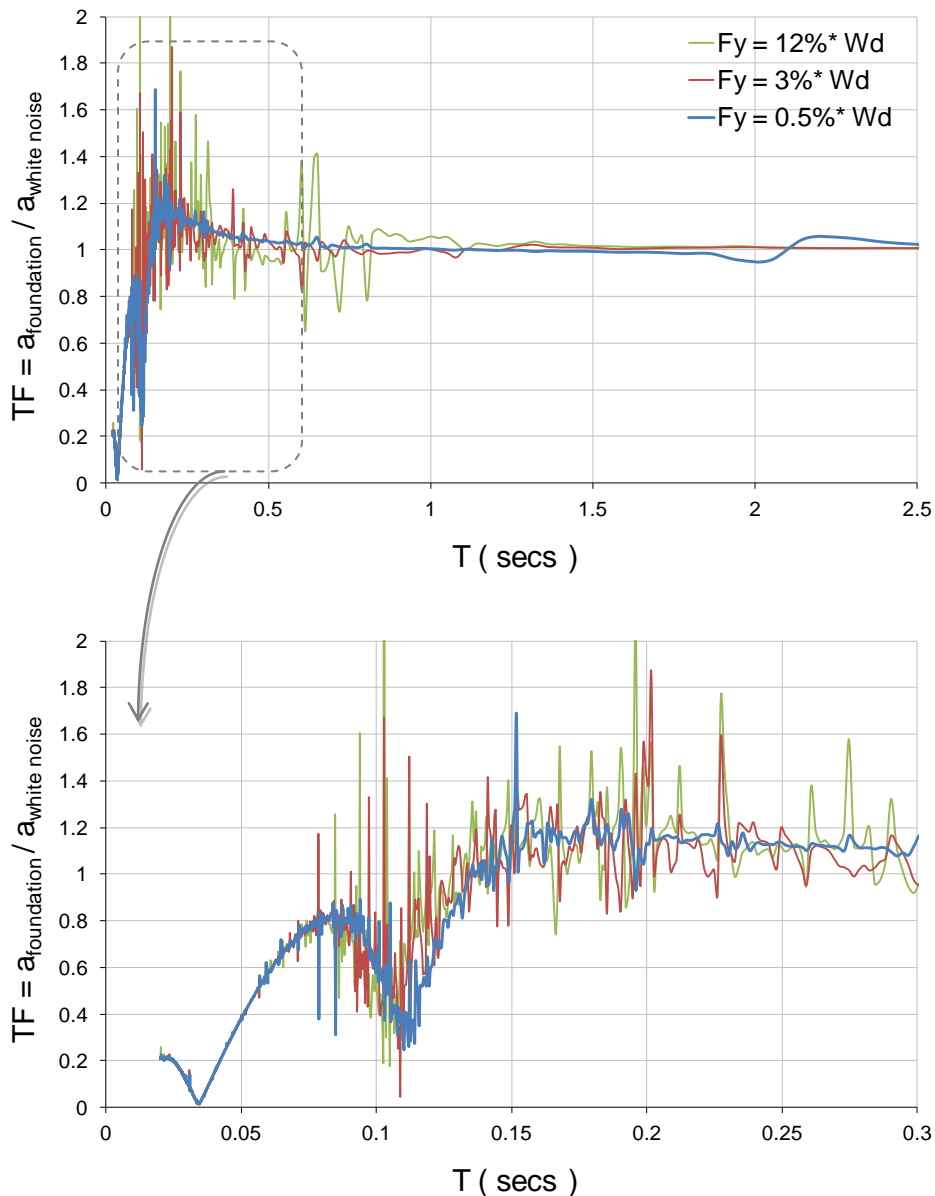


Figure 93. White Noise TFs  $a_{Type II} / a_g$ , (Bridge I, 5x5 pile group).

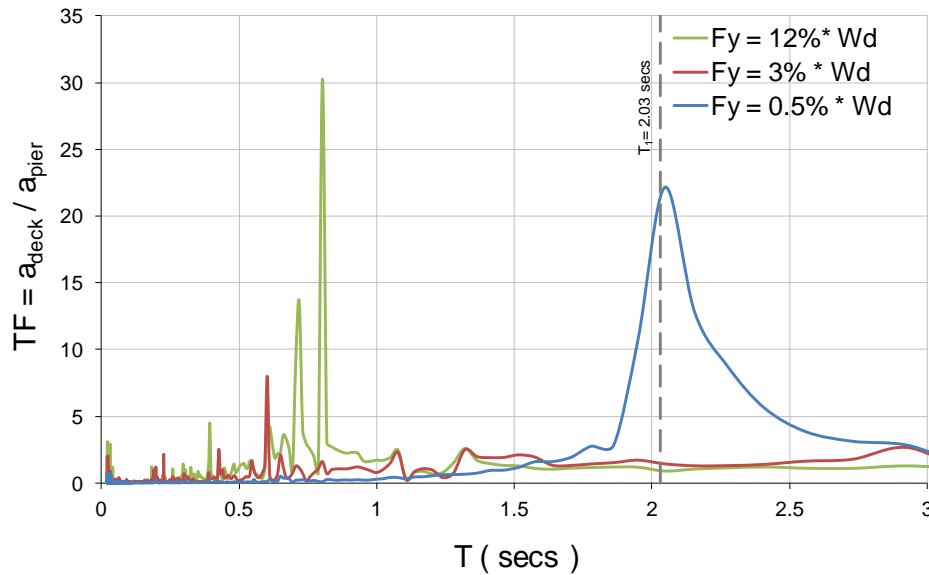


Figure 94. Transfer functions  $a_{deck} / a_{pier}$ , Bridge I, 5x5 pile group, white noise.

In *Figure 95* the TFs of the foundation's acceleration with respect to the incoming motion are shown for both Voigt and Type II models. The data plotted refer to the case of the lower friction ( $F_y/\text{weight}=0.005$ ). The red and blue dashed vertical lines are the periods from the eigenvalue analysis which are related to the foundation modes for both the Voigt and Type II models. The frequency range of the white noise signal doesn't allow the identification of system periods below  $T=0.02$  secs (max frequency = 50 Hz). Apart from the analyses performed, due to the large horizontal and rotational foundation stiffnesses the periods are expected to be very small. The conclusions that come of the TFs plots are quite clear. The existence of the soil-structure interaction that Type II model represents lengthens the periods, even though for a small amount, and makes the system more flexible compared to the system with the Voigt model. The peaks of the TFs are not in accordance with the eigenvalues and that is probably because of the linearity assumed at the case of eigenvalue solution.

*Figure 96* presents the TF between the pier horizontal acceleration and the foundation horizontal acceleration ( $TF = a_{pier} / a_{foundation}$ ). The peaks of the two TFs correspond to the eigenvalues related to the pier movement and almost coincide. Once more the SSI seems to make the pier a bit more flexible, fact that agrees with the values obtained from the eigenvalue analysis. The discrepancies observed between the peaks and the estimated periods represented by the vertical discontinuous lines may be due to the linearization of the isolation's system.

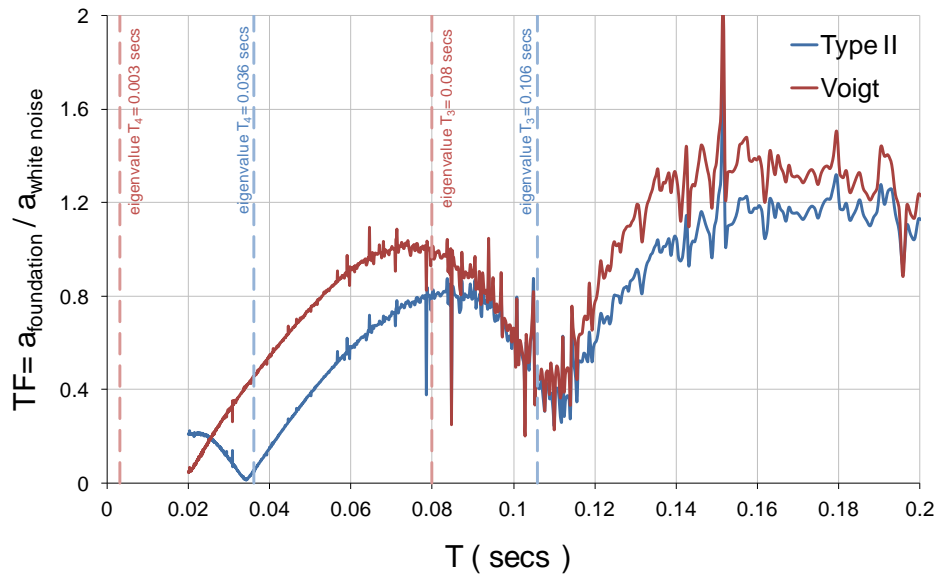


Figure 95. White Noise TFs  $a_{\text{foundation}} / a_{\text{ground}}$ , (Bridge I, 5x5 pile group,  $F_y/W_d=0.005$ ).

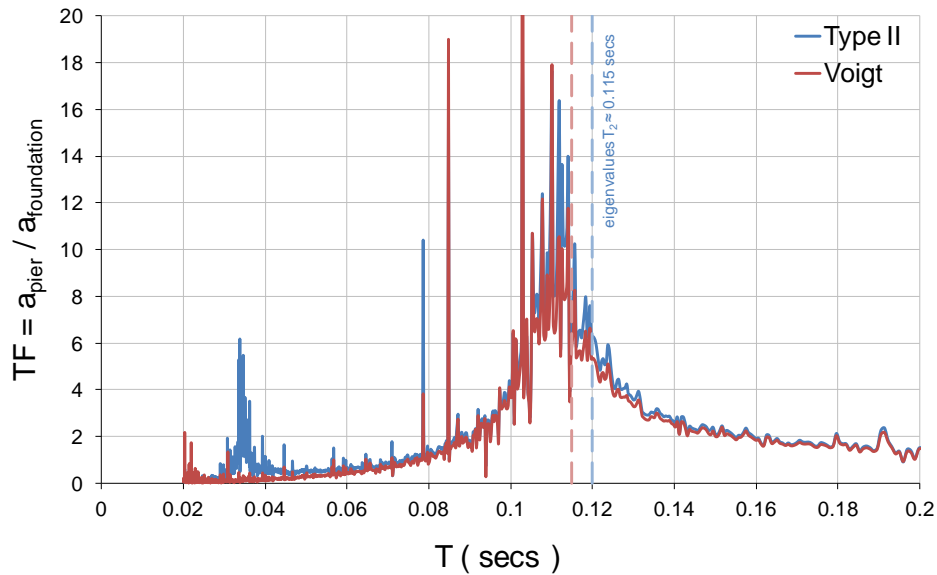


Figure 96. White Noise Transfer Functions  $a_{\text{pier}} / a_{\text{foundation}}$ , (Bridge I, 5x5 pile group,  $F_y/W_d=0.005$ ).

The concept of transfer functions (TF) of a structure subjected to a white noise signal is used now in combination with the Fourier Transform of the earthquake motion signal of interest to qualitative predict the effect of SSI on the structural response. It is done by comparing the range of frequencies which the motion’s energy is mainly concentrated with the structural system’s frequencies.

*Figure 97* shows the plots of the TFs of Bridge I ( $F_y/W_d=0.12$ ) under the white noise excitation, of the FFT of the NF12 seismic event and of the dynamic impedances of the 5x5 pile group. Considering that the predominant frequency of NF12 is around 12Hz ( $T=0.083$  sec) and the 3<sup>rd</sup> eigen-period is around  $T=0.08$  sec for Voigt model and  $T=0.106$  sec for Type II it appears that the SSI effect is not detrimental. It appears that the resonance scenario for the Voigt system is likely to happen but cannot be predicted with certainty as it is also controlled by other parameters, such as the duration of the excitation or the possible large damping. The SSI effects decrease the soil's horizontal impedance about 50% compared to the Voigt's ( $K_{x,Voigt}=421,000$  kN/m,  $K_{x,Type II}=205,000$  kN/m). On the other hand there is an extreme increase in the damping that is not shown in this *Figure 97*. The SSI with the Type II model 9 gives 1.24 times larger damping compared to the Voigt's model ( $C_{x,Voigt}= 8,416$  kN\*sec/m,  $C_{x, Type II}= 10,403$  kN\*sec/m). On the other hand, the rotational stiffness decreases up to 17% ( $K_{r,Voigt}= 17,000,000$  kN/rad,  $K_{r,Type II}= 14,100,000$ kN/rad) and the rotational damping part is amplified for about 2.3 times ( $C_{r,Voigt}= 345,483$  kN/m,  $C_{r, Type II}= 791,893$  kN/m). A significant remark concerning the above values is that the increased damping seems to outbalance the stiffness reduction of the Type II model which accompanies the SSI effects. Such an observation is going to be discussed further later. The same plots can be shown for the TFs that correspond to the pier's motion.

It would be very interesting to observe what would happen in the cases where the structure was founded on a 3x3 and a 2x2 equivalent pile groups. *Figure 98* shows the Transfer Functions of foundation accelerations to the ground acceleration of Bridge I with the Type II model for the 3 different foundations. It should be noted that the 2x2 and 3x3 pile groups are equivalent to the 5x5 pile group with same cross sectional area of the piles. It is expected not to see important discrepancies concerning the peaks of the TFs. *Figure 99* is comparing the foundation force ( $F_{Type II}$ ) versus foundation drift hysteretic loops for all three pile groups for the NF12 excitation. It is obvious that the less the piles (larger diameter), the greater the overall stiffness.

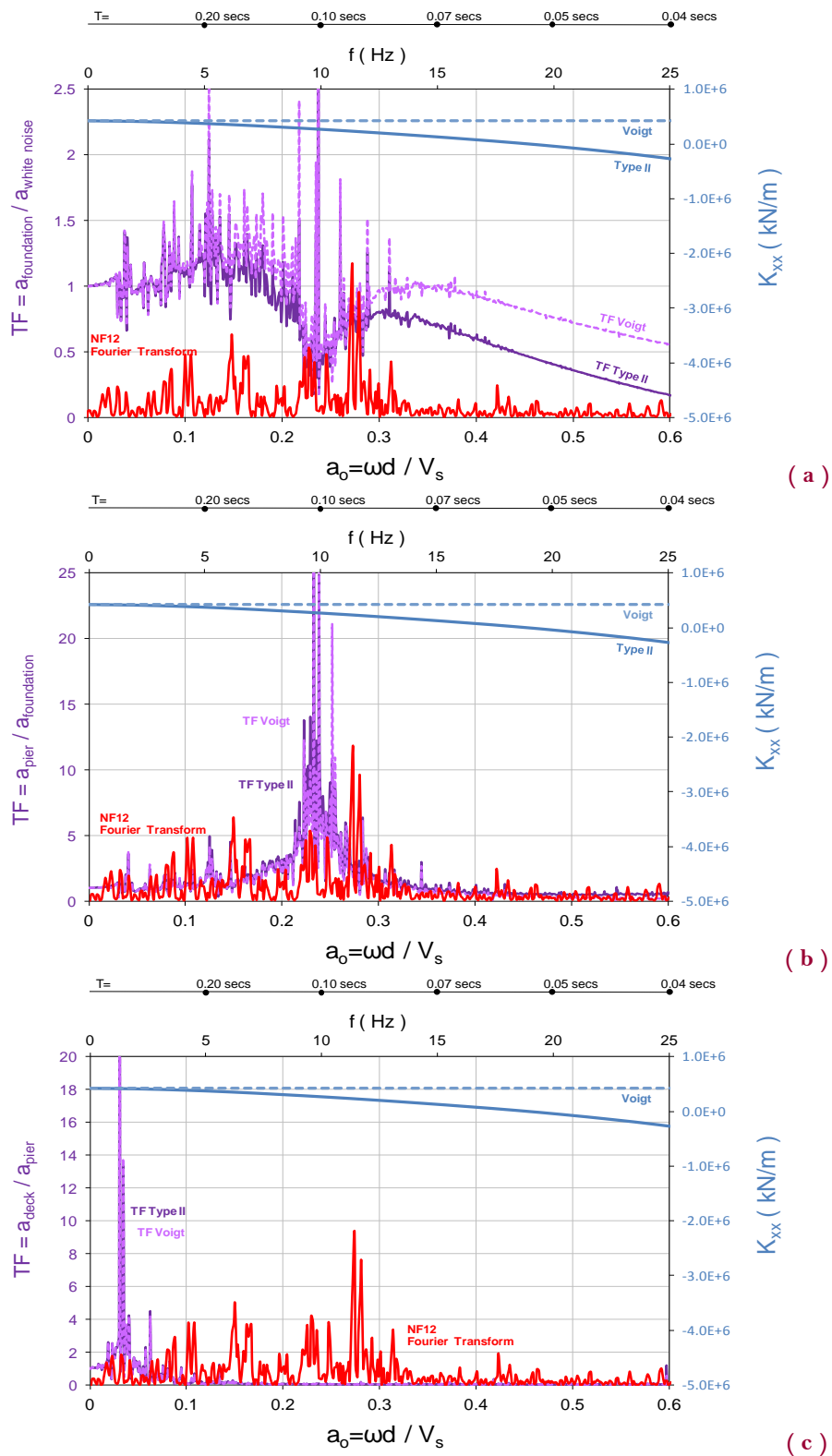


Figure 97. White Noise TFs (a)  $a_{pier}/a_{foundation}$ , (b)  $a_{foundation}/a_{whitenoise}$  (c)  $a_{deck}/a_{pier}$  of for Bridge I (purple and dashed light-purple line), Fourier Power spectrum of NF12 (red line), impedance functions of 5x5 pile group (blue and dashed blue lines).

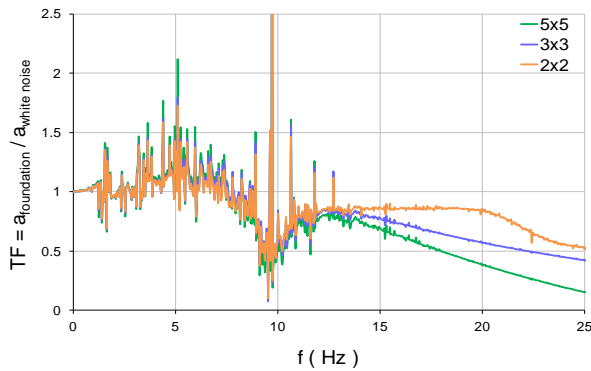


Figure 98. Transfer functions of Bridge I modeled with Type II system, for 5x5, 3x3 and 2x2 pile groups.

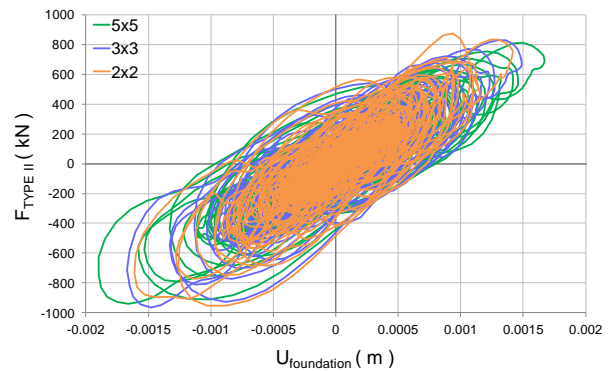


Figure 99. Graphical representation of Type II stiffnesses of Bridge I for 5x5, 3x3 and 2x2 pile groups, NF12.

## Bridge II

In order to understand the impact of NF16 on the Bridge II system, the transfer function concept is used again. Bridge II is analyzed for a low friction case (same as before,  $F_y=0.5\%*W_d$ ) and the suitable TFs are plotted so as the resonance points to be revealed and compared with the results of the eigenvalue analysis. More specifically, *Figures 100, 101 and 102* reveal the periods which are related with the isolation, the pier and the foundation motions, respectively. The peaks of the TFs are in quite good agreement with the values obtained from the eigenvalue analysis. The simplification considering the isolator to behave as a linear system has undoubtedly influenced the values of eigenperiods, as it has already been discussed for Bridge I.

In *Figures 103a, b and c* the seismic event NF16 is examined in the frequency domain, in comparison with the TFs of the system and the dynamic impedances of the soil-foundation system. The energy of the seismic motion is considered to be concentrated around 2 Hz, which is the 2<sup>nd</sup> eigen-frequency of both Type II and Voigt systems ( $T=0.46$  sec). At this frequency, the SSI effects drop the soil's horizontal stiffness up to 30% compared to the Voigt model ( $K_{x,Voigt}=1,780,000$  kN/m,  $K_{x,Type II}=1,260,000$  kN/m), while they increase the damping up to 1.2 times ( $C_{x,Voigt}= 144,864$  kN/m,  $C_{x,Type II}= 175,395$  kN/m). In addition, the rotational stiffness suffers a decrease of around 54% ( $K_{r,Voigt}= 700,000,000$  kN/m,  $K_{r,Type II}= 322,000,000$  kN/m) and the rotational damping part increases about 1.9 times ( $C_{r,Voigt}= 35,079,049$  kN/m,  $C_{r,Type II}= 65,610,813$  kN/m).

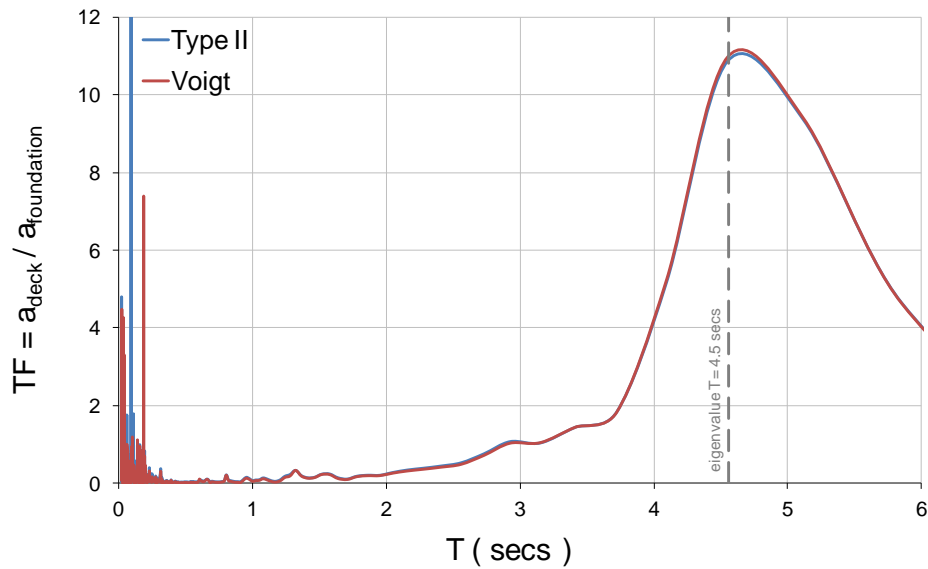


Figure 100. Transfer functions  $a_{deck} / a_{pier}$ , Bridge II, 5x5 pile group, white noise ( $F_y/W_d=0.005$ ).

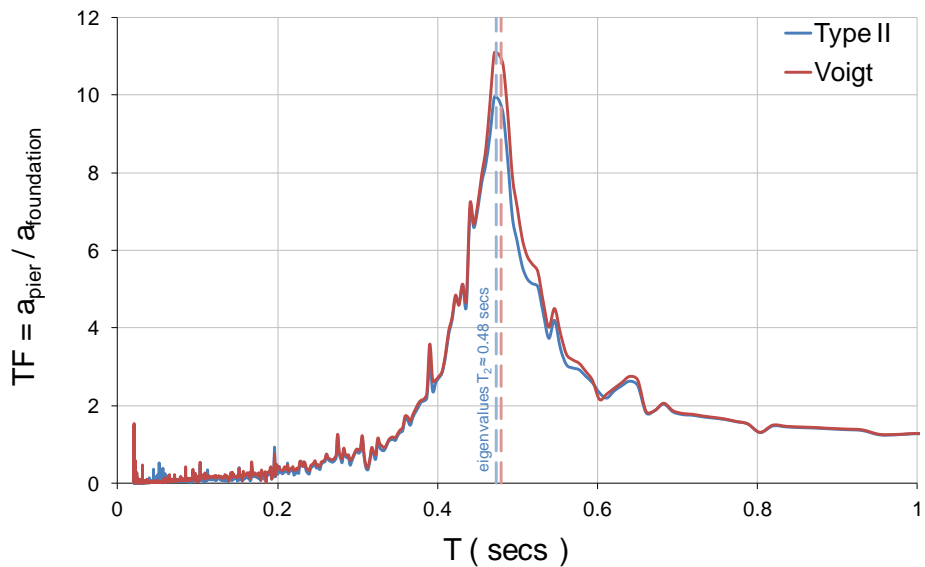


Figure 101. Transfer functions  $a_{pier} / a_{foundation}$ , Bridge II, 5x5 pile group, white noise ( $F_y/W_d=0.005$ ).

It should be noted that the TFs in Figure 103 are for the system with  $F_y/W_d=0.12$  and not the modified one with  $F_y/W_d=0.005$  as presented in Figures 100, 101, and 102. According to the discussion presented in Section 4.4.3 the non-linear hysteretic system with 12% strength masks the fundamental periods of the system and that is clear in Figure 96a where there is no distinct peak in the TFs at  $T=4.5$  secs corresponding to the post yielding period of the isolation system (with  $T_e= 1.42$  secs) but rather there are

2 peaks one at  $a_0=0.065$  ( $T=1.57$ secs) and next to it another at  $a_0=0.030$  ( $T=3.41$ secs). Both these peaks are probably effective values for the specific motion, with  $T=1.57$ secs to be the predominant.

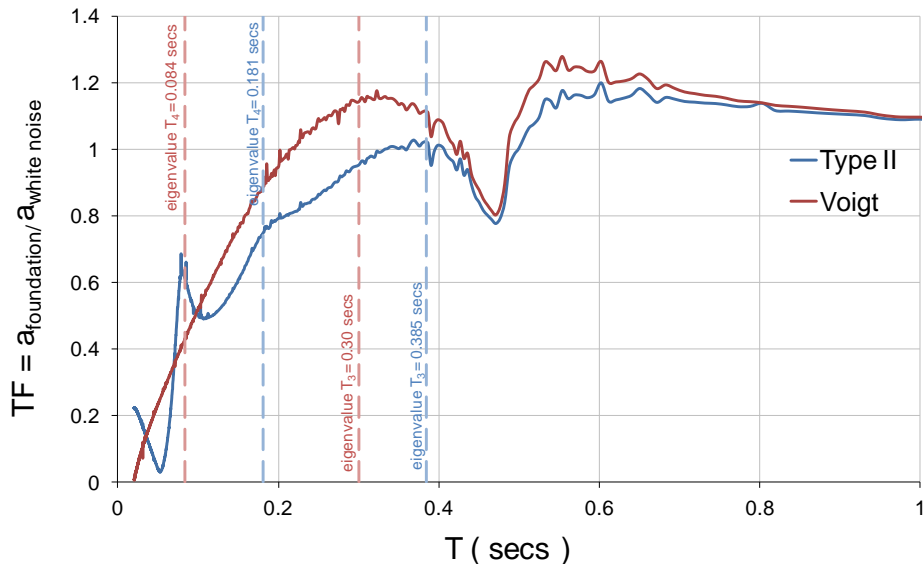


Figure 102. Transfer functions  $a_{\text{foundation}}/a_{\text{ground}}$ , Bridge II, 5x5 pile group, white noise ( $F_y/W_d=0.005$ ).

The energy/power of the seismic input is concentrated around  $T=0.5$  secs, with significant spread to larger periods. This cannot explain the effect on the isolation system response (see Figures 76, 77, 78 and 79) where the displacements are larger for the Voigt system in spite the fact that the Type II stiffness is smaller. However, from Figure 96(c) (the Voigt TF is higher than Type II) it can be deduced that the response (foundation acceleration) for the Voigt system should be larger than the Type II something which is confirmed in Figure 79 were indeed the foundation force for the Voigt system is larger than the Type II. The response of the isolation system might not be possible to be predicted directly from Figure 96 (a), because it is not affected directly by the acceleration of the ground but it is affected by the acceleration of the pier which has resulted from filtering of the ground acceleration 2 times, one through the soil-foundation springs and after through the pier.

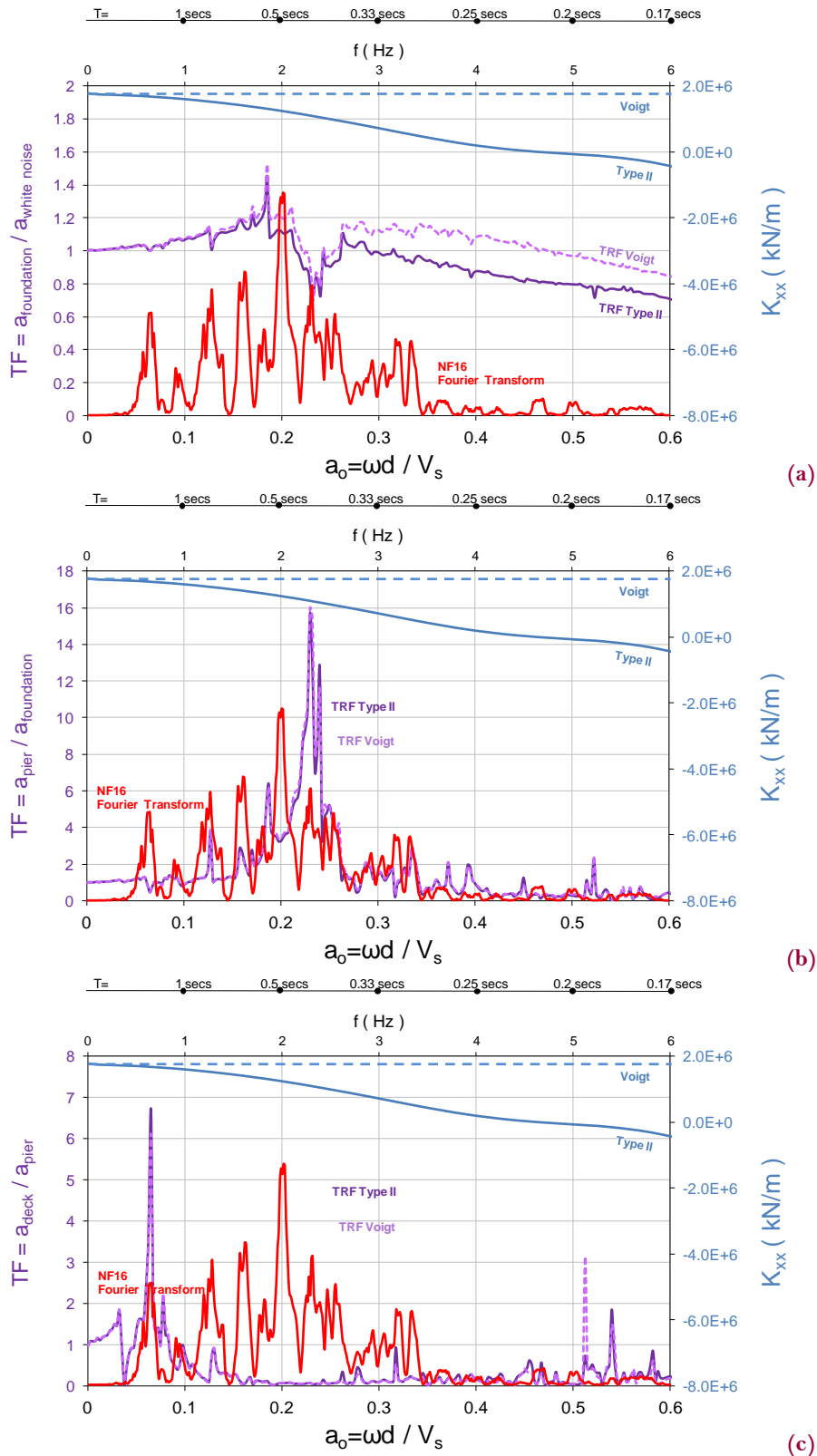


Figure 103. TFs (a)  $a_{deck} / a_{pier}$ , (b)  $a_{pier} / a_{foundation}$ , (c)  $a_{foundation} / a_{whitenoise}$  of Bridge II, FFT of NF16; (the scale of the FFT is not presented in figures) Impedance Functions 5x5 pile group

Figure 104 presents the TFs of the foundation for the three different pile groups considered in the study. In contrast to the Bridge I model these for Bridge II are different. This is supported by the findings in the groups of Figures 69, 70, 71, 72 and 78, 79, 80, 81 where there are strong differences between the 3 pile group cases for the Bridge II. Figure 105 presents the force-displacement loops of the Bridge II soil-foundation for the three pile group cases when excited by NF16 motion. It appears that for the 2x2 pile group the response is smaller as expected since this pile group is stiffer than the other two. The total stiffness that each pile group represents is increasing as the number of piles is getting smaller.

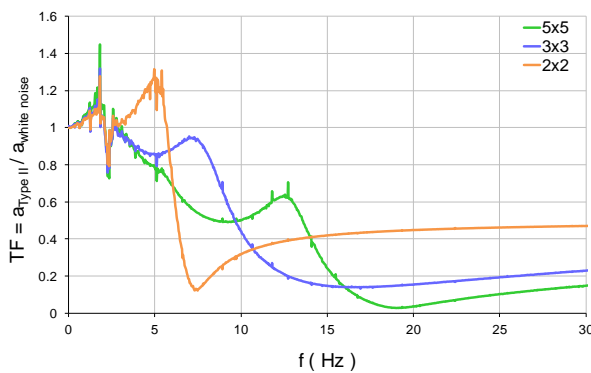


Figure 104. Transfer functions of Bridge II modeled with Type II system, for 5x5, 3x3 and 2x2 pile groups.

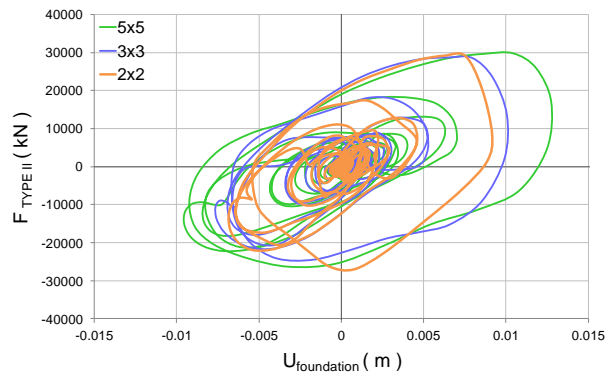


Figure 105. Graphical representation of Type II stiffnesses of Bridge II for 5x5, 3x3 and 2x2 pile groups, NF16.

In Figure 106(a) the seismic event FF11 is examined in the frequency domain, in comparison with the TFs of the system and the dynamic impedances of the soil-foundation system. This motion is the one which resulted in larger responses for the Type II model compared to the Voigt model for the isolation system response. However the response of the pier and the foundation were larger for the Voigt model. The frequency representation of the seismic input is concentrated around 2.5-4 Hz. The frequency dependent Type II model results in drop of the horizontal stiffness up to 87% ( $K_{x,Voigt}=1,780,000$  kN/m,  $K_{x,Type II}=229,000$  kN/m), while they increase the damping part up to 1.54 times ( $C_{x,Voigt}=144,864$  kN/m,  $C_{x,Type II}=222,492$  kN/m). Moreover, the rotational stiffness moves from positive to negative values ( $K_{r,Voigt}= 700,000,000$  kN/m,  $K_{r,Type II}= -429,000,000$  kN/m) and the rotational damping part increases about 2.22 times ( $C_{r,Voigt}= 35,079,049$  kN/m,  $C_{r,Type II}= 77,953,442$  kN/m).

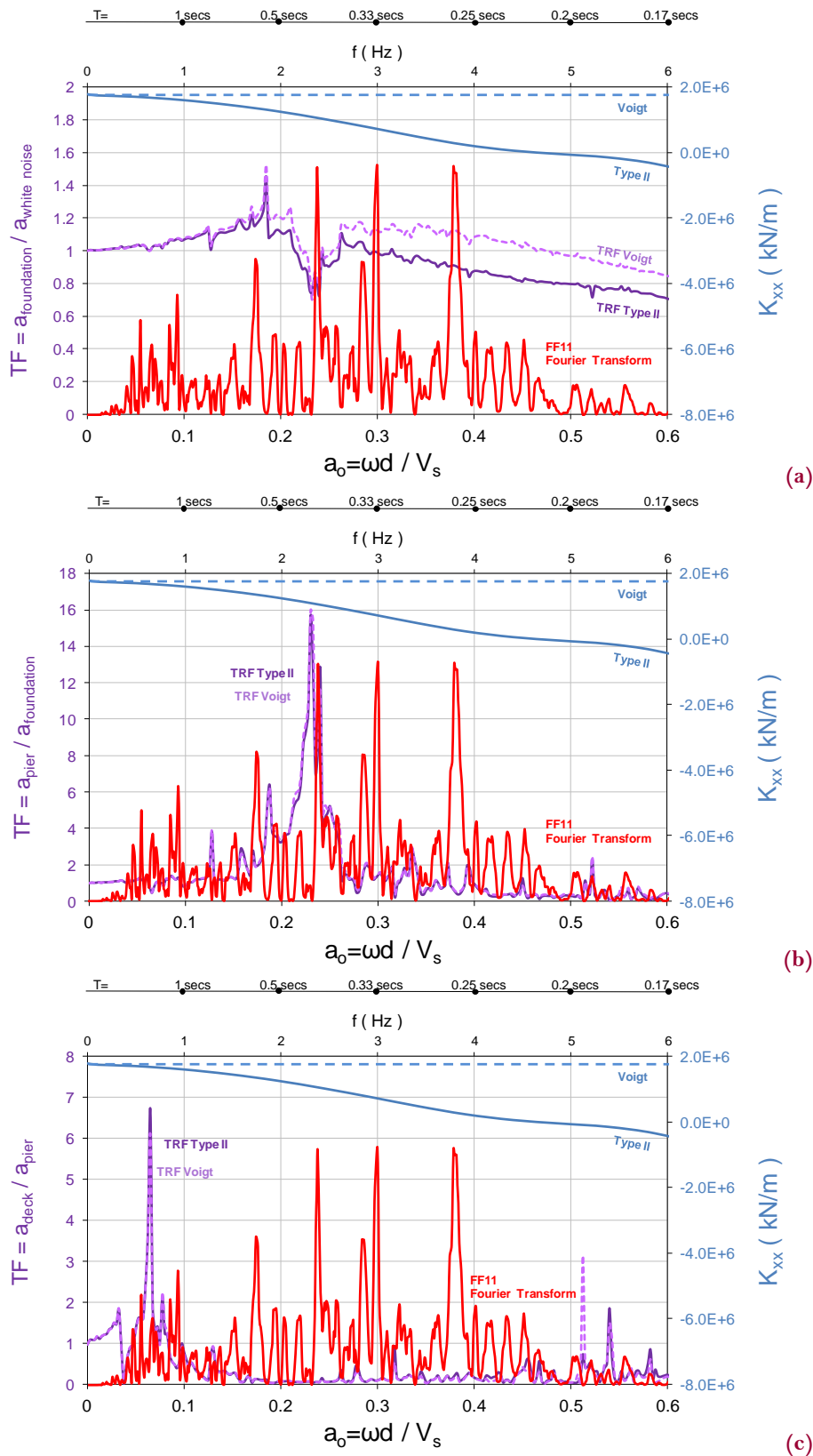


Figure 106. TFs (a)  $a_{deck}/a_{pier}$ , (b)  $a_{pier}/a_{foundation}$ , (c)  $a_{foundation}/a_{whitenoise}$  of Bridge II, FFT of FF11; Impedance Functions  $5 \times 5$  pile group.

In *Figures 106(b)* and *(c)* the vibration's main energy is compared in the frequency domain to the structure's periods, as indicated by the TFs. The seismic event excites a wide range of frequencies which contain approximately 3 of the 4 frequencies which characterize the structure with the Type II model. There is also a small amount of energy concentrated at the 4<sup>th</sup> eigenvalue of the system, that is related to the isolation's motion (*Figure 99c*,  $a_0=0-0.1$ ). At this point the damping part of the impedance function is small compared to the other points that the main earthquake's motion is located. The absence of large damping is definitely a parameter that would let the system develop large displacements and forces and even reach resonance, if the site conditions should allow it.

Considering all previous results it becomes apparent that the parameters influencing the behavior of a seismic isolated bridge are difficult to be predicted. The representative models of this study are tested for different seismic motions, foundation models, number of pile groups etc, in order to find the vulnerable aspects of the phenomenon. Undoubtedly the stiffness and mass of the structure, the geometry of the foundation (especially when it is about a flexible system), the relative stiffness of the piles and the soil, the incoming energy of the striking excitation etc., are some of the most important ones. So far, the majority of the excitations for the 2 bridge models seem to result in small differences in the displacements between the Type II and Voigt models. A reasonable explanation for this is that the presence of large damping does not allow for the stiffness differences to result in large displacement differences.

#### 4.5. Effect of $E_p/E_s$

The question that arises now is if there can be cases where the stiffness can be small and the damping also small. That would be definitely a case of interest concerning the SSI effects. The behavior of the dynamic impedance of the soil-structure system is controlled by the stiffnesses of the piles and the soil, as well as by the number of piles in the pile group. For this purpose the ratio  $E_p/E_s$  is the last parameter of studying. Bridge II, same as before, is the model of analyses (§.2.3, Table 4), founded on a 2x2 pile group with  $d=1.8$  m (same as 5x5 pile group) and  $S/d=10$ . The system will be investigated for 2 soil cases, both presented in *Table 13*. The first soil case is the same used in all the previous analyses. The second was chosen so as to represent the ratio  $E_p/E_s=1000$ , with the pile constructed by concrete. The set of seismic motions used is

the Far Field (§.3.3). It should be noted that the case of  $E_p/E_s=1000$  as shown in the table might represent an extreme case of soil properties ( $V_s=63$  m/s is very low) but close enough to the properties of the soil of the Mexico valley (Mexico City earthquake, 1985, soil structure interaction involved).

With the help of the software PILES, the impedance functions are calculated for the given frequency range ( $a_o = [0,1]$ ). *Figures 107 and 108* are the plots of the impedances for the horizontal and rotational degrees of freedom respectively, when  $E_p/E_s=300$ . *Figure 109 and 110* show the same quantities for the case  $E_p/E_s=1000$ . Although, the modulus of elasticity of the soil drops around 3 times from the first soil case to the second, the peaks and valleys of the impedances curve are almost at the same positions. On the other hand, the values change significantly and proportionally to the soil's stiffness. It is interesting to observe that the real part of the impedance which represents its stiffness is not constantly decreasing, while the imaginary part, its damping, is not constantly increasing. The peaks and valleys are the points of interest now. Depending on the excitation's main energy, the soil-foundation may react with a larger stiffness than the Voigt's model and with a smaller damping.

**Table 13. Properties of the soil profiles.**

<b>Total Thickness ( m )</b>	21.5	21.5
<b>Homogeneous / Inhomogeneous</b>	Homogeneous	Homogeneous
<b>Halfspace / Rigid Base</b>	Halfspace	Halfspace
<b>Shear Wave Velocity, <math>V_s</math> ( m/sec )</b>	110	63
<b>Mass Density, <math>\rho_s</math> ( kg/m<sup>3</sup> )</b>	1800	1800
<b>Damping Ratio, <math>\xi</math></b>	0.10	0.10
<b><math>G = \rho_s V_s^2</math> ( MPa )</b>	22	7.1
<b><math>E_s = 2(1+\nu)G</math> ( MPa )</b>	62	20
<b><math>E_p/E_s</math></b>	<b>300</b>	<b>1000</b>
<b>Poisson's Ratio, <math>\nu</math></b>	0.40	0.40

Considering the above observations, it becomes clear that the flatness of the impedances through the frequency range is controlled mainly by the ratio  $S/d$ . That is the reason why the  $2 \times 2$  pile group with  $S/d=10$  was chosen. Many other cases could have been studied, such as a stiffer bridge model, a pile group made of steel and a stiffer soil.

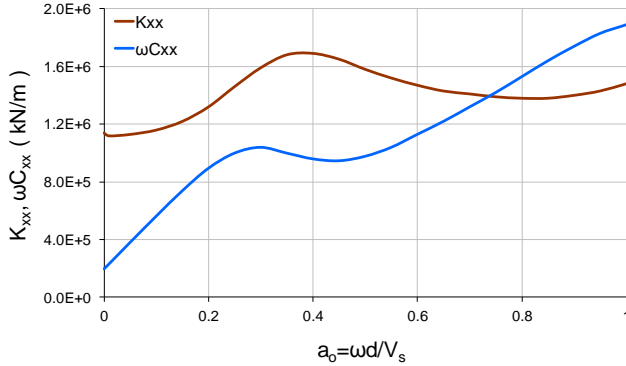


Figure 107.  $K_{xx}(\omega)$  for Bridge II, with the  $2 \times 2$  pile group, ( $d=1.8\text{m}$ ,  $S/d=10$ ,  $E_p/E_s=300$ ).

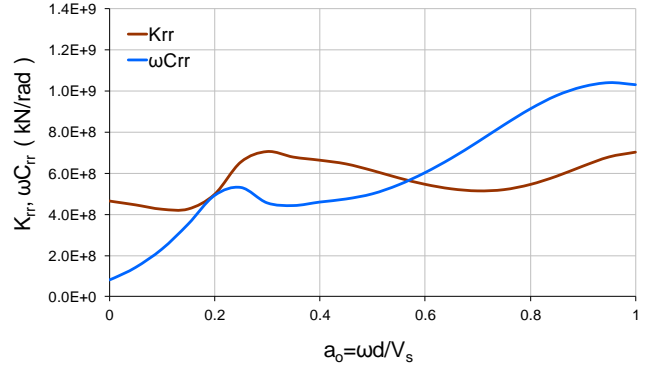


Figure 108.  $K_{rr}(\omega)$  for Bridge II, with the  $2 \times 2$  pile group, ( $d=1.8\text{m}$ ,  $S/d=10$ ,  $E_p/E_s=300$ ).

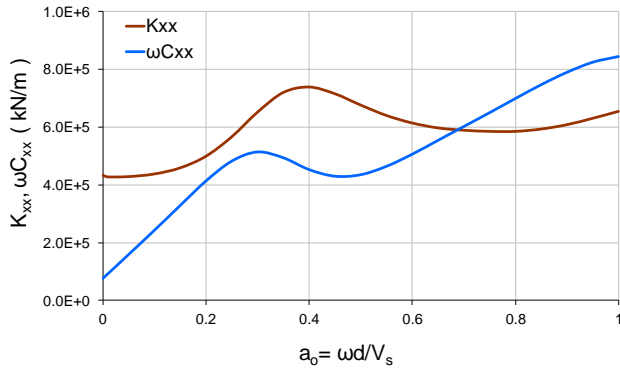


Figure 109.  $K_{xx}(\omega)$  for Bridge II, with the  $2 \times 2$  pile group ( $d=1.8\text{m}$ ,  $S/d=10$ ,  $E_p/E_s=1000$ ).

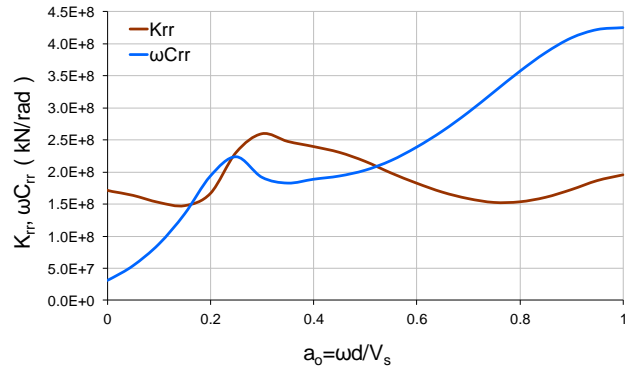


Figure 110.  $K_{rr}(\omega)$  for Bridge II, with the  $2 \times 2$  pile group ( $d=1.8\text{m}$ ,  $S/d=10$ ,  $E_p/E_s=1000$ ).

The maximum values of the Isolation Drift Ratios and Pier Shear Ratios between Type II and Voigt models (relations (40) and (41)), for the far field set of motions are shown in *Figures 111* and *112*. The frequency variation of the impedances for the  $2 \times 2$  pile group for of the specific soil conditions seems to play important role in the Type II response. For the case of  $E_p/E_s=1000$ , there is one excitation where the isolation system reaches 28% larger displacements for Type II, while for the rest of the motions the differences on the isolation drift are between +10% and -10% . For  $E_p/E_s=300$  the differences are no more than +5% or -5% between Type II and Voigt.

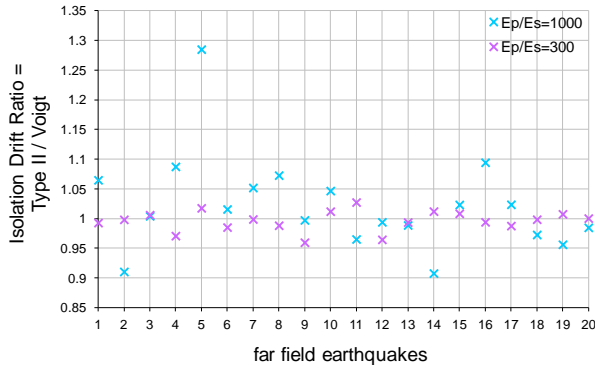


Figure 111. Bridge II IDR vs seismic motions for FF set.

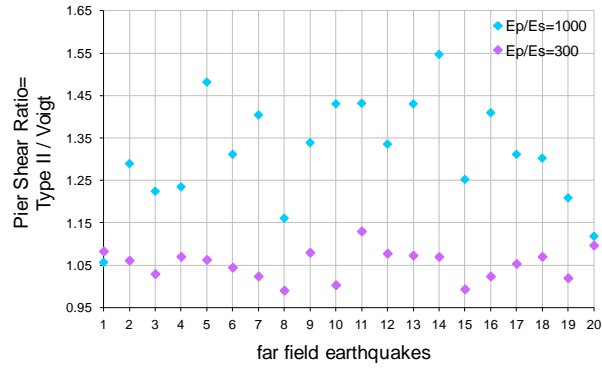


Figure 112. Bridge II PSR vs seismic motions for FF set.

The discrepancies are larger between the two models for the pier shear forces. Especially for the case of  $E_p/E_s=1000$ , there are motions that develop up to 45% larger pier shear forces when Type II model is utilized. The case of  $E_p/E_s=300$  shows maximum differences up to 17%.

Time history results are presented in Figures 113 and 114 for the FF05 seismic event, where isolation displacements, pier drifts, pier shear forces, and foundation forces are larger for the Type II model for the case of very soft soil ( $E_p/E_s=1000$ ).

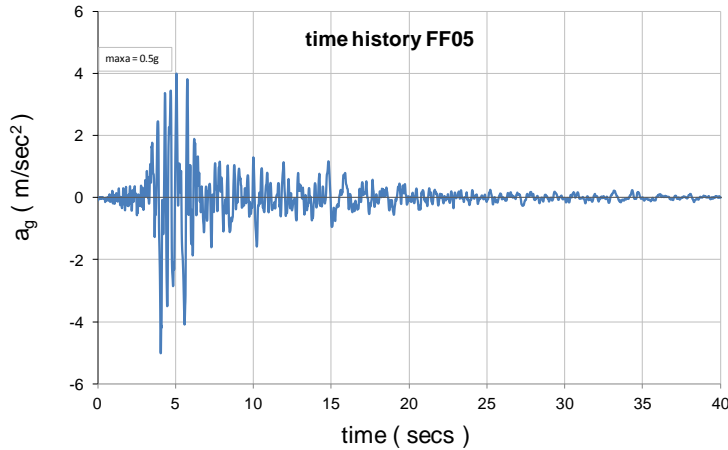
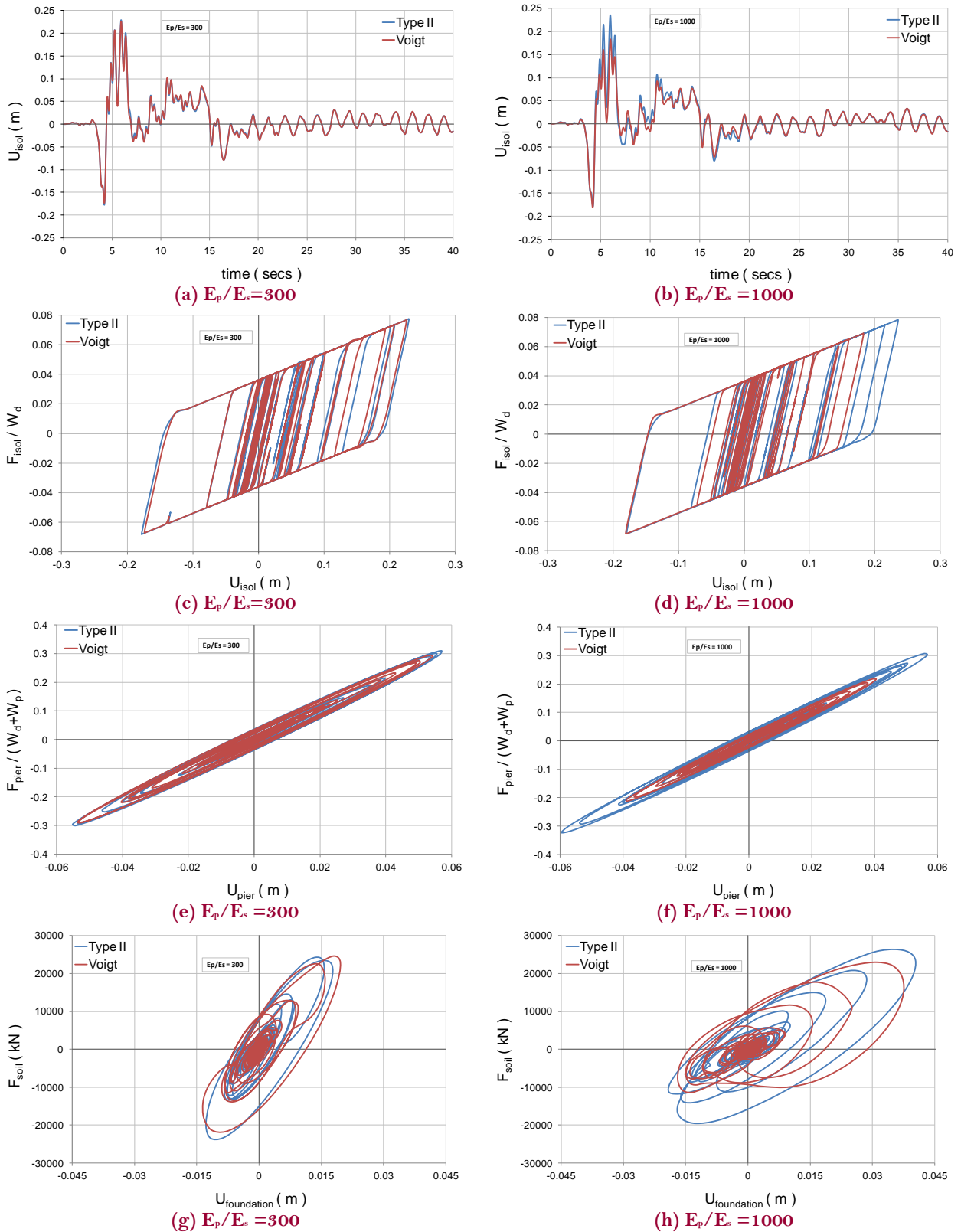


Figure 113. Time history of FF05 seismic event (1989, Loma Prieta).



**Figure 114. Bridge II with 2x2 pile group and  $S/d=10$  Responses for far field seismic motion FF05. (a) and (b) are Isolation system displacements; (c) and (d) are Isolation system hysteresis; (e) and (f) are Pier Shear vs Pier drift; (g) and (h) are Soil Foundation system hysteresis.**

Figures 115 present the soil–foundation impedances together with the input seismic motion representation in the frequency domain. The foundation spring stiffness activated in the case of Type II model is larger than the Voigt’s ( $a_0=0$ ) while the damping (tangent of the blue curve) is. Particularly for  $E_p/E_s=300$  there is a stiffness amplification with respect to Voigt of 1.4 times around  $a_0=0.5$  where most of the seismic energy is concentrated and at the same time a drop of the damping value around 4 times. The same changes hold also for the case  $E_p/E_s=1000$ , where the stiffness gets 1.25 times greater when the SSI is in action and the damping decreases around 7 times.

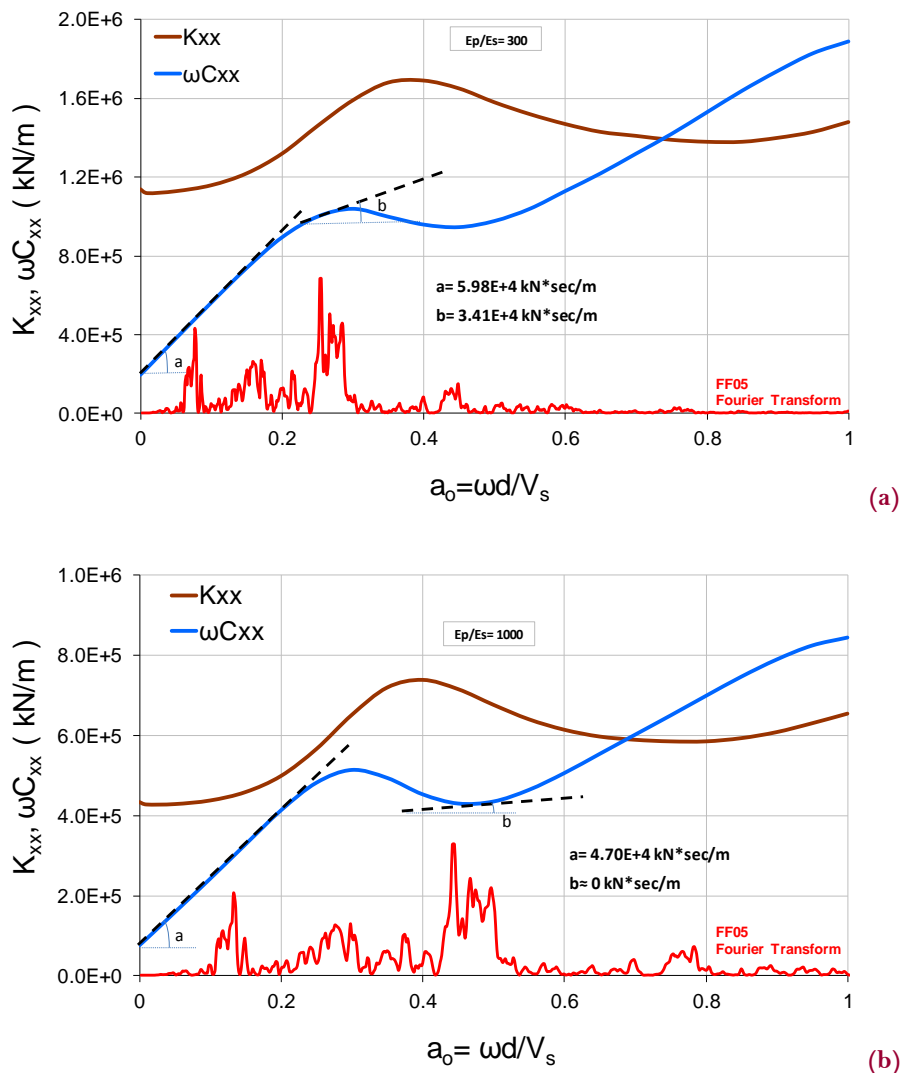


Figure 115. Fourier amplitudes of FF05 seismic event for the two cases of soil (a)  $E_p/E_s= 300$ ; (b)  $E_p/E_s= 1000$ .

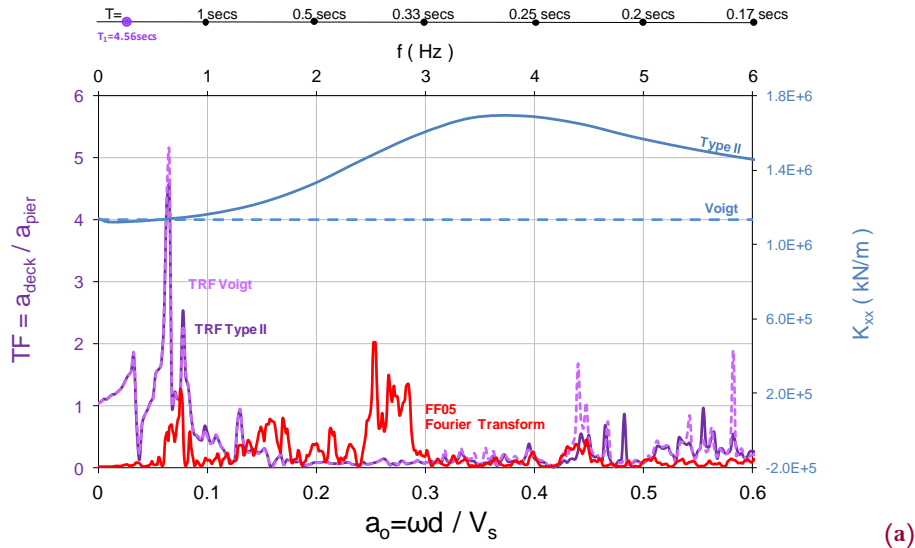
What it impressive is that so far the inverse changes had taken place during the soil-structure interaction: amplification of damping and weakening of stiffness. Before comparing the transfer functions of the system with the soil-foundation impedances and the frequency representation of the seismic input an eigenvalue analyses was performed for the Bridge II model, founded on a  $2 \times 2$  pile group, for the cases:  $S/d=10$ ,  $d=1.8\text{m}$ ,  $E_p/E_s=300$  and  $1000$ . The results of the eigenvalue analysis are presented in *Table 14*. Once again, a simplified linear isolation model was considered with damping ratio  $\xi=10\%$ , so as to represent the dissipated energy by the real bilinear isolator.

**Table 14. Eigenvalues of Bridge II, for the  $2 \times 2$  pile group,  $S/d=10$ ,  $d=1.8\text{m}$ .**

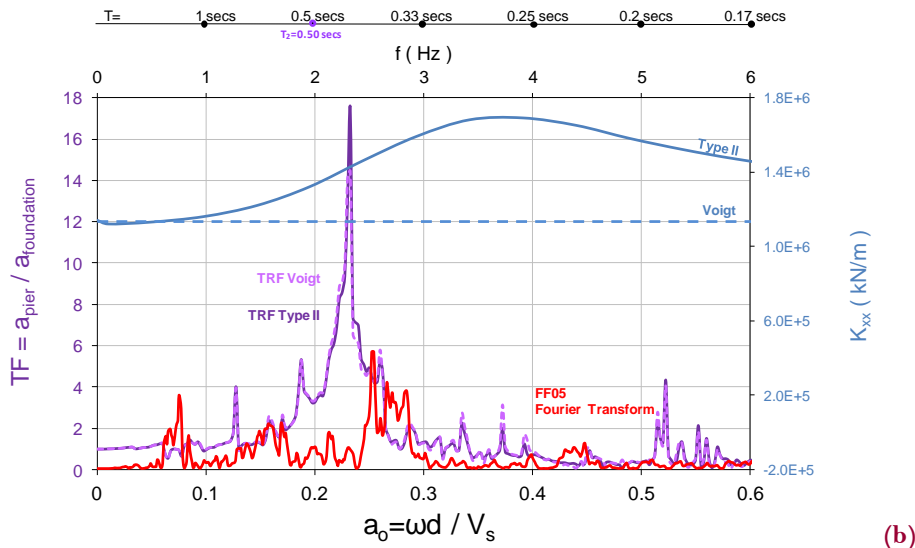
mode	Type II				Voigt			
	$E_p/E_s=300$		$E_p/E_s=1000$		$E_p/E_s=300$		$E_p/E_s=1000$	
	T (sec)	$\xi$	T (sec)	$\xi$	T (sec)	$\xi$	T (sec)	$\xi$
#1	4.563	9.60%	4.576	9.57%	4.563	9.60%	4.576	9.57%
#2	0.492	11.47%	0.890	64.85%	0.500	13.13%	0.658	45.89%
#3	0.386	30.91%	0.534	17.28%	0.360	37.38%	0.442	17.11%
#4	0.278	19.19%	0.389	14.19%	0.215	100%	0.396	100%

The eigenvalues of the structures are needed to aid the identification of the structural properties from the TRs of the non-linear hysteretic system. Based on periods of the structure from eigenvalue analysis (Table 14) and on the fact that the TF's peaks are satisfactorily show them, *Figures 116* give some explanation for the results of the previous plots, for the case that  $E_p/E_s=300$ . The three figures are combining the Fourier transform of the excitation of interest, the TFs of the accelerations between the ground and the foundation, the foundation and the pier, the pier and the deck and the impedance functions for the  $2 \times 2$  pile group. Although *Figure 115* reveals the active stiffness and damping, the final performance of the structure depends on its physical characteristics. From the 3 plots in *Figure 116*, the following are observed: a small amount of the FF05 energy enters into the structure around the isolation system frequency ( $a_0=0-1$ ), while a larger amount, excites the structure at

higher-frequencies ( $a_0=0.25-0.3$ ) around the frequencies corresponding to both the pier and the foundation. For the range of frequencies of the pier and the foundation, their corresponding stiffness increases and the damping decreases. The input energy seems to be concentrated around the period related to the Type II foundation motion and that's the main reason for the differences observed at the pier and foundation loops (Figures 114e and 114g).



(a)



(b)

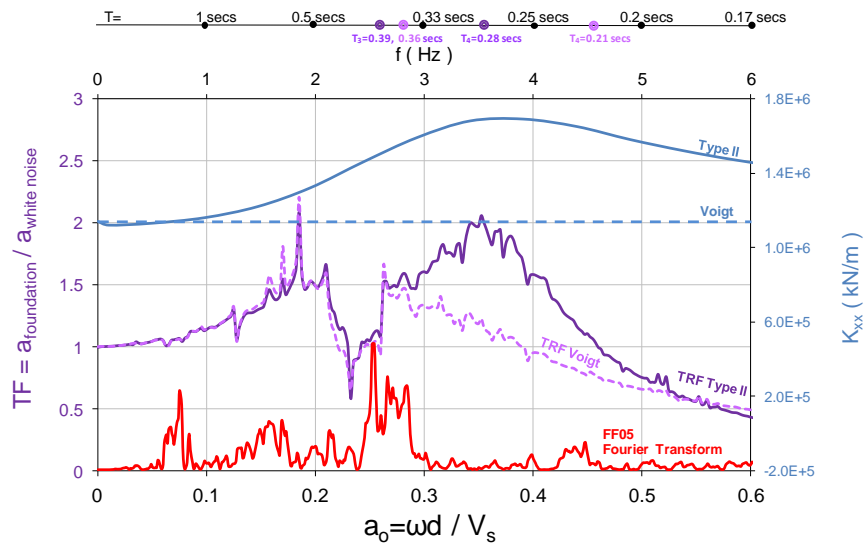
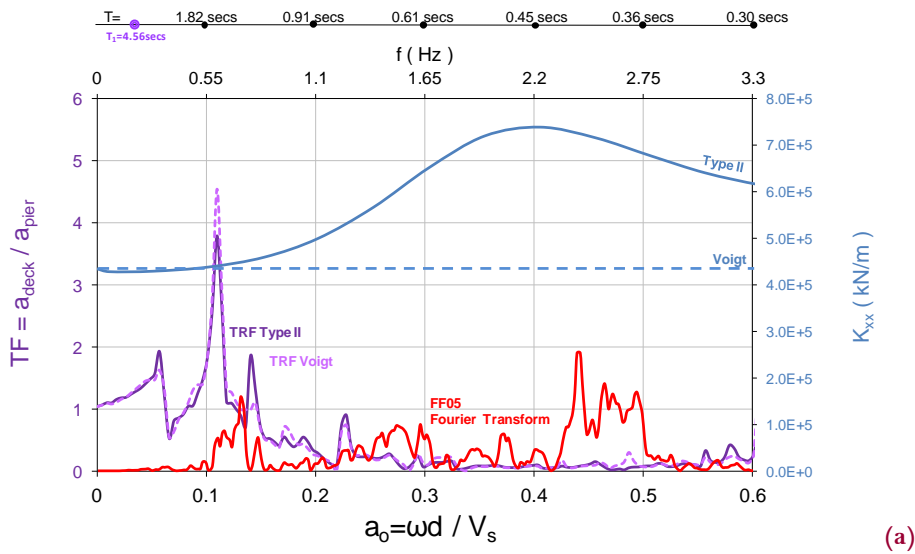
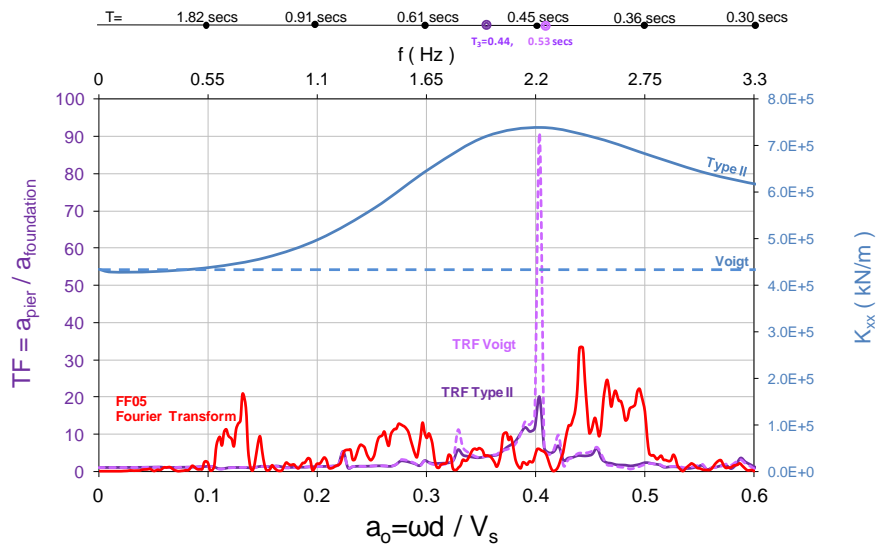


Figure 116. TFs (a)  $a_{deck}/a_{pier}$ , (b)  $a_{pier}/a_{foundation}$ , (c)  $a_{foundation}/a_{whitenoise}$  of Bridge II, FFT of FF05;  $E_p/E_s=300$ ; Impedance Functions  $2 \times 2$  pile group.

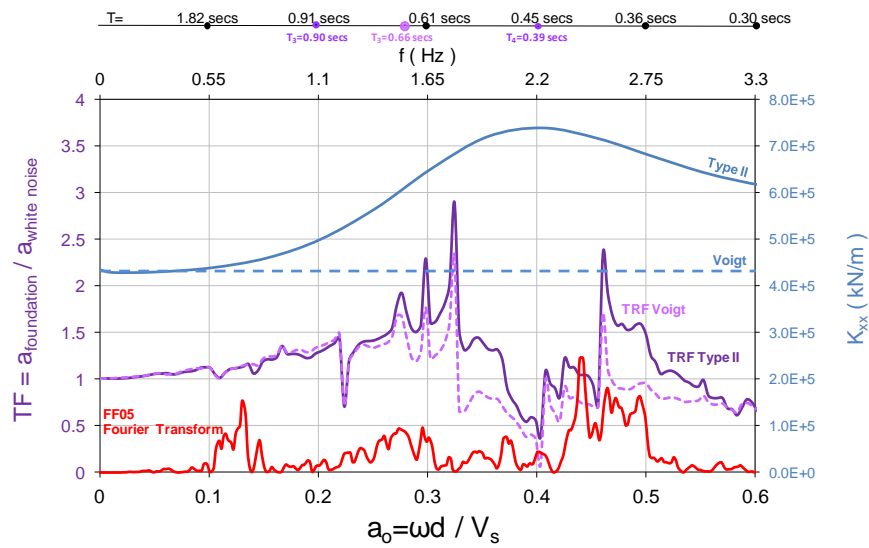
At the second soil case, where  $E_p/E_s=1000$ , the energy probably enters into the structure through the isolation and foundation systems (as seen in Figure 117). The main seismic energy activates larger stiffness for the Type II model, while the damping is almost zero. Due to the absence of damping, which finally controls the displacements, both Voigt and Type II models are expected to have large differences in their response.



(a)



(b)



(c)

Figure 117. TFs (a)  $a_{\text{deck}} / a_{\text{pier}}$ , (b)  $a_{\text{pier}} / a_{\text{foundation}}$ , (c)  $a_{\text{foundation}} / a_{\text{whitenoise}}$  of Bridge II; FFT of FF05;  $E_p / E_s = 1000$ ; Impedance Functions 2x2 pile group

# 5

## Conclusions

The chapters that compose this study are only a brief description of the so-called soil-structure interaction of seismic isolated bridges. The complexity of the phenomenon and the studies that so far treated the SSI effects as beneficial for seismic isolated structures were the initial challenges for the analyses to be performed. In the first place the differences that the SSI effects were contributing to the models, either detrimental or beneficial, were demonstrated. After the investigation of the important parameters that the SSI is vulnerable to, some more analyses were performed of a system case that would probably lead to the proof that the SSI may be detrimental. The purpose of this study is not to define in which cases the SSI effects must be taken into account or not, but to highlight the parameters that control the phenomenon and the complicity that characterizes it. Hence, the most important conclusions are:

- The misconception that treats the soil-structure interaction as always being beneficial due to the lengthening of the natural period of the total system has to be overpassed.
- The foundation's and soil's characteristics are those who determine the dynamic response of the soil. The softer the soil compared to the piles' material and the greater the distance of the piles of the group, the more sensitive to the frequency the dynamic impedances are.
- Generally, in cases of stiff foundation resting on linear homogeneous soil based on halfspace, the SSI can be satisfactorily modeled with the simple Voigt systems. The discrepancies between the Type II (gyromasses) and Voigt models are up to 10-20% for both isolation displacements and pier shear forces.
- The last case of analysis (Bridge II, 2x2 pile group,  $V_s=63$  m/sec) revealed the importance of the relative stiffness between the soil and the foundation concerning the choice of modeling of SSI. This case showed that a flexible

system, with flexible pile group resting on a very soft soil can lead to great loss of accuracy in case Voigt models are used. The differences came up to 50% for both isolation displacements and pier shear forces, with the Type II model outweighing the Voigt. This case of such a small value of shear wave velocity could be a simplified approach of the nonlinear behavior of the soil, which is the actual one.

- Apart from the dynamic impedances, the final performance of the superstructure is a matter of its properties and of the incoming energy. An attempt to define the dynamic characteristics of the system (with the SSI involved) was made in this study, both graphically (transfer functions, white noise) and analytically (eigenvalue analyses). The results are important and could be probably used for the inverse scenario: to predict in which excitations there would be a problem in case the Voigt systems were used for the SSI modeling.

---

## Bibliography

- Ucak, A., and P., Tsopelas, “*Effect of Soil-Structure Interaction on Seismic Isolated Bridges*” in *Journal of Structural Engineering*, ASCE, pp.1154-1164, July 2008.
- Saitoh, M., “*Simple Model of Frequency-Dependent Impedance Functions in Soil-Structure Interaction Using Frequency-Independent Elements*” in *Journal of Engineering Mechanics*, ASCE, pp. 1101-1114, October 2007.
- Kaynia, A. and E. Kausel, “*Dynamic Stiffness and Seismic Response of Pile Groups*”, Research Report, Publication Number: R82-03, Department of Civil Engineering, MIT, Cambridge, January 1982.
- Gazetas, G., “*Soil Dynamics: an Overview*”, *Dynamics of Foundations and Underground Structures*, Elsevier Applied Science, Chapter 1, pp. 1-39, 1987.
- Kampas, G. and N. Makris, “*Modal Identification of Freeway Overcrossings with Soil-Structure Interaction: a Case Study*” in *Structural Control and Health Monitoring*, pp.304-319, Online Publication Date: 1-Mar-2013.
- Mylonakis, G. and G. Gazetas, “*Seismic Soil-Structure Interaction: Beneficial or Detrimental?*” in *Journal of Earthquake Engineering*, pp. 277-301, April 2008.
- Ozdemir, H., “*Nonlinear Transient Dynamic Analysis of Yielding Structures*”, PhD dissertation, University of California, Berkeley, 1976.
- Wolf P.J, “*Dynamic Soil Structure Interaction*”, Chapter 1, Prentice Hall, 1985.
- Novak M. and Nogami T., “*Soil-Pile Interaction in Horizontal Vibration*” in *Earthquake Engineering and Structural Dynamics*, vol. 5, pp. 263-281, 1977.
- Makris, N. M., and J., Zhang, “*Seismic Response Analysis of a Highway Overcrossing Equipped with Elastomeric Bearings and Fluid Dampers*” in *Journal of Structural Engineering*, 130\_6\_, pp. 830-845, 2004.
- Gazetas, G and N. Makris, “*Dynamic Pile-Soil-Pile Interaction. Part I: analysis of Axial Vibration*” in *Earthquake Engineering and Structural Dynamics*, Vol. 20, pp. 115-132, 1991.

- Fan, K., Gazetas, G., Kaynia, A., Kausel, E., and Ahmad, A., “*Kinematic Seismic Response of Single Piles and Pile Groups*” in *Journal of Geotechnical Engineering*, 117\_12\_, pp. 1860–1879, 1991.
- Mylonakis, G. G. Gazetas, A. Nikolaou and O. Michaelides, “*The Role of Soil on the Collapse of 18 Piers of the Hanshin Expressway in the Kobe Earthquake*” in 12WCEE, 2000.
- Mylonakis G., Nikolaou S., Gazetas G., “*Footings Under Seismic Loading: Analysis and Design Issues With Emphasis on Bridge Foundations*” in *Soil Dynamics and Earthquake Engineering*, pp. 824–853, 2006.
- Moghaddasi, M. Cubrinovski, J. G. Chase , S. Pampanin and A. Carr, “*Stochastic Quantification of Soil-Shallow Foundation-Structure Interaction*” in *Journal of Earthquake Engineering*, pp. 820-849, July 2012.
- D.W. Marquardt., “*An Algorithm for Least-Squares Estimation of Nonlinear Parameters*” in *Journal of the Society for Industrial and Applied Mathematics*, 11(2), pp. 431-441, 1963.
- Spyrakos, C. C., “*Assessment of SSI on the Longitudinal Seismic Response of Short Span Bridges*” in *Engineering Structures Journal*, 12(1), pp 60-66, 1990.
- Spyrakos, C. C., “*Seismic Behavior of Bridge Piers Including Soil-Structure Interaction*” in *Journal of Computational Structures*, 43(2), pp 373-384, 1992.
- Resendiz, D. and Roesset J.M., “*Soil-Structure Interaction in Mexico City During the 1985 Earthquake*”, *The Mexico Earthquakes -1985*, ASCE special publication, 1987.
- Meymand, P.J, “*Shaking Table Scale Model Tests of Nonlinear Soil-Pile-Superstructure Interaction in Soft Clay*”, Ph.D. Dissertation, University of California, Berkeley, 1998.
- Celebi, M. (1998). “*Turkish Earthquakes: Two Reports. Lessons from the Adana-Ceyhan Quake and the Dinar Aftershock*” in *EERI Newsletter*, Vol. 32, No. 9, 8 pages.
- Wolf, J.P. and von Arx, G. A., “*Impedance Functions of a Group of Vertical Piles*”. *Proc. ASCE Specialty Conf. on Earthquake Engrg. And Soil Dynamics*, Pasadena, California, II, pp. 1024-1041, 1978.

- 
- Wolf, J.P. and von Arx, G. A., “*Horizontally Travelling Waves in a Group of Piles Taking Pile-Soil-Pile Interaction into Account*” in Earthquake Engineering Structural Dynamics Journal, Vol. 10, No.2, March 1982.
  - Poulos H.G., “*Analysis of the Settlement of Pile Groups*” in Geotechnique Journal, 18, pp. 449-471, 1968.
  - Gazetas, G., and Dorby, R., “*Horizontal Response of Piles in Layered Soil*” in Geotechnical Engineering Journal, 110(1), pp.20-40, 1984.
  - Gazetas, G., “*Seismic response of End - Bearing Single Piles*” in Soil Dynamics and Earthquake Engineering Journal, Vol.3, No.2, pp. 82-93, 1984.
  - Gazetas, G., and Tassoulas, J.L., “*Horizontal Stiffness of Arbitrarily – Shaped Embedded Foundations*” in Journal of Geotechnical engineering, ASCE, Vol.113, No.5, pp. 440-457, June 1987.
  - Gazetas, G., and Tassoulas, J.L., “*Horizontal Damping of Arbitrarily – Shaped Embedded Foundations*” in Journal of Geotechnical engineering, ASCE, Vol.113, No.5, pp. 458-475, May 1987.
  - Dorby, R. and Gazetas, G., “*Simple Method for Dynamic Stiffness and Damping of Floating Pile Groups*” in Journal Geotechnique, 38, No.4, pp 557-574, 1988.
  - Roesset, J.M., “*Dynamic Stiffness of Pile Groups*” in Journal Pile Foundations, ASCE, New York, 1984.
  - Sanchez-Salinerio, I., “*Dynamic Stiffness of Pile Groups: Approximate Solutions*”, Geotechnical Engineering Report GR83-5, University of Texas at Austin, 1983.
  - Makris, N., and Gazetas, G., “*Dynamic Pile-Soil-Pile Interaction. Part II: Lateral and Seismic Response*” in Earthquake Engineering and Structural Dynamics, Vol. 21, pp. 145-162, 1992.
  - De Barros, F.C. P., and Luco, J.E., “*Discrete Models for Vertical Vibrations of Surface and Embedded Foundations*” in Earthquake Engineering and Structural Dynamics Journal, 19 (2), pp.289-303, 1990.
  - Wolf, J.P., and Somani, D.R., “*Approximate Dynamic Model of Embedded Foundation in Time Domain*” in Earthquake Engineering and Structural Dynamics Journal, 14 (5), pp.683-703, 1986.